November 2021

Metastatic MAT Phenotype Driven by Noncanonical EphA2 Signaling in Melanoma

Chao Zhang
University of South Florida

Metastatic MAT Phenotype Driven by Noncanonical EphA2 Signaling in Melanoma

by

Chao Zhang

A dissertation submitted in partial fulfillment
of the requirements for the degree of
Doctor of Philosophy in Biomedical Sciences
with a concentration in Pathology and Cell Biology
Department of Pathology and Cell Biology
College of Medicine
University of South Florida

Co-Major Professor: Keiran S.M. Smalley, Ph.D.
Co-Major Professor: Patricia Kruk, Ph.D.
Vrushank Dave, Ph.D.
Uwe Rix, Ph.D.
Anne Champeaux, M.D.

Date of Approval:
November 4, 2021

Keywords: Amoeboid, Cdc42, PI3K, drug-resistant

DEDICATION

I dedicate my dissertation work to my family and important persons in my life. A deep gratitude to my loving parents Ping Zhang and QiaoMei Liu whose words always encourage and guide me for chasing my goals. Even they are in China-far away from here, they are always with me in my heart as one family.

I also would like to thank my friend Tao Han, who has supported me since the beginning of my PhD. As roommate for almost a year, Tao Han is very nice person. As co-worker, he is smart and helpful.

In the end, I really would like to appreciate someone who has always been staying with me through all the time of my dissertation work. Olga VeraPuente-was as my partner, always encourages me when I face difficulties and rough times. She is the light when I feel lost and down. I can't image how the dissertation would be going without her by my side. Now as my wife, she always shows me the brightness and smile which is such a wonderful thing in my life.

ACKNOWLEDGMENTS

This project would not have been possible without the support and help of my PI-Dr. Keiran Smalley. He is a wonderful supervisor with lots of magical and creative ideas. He always encourages and leads me to the development of the project. His knowledge and smartness always inspire and guide me for exploring the interesting questions. I'm so pride of, and grateful for working with him.

And I would also like to thank Inna Smalley. She was my mentor when I first joined the lab. She teaches me most of the experiments. Her patience and thoughtful thinking towards science influences me a lot. She is a good teacher and I'm very glad and lucky that I met her as my mentor in my early PhD period.

TABLE OF CONTENTS

LIST OF TABLES

LIST OF FIGURES

ABSTRACT

Acquired BRAF/MAPK/extracellular signal–regulated kinase inhibitor resistance in melanoma results in a new transcriptional state associated with an increased risk of metastasis. In this study, we identified noncanonical ephrin receptor (Eph) EphA2 signaling as a driver of the resistance-associated metastatic state. We used mass spectrometry–based proteomic and phenotypic assays to demonstrate that the expression of active noncanonical EphA2-S897E in melanoma cells led to a mesenchymal-to-amoeboid transition driven by Cdc42 activation. The induction of mesenchymal-to-amoeboid transition promoted melanoma cell invasion, survival under shear stress, adhesion to endothelial cells under continuous-flow conditions, increased permeability of endothelial cell monolayers, and stimulated melanoma transendothelial cell migration. In vivo, melanoma cells expressing EphA2-S897E or active Cdc42 showed superior lung retention after tail-vain injection. Analysis of BRAF inhibitor–sensitive and –resistant melanoma cells demonstrated resistance to be associated with a mesenchymal-to-amoeboid transition switch, upregulation of Cdc42 activity, increased invasion, and transendothelial migration. The drug-resistant metastatic state was dependent on histone deacetylase 8 activity. Silencing of histone deacetylase 8 led to the inhibition of EphA2 and protein kinase B phosphorylation, reduced invasion, and impaired melanoma cell-endothelial cell interactions. In summary, we have demonstrated that the metastatic state associated with acquired BRAF inhibitor resistance is dependent on noncanonical EphA2 signaling, leading to increased melanoma-endothelial cell interactions and enhanced tumor dissemination.

INTRODUCTION

Skin cancer and melanoma

Skin cancer is the most common and prevalent type of cancer in the United States and worldwide [1, 2]. It has been reported that almost 9,500 cases of skin cancer are diagnosed every day, with 2 people dying from it every hour in the U.S. [3, 4]. The incidence rate has increased dramatically over the past decades [4] and it is estimated that 20% of Americans will be diagnosed with skin cancer by the age of 70 [5, 6]. Skin cancer has the following major types: basal cell carcinoma (BCC), squamous cell carcinoma (SCC), and melanoma [3, 7]. The BCCs and SCCs are classified as non-melanoma skin cancers and arise from oncogenic transformation of keratinocytes [8, 9]. There are also rare and uncommon types of skin cancers such as Merkel cell carcinoma (MCC) and dermatofibrosarcoma protruberans [10, 11]. BCC is the most prevalent form of skin cancer with more than 4 million cases diagnosed each year in the U.S. [3, 7]. SCC is the second common form of skin cancer with more than 1 million cases each year in the U.S. [3].

Melanoma is the most aggressive form of skin cancer and results in the most deaths, although it only accounts for around 1-2% in all skin cancers [12]. The incidence rate of new melanoma cases is rising at a rate of 1-3% every year (roughly 2% in 2020), although the incidence rates are decreasing in many other cancer types [4, 13]. According to the estimation of the American Cancer Society (ACS), approximately 106,110 people will be diagnosed with invasive melanoma in the U.S. for 2021 [14]. Among them, 62,260 and 43,850 new cases in male and female are expected to be detected, respectively [14]. Approximately 7,180 people will die due to melanoma including 4,600 males and 2,580 females [14]. White people are almost 20 times more likely to develop melanoma in lifetime than black people [15, 16]. The average of age melanoma diagnosis

is 63 years of age [16, 17]. Below the age of 50 more females are diagnosed with melanoma than males, a likely consequence of tanning behavior [4]. Over the age of 65, 2-3 times more men are diagnosed with melanoma than women [4]. Although melanoma is mostly found in elderly people, it is still one of the most prevalent cancers found in young adults, typically young females [18-20]. Around 2,400 young people between the age 15 and 29 were diagnosed with melanoma in 2020 according to ACS [4]. The financial burden of skin cancer is very high. The average of annual cost for treatment of skin cancer is nearly $8.1 billion in the U.S., including $4.8 billion for non-melanoma skin cancers and $3.3 billion for melanoma [2].

The ABCDE rule is adopted to characterize unusual moles, which may be the precursor of melanoma according to the following criteria: asymmetrical shape (A), irregular border (B), changes in color (C), diameter (C) and evolving (D) [21-23]. The medical term for these moles is *nevi*, and these are very common with most people having an average of 10-40. Usually, they are harmless as small brown, tan spots [24, 25]. Interestingly, nevi have a high frequency of BRAF mutations, the same ones commonly found in melanomas [26]. Several studies have shown that more than 80% cases of nevi samples harbor BRAF V600E mutation. These studies strongly suggested that although the BRAF mutation is common, it is not sufficient on its own to cause malignant transformation of the melanocytic nevi. The acquisition of a BRAF mutation on its own typically pushed melanocytes into senescence, with additional mutations being required for melanoma development [26-28]. Although the rate at which nevi transform into melanoma is very low (range 1 in 33,000 to 1 in 200,000), up to 30% of melanoma arise from either pre-existing nevi or in the vicinity of existing nevi [29-31]. Despite this, studies indicate that the majority of cases of melanoma arise *de novo* rather than from existing moles [32-34].

Based on the growth pattern, melanoma is histologically classified as following groups: superficial spreading melanoma, nodular melanoma, lentigo maligna melanoma and acral lentiginous melanoma [35-37]. These different subgroups are generally associated with specific body location (e.g., the palms and soles for acral melanoma) and on skin that is either sun-exposed or non-sun

exposed [38, 39]. Superficial spreading melanoma is the most frequent type of melanoma, which is mainly found in arms, legs, and main body (back) [36, 40]. Nodular melanoma typically arises on the chest, back and face, and grows much faster than the other types, preferring to invade into the skin [41-44]. Elderly people usually develop lentigo maligna melanoma on the areas highly exposed under the sun like the ears, arms, and face [17, 45]. Acral lentiginous melanoma is rare case of melanoma and is the most prevalent form of melanoma in people with dark skin including Hispanic, Asian and black people [46, 47]. Hand's palms, feet's soles and the area under the nails are the typical areas associated with the development of acral melanoma [48, 49]. However, these areas are usually highly protected from exposure to the sun [46, 50, 51], suggesting different mechanism driving these melanoma types.

A number of factors are considered to increase the risk of melanoma development. Extreme ultraviolet (UV) radiation from the sun or tanning beds is the major risk factor [52-54]. Research show that more sunburn increases the chance of developing melanoma [55, 56]. The number of atypical moles [57, 58] or a family history of melanoma are other factors indicating the potential risk [59, 60]. Besides that, people with fair skin or compromised immune system are also at higher risk for melanoma development than those without them [61-64].

The 5-year survival rate for melanoma depends upon the stage [65, 66]. For early melanoma patients (e.g., Stage 0 and I called melanoma *in situ* which is a localized tumor), the 5-year survival rate is above 90% (Cancer Facts and Figures 2020. American Cancer Society). However, the rate dramatically decreases to around 15% in late-stage melanoma patients (e.g., Stage IV as tumor metastasis beyond regional lymph nodes) who have metastases [66, 67].

Stages of melanoma

Melanoma is a deadly cancer because of its propensity to metastasize early. It is somewhat unique that even very thin tumors (~1mm) at diagnosis may have already seeded to distant organs. From a clinical perspective, cancer staging is a key criterion that defines the level of disease

progression and dictates the treatment plan. The staging process of melanoma in clinic is determined by the following several aspects. The Breslow Depth system is used to measure how far the melanoma has vertically grown into the dermis in millimeters (Figure 1) [65, 68]. It is an accurate and helpful method that evaluates and predict the extent of melanoma progression and is correlated with prognosis and survival. Generally speaking, the extent of invasion into dermis, the greater the chance it has spread to other parts of body [65, 68]. Tumor ulceration is also a high-risk indicator of tumor prognosis and poor outcome [69, 70]. Metastasis to distant lymph nodes or other organs, such as lung or liver, is also a marker of poor prognosis and tumor aggressiveness [71, 72].

The stages of melanoma include the following levels using five Roman numerals (0 through IV). Within each stage, the letters A, B, C and D are used to further classify the extent of tumor progression.

In stage 0, the tumor is still restricted in the outer layer of the epidermis. Since it is little invading, likelihood of metastasis is low. This is often known as melanoma *in situ*.

In stage I, there are cancer cells in both the epidermis and dermis, and the tumor can be up to 2mm thick. There is no spread to nearby lymph nodes or distant organs. The risk of metastasis is still low. It can be ulcerated or not. The two subgroups stage IA and stage IB are differentiated by depth of tumor and ulceration. The tumor in stage IA is generally less than 0.8 mm and not ulcerated. The tumor in stage IB is normally between 1.0 mm and 2.0 mm and not ulcerated. However, if the tumor is less than 0.8 mm but with ulceration, it is considered to be stage IB [73, 74].

In the stage II, the cancer cells are found in both epidermis and dermis with at least 1 mm thickness or might be even thicker than 4 mm. It could be ulcerated or not without any spread to nearby lymph nodes or distant organs. There are three subgroups in this stage as IIA, IIB and IIC. In the stage IIA, the thickness of tumor is 1.01-2.0 mm with ulceration, or the thickness is 2.01-4.0 mm but without ulceration. In stage IIB, the tumor is between 2.01- and 4.0 mm thickness and

is ulcerated or the tumor is larger than 4.0 mm without ulceration. In stage IIC, the tumor is larger than 4.0 mm and ulcerated [73, 74].

In the stage III, the cancer cells are usually found in the local lymph nodes but not in distant organs. There are four subgroups in this stage. In stage IIIA, the tumor is less than 2.0 mm thick with or without ulceration. It can spread to 1-3 nearby lymph nodes. In stage IIIB, if there is no detection of the primary tumor, it has either spread to only one nearby lymph node or the tumor has spread to the nearby skin and is in transit to the nearby lymph nodes. If the tumor is larger than 4.0 mm thick, either it has spread to 1-3 nearby lymph nodes or has spread to a nearby small area of skin and is on the way to reach the nearby lymph nodes. In stage IIIC, if there is no detection of the primary tumor, either it has spread to 2 or more nearby lymph nodes with at least observation of 1 spreading or it has spread to a chain of lymph nodes. It is also considered IIIC if the tumor is larger than 4.0 mm thick with ulceration and spreads to 1 to 3 nearby lymph nodes. In stage IIID, the tumor is generally larger than 4.0 mm thick with ulceration. It has either spread to 4 or more nearby lymph nodes or spread to a nearby chain of lymph nodes. [73, 74]

In the stage IV, the cancer cells have disseminated to distant lymph nodes and other organs such as the liver, lungs, and brain. In stage IV disease, the letter M represents metastasis and is used to define the level of spread. Metastasis of melanoma cells to distant skin and soft tissue, including muscle, is considered M1a. Metastases found in the lungs are consider M1b. Metastasis found in the internal visceral organs is considered M1c. Metastasis found in central nervous system (CNS) is considered M1d [73, 74].

Classification by driver mutations

Melanoma develops due to a combination of environmental and genetic factors results [75, 76]. The accumulation of UV radiation results in DNA damage, inflammatory reactions, and increased stress of oxidative free radicals [77-79]. This cumulative damage leads to genetic mutations,

including those in key oncogenes and tumor suppressors that drive melanoma development [80-82].

Melanoma has the highest number of somatic gene mutations of all cancers [83-85]. Among these, specific genes have been identified as oncogenic drivers of melanoma development, such as those implicated in increased growth, survival and invasion [84, 86]. Specifically, activating mutations in the serine-threonine kinase BRAF is the most prevalent driver oncogene in melanoma, being found in nearly 50% cases of cutaneous melanomas that arise on sun-exposed skin [87-89]. Although multiple mutations in BRAF have been identified, the overwhelming majority (>80%) are valine to glutamic acid substitutions, the so-called BRAF V600E mutation [88, 90]. Other frequent BRAF mutations include the V600K and V600R mutations representing around 20% and 7% cases, respectively [87, 91]. Besides BRAF mutations, NRAS alteration is the second leading mutation found in cutaneous melanoma, comprising approximately 20% cases [82, 92]. In comparison to cutaneous melanoma, BRAF and NRAS mutation are rare in patients with mucosal or acral melanomas [93, 94]. However, KIT mutations are identified in almost 20% of these patients [95-97]. Melanoma can also be inherited, with rare cases of families with increased melanoma risk being reported [98, 99]. Familial melanoma accounts for up to 10% of all cases [59, 100] and is typically associated with inherited mutations in CDKN2A and MC1R [59, 80, 98, 99, 101].

The development of next-generation sequencing (NGS) technologies, especially whole exome (WES) or whole genome sequencing (WGS) have proven to be powerful tools for mapping the genetic landscape of melanoma [85]. Although the frequency of somatic mutations varies between 0.001 per megabase (Mb) to more than 400 per Mb in different cancers, melanoma has the highest somatic mutations frequency (range from 0.1 to 100 per mb) of all cancers [85]. The high mutational burden of melanomas has been ascribed to the causative role of UV radiation in melanoma development, with the vast majority of mutations in melanoma being of the C>T type (e.g. UV signature mutations). Sequencing of hundreds of melanoma cell lines and patient

specimens as part of the Cancer Genome Atlas (TCGA) Network has provided a comprehensive picture of the mutational landscape, allowing melanomas to be sub-divided into 4 distinct genetic sub-groups: mutant BRAF, mutant NRAS, mutant NF1, and triple-wildtype [102]. BRAF and NRAS are considered initiating events in melanoma and have been found in most cases [87]. The constitutive activation of the MAPK pathway results from these mutations, which potentially promote the survival and proliferation of melanocytes. Besides the activation of pro-oncogenic driver mutations, silencing of key tumor suppressors such as PTEN and CDKN2A, as well as the reactivation of the telomerase activity via TERT have also been implicated in melanoma development [84, 102]. PTEN is an important regulator of the PI3K/AKT pathway; its loss leads to activation of AKT, particularly an increased expression of phosphorylated AKT at Ser-473. Subsequently, the upregulation and activation of AKT mediated by PTEN loss leads to changes in apoptotic signaling which facilitates increased cell survival and tumor progression [103-105]. Mutations in the CDKN2A gene are found in 20-40% of melanoma families. Mutation or deletion of CDKN2A gene leads to dysfunction of the p16(INK4A) protein which normally blocks the activation of cyclin D–CDK4/6 complex. Without the regulation of p16(INK4A) protein, the cells acquire the ability to undergo uncontrolled growth and division [80, 106, 107]. In addition, mutations and copy number losses in p53 occur frequently in cutaneous melanoma [108, 109]. Even for wild-type (WT)-p53 melanoma cells, the amplification of negative regulators impairs the activity of p53 to promote cell survival and block the p53-mediated apoptosis. MDM4, which is a negative regulator of p53 and a key factor to suppress p53 activity through binding with it, is upregulated in a large percentage of stage I-IV human melanomas. Similarly, MDM2 binding to the p53 transactivation domain leads to the suppression of its transcriptional activity. MDM2 mediates ubiquitination of p53, and then degradation as an E3 ubiquitin ligase [110-112].

The development of single-cell RNA sequencing (RNA-seq) technology has further allowed the genotypic and phenotypic heterogeneity of melanoma to be unraveled [113]. These data have provided new insights into the different cell types (such as malignant, immune, stromal, and

endothelial cells) present in the melanoma microenvironment. These analyses have further highlighted the presence of multiple cell states within the same tumor, which have shown differences in things such as cell cycle states and drug resistance [113]. At least two co-existent transcriptional cell states have been identified in the same tumor including those with high levels of the MITF transcription factor and those with low MITF expression with increased levels of AXL kinase [113-118]. There is evidence that MITF can also function as an oncogene with amplification of MITF being identified in up to 15-20% of human metastatic melanomas [119]. High expression of MITF was also found in melanoma samples from patients who had relapsed on the combination therapy of BRAF and MEK inhibitors [120]. These findings suggest that the high levels of MITF promote differentiation whereas the low expression of MITF indicate an increased metastatic potential [120-122]. This central regulatory role of MITF has demonstrated the phenotypic diversity of melanoma cells that can adapt to changes in the tumor microenvironment to promote the tumor progression [123-125].

Treatment of metastatic melanoma

As previously described, over 50% of all melanomas harbor activating BRAF mutations. Activating BRAF mutations drive the mitogen-activated protein kinases (MAPK) pathway, an important signaling cascade that is responsible for the uncontrolled growth of melanoma cells through increased cyclin D expression, suppression of pro-apoptotic proteins such as BIM and BMF and increased expression of pro-survival proteins such as MCL-1 [126, 127]. In addition to this, MAPK signaling also contributes to increased melanoma survival via the inhibition of BAD and BIM, two proapoptotic BH3-only proteins [128, 129]. Activated ERK1/2 is the major effector of the MAPK pathway that exerts its effect by translocating to the nucleus and regulating transcription factors through phosphorylation such as proto-oncogene c-Fos, proto-oncogene c-Jun, ETS domain-containing protein Elk-1, proto-oncogene c-Myc [130, 131]. Constitutive MAPK signaling also contributes to metastasis through the regulation of MMP-2 and MMP-9, leading to degradation of

the tumor extracellular matrix [132, 133]. ERK/MAPK signaling pathways additionally activates transcription factors to enhance the transcription of VEGF, which enhances the blood vessel formation [134].

The addiction of melanoma cells to the MAPK signaling pathway makes it an excellent therapeutic target and numerous BRAF and MEK inhibitors have been developed clinically to target this pathway. The first BRAF inhibitor used in clinical trials to treat melanoma was sorafenib, which actually is a multi-kinase inhibitor targeting BRAF, CRAF, c-KIT and vascular endothelial growth factor receptor (VEGFR) [135]. In preclinical studies of human melanoma cell xenografts in nude mice, sorafenib did induce growth arrest of the tumor but did not cause any regression [135, 136]. In randomized phase III clinical trials, sorafenib did not cause any significant improvements in response rate or progression-free survival compared to the original chemotherapy combination of paclitaxel and carboplatin. The failure of sorafenib was potentially due to its incomplete level of BRAF inhibition [137, 138]. Surprisingly, in renal cell carcinoma which largely relies on the signaling of VEGFR but not BRAF, sorafenib did exhibit strong efficacy and was FDA-approved on December 20, 2005 [139].

The demonstration of BRAF V600E as a *bona fide* therapeutic target for melanoma was not confirmed until the development of the second generation of BRAF inhibitor PLX4032 (vemurafenib) [140]. This drug works by selectively targeting the active form of BRAF (with some selectivity for the BRAF V600E mutant) and blocks the signal transduction between BRAF and MEK at a concentration 10 times lower than sorafenib, while exhibiting minimal activity on other kinases [141]. In preclinical studies, the PLX4032 exhibited strong efficacy against BRAF-mutant melanoma cell lines and BRAF mutant mouse melanoma models. In phase III clinical trials, vemurafenib significantly improved progression free survival (PFS) and overall survival (OS) compared to dacarbazine (chemotherapy) [142]. In light of these striking results, vemurafenib (Zelboraf) was approved by the FDA on August 17, 2011 for treatment of metastatic or unresectable BRAF-mutant melanoma [143].

Following the success of vemurafenib multiple other BRAF inhibitors were FDA-approved. Among these, the BRAF inhibitor dabrafenib showed remarkable results. In the phase III, BREAK-3 trial, dabrafenib improved the median PFS from 2.7 to 5.1 months compared to dacarbazine chemotherapy in the patients with BRAF-mutant metastatic melanoma. The remarkable results of the BREAK-3 led trial led to the FDA-approval of dabrafenib in May 2013 [144-148].

MEK is a direct downstream effector of BRAF and is directly responsible for the phosphorylation and activation of ERK, the major effector kinase in the MAPK pathway. This led to the possibility of MEK being an alternative therapeutic target for treating BRAF-mutant melanoma [149]. In studies in BRAF-mutant xenografts, the pharmacological blockade of MEK effectively inhibited tumor growth. Based on these important studies, the phase III METRIC trial was conducted to evaluate the efficacy of single agent MEK inhibition in metastatic melanoma patients with BRAF V600E/K mutations [150]. These studies demonstrated that the MEK inhibitor trametinib significantly enhanced the median PFS and OS around 6 months and trametinib was FDA-approved in May 2013 for treatment of BRAF-mutant metastatic or unresectable melanoma patients [151].

Although single-agent BRAF or MEK inhibition exhibited impressive anti-tumor effects against BRAF-mutant metastatic or unresectable melanoma patients, the average PFS was generally short at around 7 months [144, 152]. Moreover, several potential BRAF inhibitor resistance mechanisms were uncovered including NRAS mutations, MEK1 mutations and BRAF truncation mutations [153-156]. As MAPK reactivation seemed to be the major resistance mechanism to BRAF inhibition, it seemed likely that combined BRAF-MEK inhibition could overcome it. This concept was demonstrated *in vitro* [157-164]. Further, a number of clinical trials were undertaken to test the concept of dual BRAF-MEK inhibitor therapy, and all proved to highly successful, increasing the PFS and OS compared to single agent BRAF inhibitor therapy alone [165-168]. Among all these trials, the phase III trial COMBI-v, which compared the combination therapy of dabrafenib and trametinib with vemurafenib monotherapy, was the most exciting and highly

anticipated, demonstrating that the combination therapy significantly improved the median PFS from 7.3 to 11.4 months and OS from 65% to 72% respectively. Meantime, the combination therapy reduced potential side effects, such as the development of cuSCC compared to BRAF monotherapy [169]. Because of these remarkable outcomes, the combination therapy was FDA-approved and is now one of the standard treatments for BRAF-mutant metastatic or unresectable melanoma. At this time, the OS rates are 37% at 4 years and 34% at 5 years from the above trial COMBI-v which finished in 2019. It is clear that a significant proportion of patients gain long term benefit from BRAF inhibitor therapy [169].

Another significant systemic therapy for advanced melanoma is immunotherapy. The most successful of these are strategies to target inhibitory immune checkpoints, such as the inhibition of Programmed cell death protein 1 (PD-1). This protein is expressed on the surface of T cells, as well as other immune cells such as regulatory T cells, B cells, myeloid cells and natural killer cells. The binding of PD-1 to its ligand PD-L1, which is mainly expressed in the cancer cells, has been identified as a novel immune escape strategy that protects cancer cells from being attacked by T cells. Hence, inhibition of the T cell communication with cancer cells and the interaction between the PD-1 and PD-L1 would potentially enhance the T cells activation and recognition for eliminating cancer cells.

In clinical trials, targeting of PD-1 through the blocking antibody nivolumab, which prevents the binding of PD-1 to PD-L1, improved the median PFS and OS of patients with advanced melanoma compared to chemotherapy. Further studies showed that the combination of anti-PD-1 with anti-CTLA4 (nivolumab and ipilimumab) showed better efficacy compared to each monotherapy, albeit with more severe side effects. Nivolumab was FDA-approved as a monotherapy for advanced melanoma patients with wild-type BRAF as well as those with a BRAF V600E mutation. The combination therapy of the nivolumab and ipilimumab was quickly approved by FDA as the treatment for advanced melanoma patients with wild-type BRAF [170-172].

Escape from targeted therapy (BRAF inhibitor)

As mentioned in the above section, BRAF inhibitor therapy is associated with a rapid onset of resistance. Numerous mechanisms of resistance have been identified and these can be classified as either intrinsic/primary resistance or acquired/secondary resistance [173-175].

In the early clinic trials, it was found that approximately 20% of the BRAF V600E mutant melanoma patients did not respond to BRAF inhibitors. Genetic sequencing studies identified multiple potential mediators of intrinsic resistance including loss of PTEN, RAC1 mutations, loss of NF1, overexpression of MAP3K8 and Hepatocyte growth factor (HGF) secretion. As a critical tumor suppressor, loss of PTEN directly cause the constitutive activation of PI3K/AKT pathway which promotes cell proliferation despite BRAF inhibition. RAC1, as the GTPase effector of RAS, plays important roles in cell proliferation and motility. The RAC1 P29S mutation has been confirmed to maintain the activation of the MAPK signaling. NF1, is a tumor suppressor of RAS, whose mutation leads to upregulation of RAS; this activates different isoforms of RAF, like CRAF, which reactivates the MAPK pathway. The MAPK/ERK pathway could also be independently re-activated by other MAPK isoforms such as MAP3K8 (also called COT). Resistance-conferring signals can also come from the tumor microenvironment. As one example, the binding of HGF secreted by stromal cells with its receptor MET reactivates the MAPK/ERK and PI3K/AKT pathways. There is also evidence that host cells can secrete IGF, PDGFR and EGF to reactive MAPK and PI3K signaling in melanoma cells leading to resistance [154, 159, 160, 163, 175-181].

In the presence of BRAF inhibitors, the different RAF isoforms including ARAF and CRAF can compensate for the suppression of BRAF. The CRAF-BRAF heterodimers or homodimers and the flexible switching among these RAF isoforms are able to reactivate the ERK pathway. The mutant RAS bound to GTP cannot be reversed to the inactivated state by binding with GDP. The constitutive activation leads to the increased dimerization of BRAF V600E. It allows the escape from BRAF inhibitors because the blockage is only effective on the monomeric BRAF V600E. New types of BRAF inhibitors have also been developed which inhibit both mutant BRAF

monomers and dimers, such as PLX8394. This drug works by targeting BRAF homodimers and BRAF-CRAF heterodimers, but not CRAF homodimers or ARAF-containing dimers [182-184].

Although gatekeeper mutations in BRAF have never been identified as a resistance mechanism, other genetic changes to BRAF can decrease BRAF inhibitor sensitivity. The most common of these is the alternative splice mutant of p61BRAF V600E which can form dimers without RAS activation reactivating MAPK signaling. Besides that, increased BRAF gene copy number gain can dramatically increase the level of BRAF V600E expression, enhancing the spontaneous dimerization of BRAF V600E. Mutations in downstream targets of BRAF such as the mitogen-activated protein kinases, MEK1/ MEK2 could also mediate the resistance to BRAF inhibitors. These work by increasing ERK activity in the presence of BRAF inhibitors [90, 155, 173, 185].

In addition to the reactivation of MAPK pathway, alternative pathways such as PI3K/AKT can also mediate BRAF inhibitor resistance. It has been demonstrated that there is active crosstalk and communication between the PI3K/AKT pathway and the MAPK pathways and that inhibition of either pathway would potentially lead to the upregulation of the other one. Upregulation of the PI3K/AKT pathway resulting from genetic mutations has been identified in 22% melanoma with acquired resistance to BRAF inhibitors. Studies found that the AKT levels increased significantly just within the few days of treatment with BRAF inhibitors. The abnormal overexpression of PI3K/AKT can then maintain tumor survival and proliferation in the face of drug treatment. Activation of PI3K/AKT signaling can be mediated by growth factors such as PDGFR-β and IGF-1R binding to receptor tyrosine kinases (RTKs). In addition, AKT signaling could be also enhanced by activating mutations in PI3K and AKT, which prevents apoptosis and increase proliferation of tumors [186-188].

Besides the acquisition of mutations, phenotype switching is another strategy by which melanoma cells evade from targeted therapy. Studies have shown that phenotype switching is mediated by the transcription factor MITF, which is an important transcriptional mediator of melanocyte differentiation, proliferation and metabolic rewiring. Melanoma cells are extremely heterogeneous

and have different levels of MITF at the single cell level. Studies show that MITF levels inversely correlate with expression of the RTK AXL, which while not a driver of the de-differentiated state, identify melanoma cells that are less dependent upon MITF. Analysis of individual cells have shown that the MITF-high/AXL-low dictates a differentiated, proliferative phenotype while the MITF-low/AXL-high associates with a de-differentiated, invasive phenotype. The MITF-low/AXL-high drug-resistance phenotype is a common feature in BRAF mutant melanoma cell lines [120-123].

The metastatic cascade

Metastasis is the major complication of advanced melanoma and accounts for the majority of mortality and morbidity associated with the disease [66]. The metastatic cascade describes how the tumor cells from primary lesions can escape the initial tumor, survive, grow, migrate, and then finally form new tumors in distant tissues and organs. The major processes in this cascade includes the following steps: local invasion, intravasation, survival in the circulation, arrest at distant organ site and extravasation, micrometastasis formation and then metastatic colonization. Studies show this process to be highly complex and dependent upon the ability of the melanoma cells to form new interactions with microenvironment, acquire new epigenetic/genetic lesions, and increase their cellular plasticity [189, 190].

The first step in the metastatic cascade is the escape of individual cells from the primary tumor which then migrate and cross the basement membrane. At this time, the cells tend to adopt an undifferentiated sate which can be characterized by an epithelial-mesenchymal transition (EMT). In the EMT state the cells are more invasive and can survive when detached from pro-survival cues from their tissue niche. Even though melanoma cells are not epithelial cells, they adopt similar mechanisms in this initial step of metastasis. After successful invasion through the basement membrane, the invading cancer cells secrete multiple proteases such as matrix metalloproteinase (MMP)-1, -2, and -9 that allow them to degrade the surrounding extracellular

matrix (ECM). Once the tumor cells enter nearby capillaries or nearby lymphatics, they are able to form the new vessels via angiogenesis by secreting angiogenic factors, such as the vascular endothelial growth factor (VEGF) [191, 192].

Survival in the circulation system is another challenge for metastasizing tumor cells. To be successful they must be able to withstand the high levels of fluid shear stress and evade attack from the immune system. Studies show that less than 1% of circulating tumors cells (CTCs) in the blood are able to survive for long enough to form new metastases at new sites. One strategy used by the tumors is the secretion of thrombin, and cathepsin B which leads to the aggregation of platelets around the tumor cells, conveying some protection from immune attack, as well as aids the tumor cells in their arrest in capillaries at distant sites, facilitating extravasation [193, 194]. Extravasation is necessary for metastasis in distant organs. In this regard, tumor cells may express specific cell surface proteins and adhesion molecules that convey affinities for specific organs. Brain metastasis is a serious complication of advanced melanoma that progresses rapidly and is associated with an average survival of around 3 months, constituting nearly half of all melanoma deaths [195]. Currently, targeted therapies and immune checkpoint inhibitors have less efficacy against melanoma brain metastases than at other organ sites [196, 197]. The migration mechanisms of the melanoma cells to the brain and tumor formation are still unclear. The brain constitutes a unique organ site that is protected by the blood-brain barrier (BBB), a mostly impermeable barrier that surrounds most of its blood vessels [198, 199]. The main functions of the BBB are to protect the brain from toxins, pathogens and macromolecules which might cause damage to brain [198, 200]. This barrier consists of several major cell types such as brain endothelial cells, astrocytes and pericytes [198-200]. The brain endothelial cells are tightly connected by tight junctions (potentially regulated by ZO-1, claudins and occludins) and surrounded by a basement membrane, which form the main interior barrier [199-201].

Projections from astrocytes around the endothelial cells called astrocytic end-feet play a significant role in regulating the brain endothelial cell behavior [201]. The projections are involved

in the signaling that induces the endothelial cells to form the tight junctions [202-204]. They also play a key role in controlling the transient opening of the barrier to allow important substances to cross the BBB [202, 203, 205]. The factors secreted by astrocytes are also highly involved in the regulation of the BBB [203, 206, 207]. One of the most important pathways is the Hedgehog (Hh) signaling cascade related to the secretion of Sonic Hh (SHh) by astrocytes [207]. The expression of junctional proteins is induced by activation of the Hh pathway [206, 208]. In genetically engineered mouse models, loss of the signal transducer Smo on BBB endothelial cells led to the dramatic increase of BBB permeability and downregulation of junctional protein expression [206, 208]. Another secreted angiogenic factor by astrocytes, VEGF, decreases the stability of the BBB during inflammatory conditions [209, 210]. Angiopoietins (Ang1) produced by perivascular cells, including astrocytes, are co-expressed with VEGF to enhance the BBB integrity when VEGF disrupts BBB function [211]. Besides, angiotensin-converting enzyme-1 (ACE-1), also produced by astrocytes, converts angiotensin I into angiotensin II, which interacts with type 1 angiotensin receptors (AT1) expressed by BBB endothelial cells [212].

Pericytes also contribute to the BBB integrity by polarizing the astrocyte end-feet, which interact with the cerebral microvasculature [213]. Also, the pericytes potentially regulate transcytosis and control of extracellular matrix deposition [214]. The signal transduction correlates with platelet-derived growth factor B (PDGF-B), transforming growth factor-β (TGF-β) and Notch, which are highly involved in the crosstalk and functional coupling between pericytes and endothelial cells [215]. Mice that are null for Pdgfrb show signs of a leaky BBB during embryogenesis [213, 216]. The binding of TGF-β secreted by endothelial cells to TGFβR2 in pericytes activates the ALK5-Smad2/3 pathway and leads to inhibition of endothelial proliferation but promotes endothelial cell maturation, including BBB formation [217]. The survival and attachment of pericytes to endothelial cells was potentially related to Notch signaling [214, 218, 219].

The successful development of brain metastases is generally related to the disruption of BBB integrity. This can be mediated through multiple mechanisms including the adoption of a rounded

cancer cell phenotype with cytoplasmic protrusions that can push the endothelial cells apart. The release of angiopoetin-2 and the expression of multiple pro-invasive integrins on the cancer cells can also help their migration through the BBB [220, 221]. Meanwhile, proteases such as MMP-9 released by melanoma cells have the potential to degrade the basement membrane of the BBB [222]. Another protease, cathepsin-S, can cleave the BBB tight junction protein JAM-B and promote brain metastasis [221].

The brain microenvironment has also been implicated in brain metastasis development. The cancer cells interact with multiple cell types mainly including microglia, oligodendrocytes and astrocytes. The astrocytes are the major non-neuronal cell type and comprise approximately 50% of the total cells in brain [223]. These can be activated (called re-active astrocytes) following interaction with cancer cells and lead them to secrete many growth factors, chemokines and cytokines such as IL-6, TNF-α and IL-1β, which all promote tumor cell survival [224-227]. The expression of multiple pro-survival genes in brain-resident cancer cells including BCL2L1, TWIST and pro-invasive matrix metalloproteinases such as MMP-9 were induced by these reactive astrocytes [226, 228].

One major target mediated by astrocytes was expression of the tumor suppressor PTEN [229]. Studies in breast cancer xenograft models have demonstrated that the loss of PTEN was typically found only after the cells metastasize to the brain, and that PTEN expression was restored after the cancer cells were removed from the brain [229]. The unique microenvironment of brain compared to other organs also suggests that a series of signaling pathways might contribute to the brain metastatic potential of cancer cells. Michael A. Davies group showed an upregulation of the PI3K/AKT pathway and reduced PTEN expression in 60% of the brain metastasis samples comparing a series of non-matched cranial and extracranial melanoma metastases through reverse phase protein array (RPPA) and immunohistochemistry [187]. Specifically, the phosphorylation of AKT at S473 and T308, and GSKα/β were elevated. This finding was also confirmed later by immunohistochemistry. However, in a subsequent study, the loss of PTEN was

not frequent even in specimens with high AKT level [187, 230]. Other groups have used gene expression profiling approaches to identify the potential drivers for development of melanoma brain metastasis [231]. The phospho-inositide binding protein PLEKHA5 was identified to be highly correlated with the risk of melanoma brain metastasis. Silencing of PLEKHA5 led to the decreased viability and migration of cerebrotropic melanoma cells in an *in vitro* BBB model [231]. Other signaling pathways such as the JAK/STAT3 pathway has also emerged as a key driver of cell proliferation and angiogenesis in brain metastasis models [232]. In nude mice, the potential to develop brain metastases increased following STAT3 expression in melanoma cells. Furthermore, the upregulation of STAT3 resulted in elevated angiogenesis *in vivo* and increased invasive capacity in melanoma cells *in vitro*. The expression of VEGFR, bFGF and MMP-2 were also enhanced due to the increased STAT3 [232].

One important question for the brain metastasis field is whether the brain metastases harbor distinct genetic alterations compared to those in primary tumors. A recent study addressed this by undertaking whole-exome sequencing of 86 matched pairs of primary tumors and brain metastases [233]. It was found that 46 of 86 (53%) cases harbored the distinct, potentially actionable mutations in the brain metastases comparing to paired primary tumors. Some of the key alterations identified were mutations in CDKN2A and in the PI3K/AKT/mTOR pathway. Potential deleterious mutations in HER2/EGFR were detected in the brain metastasis samples as well as alterations in genes in the MAPK pathway [233]. Recent advances in multi-photon *in vivo* imaging have allowed the process of brain metastasis to be studied in real-time. These studies were based upon red fluorescent protein (RFP) labeled cancer cells injected intra-arterially and then followed live as they invaded into the brains of nude mice. The first step observed was an initial arrest at the blood vessel branches. The melanoma cells moved slowly through the blood flow in brain micro-vessels and moved very slowly in smaller vessels, arresting at the vascular branch points or small micro-vessels due to size restriction [234]. The second step was early extravasation which directly determined the future success of metastasis growth. The time for the

initiation of extravasation varied from 1-9 days. Imaging showed that the cancer cells in the process of extravasation displayed a morphological change. The part of cell in the vascular wall was quite narrow explaining how the cells were able to squeeze into the gaps or holes in the vascular wall [234]. The third critical step was perpetuation of a perivascular position. The cells extravasating out of the vascular wall were only successful in forming micro- and macrometastases when the cells had a close physical contact with the abluminal surface of vascular endothelial cells. The cells without direct contact to the surface of micro-vessel regressed gradually [234].The last step for successful macrometastasis formation was the angiogenesis or vessel cooption. The melanoma brain tumor burden formation was strongly dependent on the interaction of the micrometastases with the preexisting microvasculature. Generally, the cells began proliferation gradually along the microvessels and formed the vascular loop around the vessels for further angiogenesis once the macrometastases were formed. The initial micrometastases in poorly vascularized locations regressed later, suggesting that the adoption of appropriate preexisting blood vessels was critical for the further successful formation of macrometastases in melanoma cells [234].

Another factor involved in the homing of tumor cells to specific organs is the expression of soluble factors from the host organs themselves. It is known that the secretion of chemokines from the tumor cells can drive organ-specific metastasis through binding with chemokine receptors from different organs [235].

Mesenchymal to amoeboid transition (MAT)

The process of metastasis requires cancer cells to undergo physical changes that allow them to physically squeeze through the basement membranes and in and out of blood vessels. Although the process of EMT is a critical transcriptional program involved in the increased motility and stemness that contributes to this, there are other mechanisms that may be involved. One other process is the mesenchymal-to-amoeboid-transition (MAT) in which the cells adopt a rounded

shape that utilize physical force to squeeze through gaps in the ECM and between blood vessels. It is known that cancer cells can switch between mesenchymal and amoeboid states in response to environmental cues [236, 237].

Cancer cells in the mesenchymal state have an elongated spindle-like shape. These highly polarized cells have one or more leading pseudopods that form the leading edge. The translocation of the mesenchymal cells starts with the leading edge, which consist of actin-rich filopodia and lamellipodia. At its poles, the cells are adhesive to the ECM and attach to the contracted actin fibers that generates the traction force. The velocity of cancer cells in mesenchymal mode is approximately 0.1–0.5 μm/min in 3D matrices. The moderate change of focal adhesions during the translocation can cause the movement to slow [238]. Mesenchymal motility depends on extra-cellular matrix (ECM) proteolysis through production of MMPs. These MMPs generally are upregulated and activated during the tumor progression and are required for the cancer cells to migrate through the matrix. Collagen is a major constituent of the connective tissue matrix that is degraded by these proteases. It was noted that even following inhibition of MMPs, the cancer cells could still migrate through the ECM, suggesting the existence of a non-protease mediated mechanism of cell migration. It was found that this motility was mediated through the cells switching to an amoeboid phenotype that could physically squeeze through gaps in the ECM [237, 239, 240]. Further studies showed that the amoeboid cells attach to the ECM in a low-adhesion manner allowing the cancer cells to translocate in 3D matrices with higher velocities than the mesenchymal mode. Studies have shown the motility of cells adopting the amoeboid state to move at 2 μm/min (such as A375-m2 melanoma cells), and up to the highest rate of 25 μm/min for lymphocytes moving through 3D collagen gels [241-243].

The amoeboid migration mode is largely dependent on the extreme contractility of actomyosin and remodeling of the cytoskeleton. The signaling mechanisms involved in the control and regulation of the actin cytoskeleton and actomyosin contractility are associated with the Rho family of small GTPases such as Rho, Cdc42 and Rac1. Each of them mediates specific changes

of actin cytoskeleton. Rac controls the formation of lamellipodia by driving actin assembly. Cdc42 drives actin assembly for filopodia. And stress fiber formation is stimulated by Rho. These small GTPases are activated as GTP-bound state through guanine nucleotide exchange factors (GEFs) and also could be inactivated as GDP-bound state by GTPase activating proteins (GAPs) [244].

Several studies have shown that different signaling can regulate this MAT. Rho-GTP is activated by RTKs, G protein coupled receptors (GPCRs), cytokines and integrins to further activate their downstream targets, the Rho-associated kinases ROCK1/2. This promotes actin stress fiber formation and actomyosin contractility. The activated ROCK/Rho signaling causes the phosphorylation of its downstream target MLC2, which is the major regulator of the actomyosin contractility [237, 243, 245, 246]. The silencing of Rho/ROCK signaling in amoeboid cancer cells leads to the reversed transition, from the amoeboid to the mesenchymal state [243, 246].

Rac has been found to regulate the plasticity of tumor cell movement as well. Rac typically becomes activated by binding of NEDD9 to the DOCK3 GEF (DOCK is the second major family of GEF), which forms a complex that promotes mesenchymal movement and blocks the amoeboid phenotype through decreasing actomyosin contractility in melanoma cells. However, in the amoeboid state, Rac is inactivated [243].

Another member of Rho family, Cdc42, is activated by DOCK10 GEF and can also induce the MAT and cell invasion. DOCK10 silencing leads to the amoeboid to mesenchymal transition associated with decreased MLC2 phosphorylation and increased Rac1 activation. The effectors of Cdc42 N-WASP and Pak2 are also necessary to maintain the amoeboid phenotype. Blocking Cdc42 results in transition from the amoeboid phenotype [247]. In B16 melanoma cells, the receptor tyrosine kinase EphA2 has been reported to upregulate Rho-GTP, promoting amoeboid-like migration [248].

Recently, the WNT11-FZD7-DAAM1 signaling has been identified as a driver of amoeboid invasion and is associated with tumor initiating abilities in melanoma. Specifically, single-sample gene set enrichment analysis (ssGSEA) was performed comparing the following different

conditions: amoeboid A375M2 melanoma cells, amoeboid A375M2 melanoma cells treated with ROCK1/2 inhibitors (ROCKi) or blebbistatin, a direct Myosin II inhibitor and A375P melanoma cells with lower Myosin II activity. The Wnt and TGFβ signaling were the most significant enriched network. WNT11 knockdown led to the decrease of Myosin II activity and a more mesenchymal-like cell shape. WNT11 depletion also result in increased adhesion of WM1361 cells to keratinocytes and reduced invasion through type 1 collagen matrices. The receptor FZD7 and its co-receptor RYK of WNT11 were both consistently increased in metastatic melanomas [249].

EphA2 signaling and its role in melanoma metastasis

The Ephs constitute the largest family of receptor tyrosine kinases (RTKs) [250-252]. They can be classified in two groups, EphA and EphB, according to the binding affinity for two different ligands, Ephrin-A and Ephrin-B [253-255]. Thus far, a total 16 Eph members have been identified in animals including EphA (1-10) and EphB (1-6), with EphA9 and EphB5 being only found in birds [255-257]. Members of the Eph family play a vital role during embryonic development in the boundary formation of tissues, remodeling of bone, cell migration, axonal guidance and organization for vascular system [258-262].

EphA2 was first identified in 1990 through the investigation of highly conserved regions of protein tyrosine kinases in cDNA libraries of the human epithelial HeLa cell line [263]. EphA2 is a 130 kDa Type-1 transmembrane glycoprotein receptor with 976 amino acid residues [264, 265]. The structure of EphA2 consists of several distinctive domains for signal transduction [259, 262, 266, 267]. The extracellular domain comprises a ligand binding domain, which connects with two fibronectin III-type repeats through a cysteine-rich domain [255, 268]. This part regulates the responses to the binding of ligands [255, 268]. The intracellular domain harbors the intrinsic enzymatic activity which consists of the following domains: a juxtamembrane region, followed by a kinase domain, a SAM domain and a PDZ domain-binding motif [269, 270]. The phosphorylation of the tyrosine residues on both the juxtamembrane region and kinase domain activate the

signaling transduction by interacting with other signaling proteins [269, 270]. Receptor dimerization is regulated by a SAM domain [270-272]. Protein-protein interactions are mediated by the SAM and PDZ domains [273]. There is evidence that EphA2 plays a significant role in the regulation of many key cellular processes in mammalian development [259, 262]. For example, these are the major functions in which they have been implicated:

1) Expression and colocalization of EphA2 and EphA5 in similar regions have been identified in early lens development. EphA2 expression has been found not only in the lens epithelium but also the lens fiber region, as well as the junction regions between the lens fibers and epithelium at various developmental stages [259, 274, 275]. EphA2 mutation or impaired function were highly correlated with cataract formation in the eye [276].

2) The expression of EphA2 is markedly increased during the development of the kidney [277]. It has been shown that the process of branching morphogenesis of Madin-Darby Canine Kidney (MDCK) cells is under the regulation of EphA2. In this context, EphA2 activation led to RhoA inactivaton and subsequent dephosphorylation of Thr-567 of Ezrin, which is a linker that connects plasma membrane and actin cytoskeleton, resulting in the cell shape change (from flat to columnar shape) [278].

3) EphA2 signaling is critical for the initiation of bone remodeling, particularly the stimulation of bone resorption [279]. And simultaneously, osteoblastogenesis is repressed by this signaling as well [280].

4) During the branching morphogenesis of the mammary gland, expression of EphA2 plays a critical role [281]. The proliferation and branching of the mammary epithelium is known to be inhibited when EphA2 function is blocked [282].

5) EphA2 expression has been detected during the growth and formation of the otic placode (which develops in the vertebrate inner ear). Currently, its exact function remains unclear [283].

Besides the key functions of EphA2 in normal cell processes and development, there is good evidence implicating abnormal expression of EphA2 in cancer, particularly colorectal, ovarian,

lung and prostate cancers [284-287]. Under physiological conditions, EphA2 receptor signaling is driven through Ephrin-Eph ligand binding between ligand and receptors at the cell surface of adjacent cells that relies on cell-cell contact and cell-cell interaction [257, 288-290]. Different from the conventional soluble factors, these ligands exhibited functions in membrane-bound form and also suggested that the activation of receptor needs the direct cell-to-cell contact [257, 291]. The membrane attachment plays a key role in ligand aggregation, which is necessary for receptor activation [291]. Chen et al. also showed that spatially modulated ephrinA1:EphA2 signaling promotes cell motility through regulation of contractility and focal adhesions [288]. Canonical EphA2 signaling involves tyrosine autophosphorylation at multiple residues including Tyr587, Tyr593, Tyr734, and Tyr771 on the EphA2 cytoplasmic domain [292].

In addition to these interactions, there is also evidence of other mechanisms of EphA2 signaling which are referred to as non-canonical signaling [293-296]. This noncanonical signaling is largely ligand independent and can involve phosphorylation of EphA2 at S897 [293, 297]. The molecular regulation of Ser-897 phosphorylation on EphA2 was first reported in glioma in 2009 [298] and can be induced by AKT activated by serum stimulation or growth factors [298]. The colocalization of EphA2 and phospho-Akt in glioma cell lines was also validated by immunofluorescence staining [298]. Furthermore, it has been demonstrated that the EphA2 S897 phosphorylation and Akt S473 phosphorylation were co-localized in human glioma specimens [298].

All the above evidence suggested that this non-canonical pathway involves phosphorylation of EphA2 by AKT and serves to reverse the function of EphA2, promoting cancer cell survival, proliferation, metastasis as well as regulation of acquired drug resistance and maintenance of a cancer stem cell phenotype [293, 298]. This contrasts with classical EphA2-Ephrin A1 signaling that reduces AKT signaling, cell motility and cell growth [299-302].

Besides the catalyzation by AKT, a number of groups have investigated the upstream kinase responsible for phosphorylation of EphA2 at S897. Some reports have identified downstream MAPK pathway mediators such as p90 ribosomal S6 kinases (RSK), mainly RSK1 and RSK2,

directly lead to EphA2 S897 phosphorylation. The RSK–EphA2 signaling regulates cell migration and invasion in metastatic breast cancer cells [303]. In addition, the EphA2 S897 phosphorylation was induced by protein kinase A (PKA) in forskolin-stimulated prostate cancer cells [297]. Other work has focused on non-small cell lung cancer (NSCLC) and showed treatment with the RSK inhibitor BI-D1870 to inhibit phosphorylation of S897 EphA2 in a time-dependent manner [304]. Furthermore, the MEK Inhibitor PD0325901 was noted to inhibit the phosphorylation of both RSK and EphA2 S897 [304].

High expression of EphA2 receptor has been found in many cancers, with its expression being correlated with metastatic potential and tumor progression [265, 295, 305, 306]. One cancer type known to express EphA2 is human glioblastoma (hGBMs) [307]. The mRNA expression level of EphA2 is dramatically higher in the hGBMs compared to normal brain tissues and low-grade gliomas. Furthermore, the EphA2 mRNA and protein levels has been detected with 2 to 300-fold higher in a subpopulation of hGBM cells, called tumor-propagating cells (TPCs), compared to their original hGBM tissue. The TPCs have been identified in a number of different solid tumors such as breast cancer, colon cancer and leukemia [308-310], and are characterized by stem-like features such as self-renewal, initialing and potential differentiation [311, 312]. However, once TPCs have differentiated and lost their stemness, EphA2 expression was significantly downregulated [313]. These findings are highly suggestive of a role for EphA2 in the stem-like state of TPCs. In agreement with this idea, the fluorescence-activated cell sorting (FACS) of isolated hGBM cells based upon expression levels of EphA2 have demonstrated the fraction with high level of EphA2 to be more clonogenic than those with low EphA2 expression. Implantation of these cells into mice show high EphA2 expression to be associated a shorter survival rate (median 4 months) than those with low levels of EphA2 cells (median 7 months) [307]. In glioma cell lines and primary glioma cultures, EphA2 was strongly downregulated by treatment of ephrin-A1 through receptor internalization [314, 315]. Furthermore, use of the ephrinA1-Fc fusion protein also downregulates EphA2 levels in hGBM TPCs but only has limited effects on EphA2

expression at the hGBM periphery, which is less tumorigenic. Treatment with the fusion protein also caused the TPCs to lose stem-like features such as self-renewal and to undergo astroglial differentiation [307]. These studies further suggested that EphA2 is important for maintaining the stemness of TPCs, a finding confirmed by siRNA knockdown of EphA2 in TPCs [307]. The potential inhibitory mechanism of EphA2 downregulation upon TPC function was caused by increased ERK phosphorylation as well as moderate Akt and FAK activation [316]. Significantly, the inhibition of ERK partially restored the clonogenicity in TPCs after EphA2 knockdown [316].

The phosphorylation of EphA2 at Serine 897 promotes oncogenic activity in cancer cells, and these effects are largely independent of EphA2 binding to its ligand EphrinA1 [298]. A role for S897 phosphorylaion of EphA2 was identified in hGBM TPCs, compared to non-TPCs. The effects of the ephrinA1-Fc fusion protein in hGBM were investigated in preclinical models with treatment being given 1) before the transplantation of hGBM TPCs (cell culture in treatment of ephrinA1-Fc); 2) just after the transplantation; 3) treatment until the growth of detectable tumors. Compared to the control group of hGBM TPCs only, all the three groups receiving the ephrinA1-Fc treatment had smaller tumor sizes and a better overall survival. Similarly, the suppression of tumor growth *in vivo* was also observed after the knockdown of EphA2 by siRNA in hGBM TPCs. In sum, this work identified EphA2 as a potential therapeutic target in hGBMs and showed that ephrinA1-Fc had impressive levels of efficacy [307].

Miao et al. also reported that EphA2-AKT crosstalk promotes the invasion of glioma stem cells (GSCs) *in vivo* and regulates stemness [316]. GSCs are highly involved in tumor proliferation, acquired resistance and have high invasive capacity [317-323]. In this system, the Akt-EphA2 signaling axis was maintained in the absence of ephrin-A ligands and was then inhibited following ligand stimulation *in vitro* [298, 324].

Multiple other cancers have been found to rely upon non-canonical EphA2 signaling. Recent work has identified a role for S897 EphA2 signaling in the invasive phenotype in NSCLC that occurs following VEGFR inhibitor therapy [304]. The finding that VEGFR inhibition upregulates an

EphA2-driven aggressive phenotype in NSCLC, which potentially increases metastatic potential, is thought to underlie the lack of efficacy of anti-angiogenic therapies in this cancer [304]. The authors showed that knockdown of VEGFR2 in the NSCLC cell line H441 led to the aggressive phenotype, and increased invasion into collagen. Similarly, after treatment of ZD6474-the potent dual inhibitor of VEGFR2, the NSCLC cell lines H441 and H1975 displayed a stronger invasion ability than non-treatment groups [304]. To further validate that these findings were due to the inhibition of VEGFR2 *in vivo*, a mutation V916M on VEGFR2 was introduced into H441 cell line which blocked the binding of inhibitor ZD6474 to VEGFR2. After injection of these cells into nude mice, the number of lung metastases observed were much higher in the control groups compared to the groups with modified cell line. Immunoprecipitation of VEGFR2 and EphA2 in H441 and H1975 cell lines revealed the two receptors to form a complex [304]. However, after treatment with the VEGFR2 inhibitor, the association of the VEGFR2/EphA2 complex decreased by Proximity Ligation Assays (PLAs) [304]. Further investigation showed that shRNA knockdown of EphA2 blocked cancer cell invasion after treatment with ZD6474. Similar effects were also seen *in vivo* with the number of lung metastases dramatically decreasing in mice injected with H441 EphA2 knockdown cells compared to control ones treated with ZD6474. These results strongly supported that EphA2 is a key mediator of the invasive phenotype in response of VEGFR2-targeted therapy [304].

Following the observation that non-canonical EphA2 signaling (S897 phosphorylation) drove the oncogenic behavior of hGBMs, there were attempts to explore this in other cancer types including NSCLC [298, 316]. It was noted that introduction of the inactive (S897A) EphA2 mutant into NSLCS cell lines (H441, H1975) significantly decreased their ability to invade in *in vitro* through invasion assays. The injection of these S897A EphA2 mutant cell lines into lungs of mice, was associated with a reduced metastatic burden compared to normal EphA2 groups [304].

Other studies have shown that EphA2 phosphorylation at S897 was highly correlated with the aggressiveness of Ewing sarcoma (ES) tumors [325]. ES is the second most common bone

malignancy affecting children and young adults [325, 326]. In this instance, the ligand independent EphA2 signaling is driven by a regulatory feedback loop involving the ERK signaling pathway [325]. In colorectal cancer (CRC), high levels of EphA2 expression are strongly associated with the high expression of stem cell markers CD44 and Lgr5 from colorectal tumors [295]. This indicates that EphA2 may be crucial in colorectal tumor progression, with EphA2 downregulation being associated with the decrease of cell migration and invasion [295].

Our lab also has found that ligand-independent EphA2 signaling led to adoption of a targeted therapy-mediated metastatic melanoma phenotype [327]. Our comprehensive phospho-proteomics identified the EphA2 and its phosphorylation at S897 were highly involved in the BRAF inhibitor resistance by comparing the naïve with resistant melanoma cell lines. The resistant cells show much higher expression of EphA2 and its phosphorylation than the paired naïve cells. Moreover, in patient specimens, the metastatic lesions had more total and phosphorylation of EphA2 than primary lesions by immunohistochemical staining. This invasive phenotype mediated by ligand independent EphA2 signaling was dependent on AKT and reversible by PI3K and AKT inhibition [327].

Similarly, in lung cancer, patients developed resistance to EGFR tyrosine kinase inhibitors (TKIs) eventually [285]. The abnormal overexpression of EphA2 was detected in the EGFR TKI resistant tumor cells. Inhibition of EphA2 by the small molecule inhibitor, ALW-II-41-27, led to the decrease of survival and proliferation in erlotinib (an inhibitor of EGFR) resistant tumor cells. Furthermore, the ALW-II-41-27 also inhibited tumor growth *in vivo.* Above all, EphA2 played a critical role in maintaining the cell survival and proliferation in response to the treatment of TKIs and would be the potential therapeutic target in TKI resistant tumors [285].

In addition, ligand independent EphA2 activation by arachidonic acid induced the metastatic behavior in prostate cancer cells [328]. It was noted that ligand independent EphA2 stimulated by arachidonic acid further promoted prostate cancer cell invasion and that EphA2 expression was higher in invasive cell lines compared to weakly invasive cell lines [328].

Models of melanoma

The past 10 years have seen major improvements in the treatment of advanced melanoma, leading in the reduction in melanoma deaths over the past 3 years. These improvements in survival have come from the development of targeted therapies such as BRAF inhibitors and the BRAF-MEK inhibitor combination and new immunotherapies like anti-PD1 and anti-CTLA-4. Recent reports indicated that treatment with dabrafenib plus trametinib (211 in the COMBI-d trial and 352 in the COMBI-v trial) was associated with overall survival rates of 37% at 4 years and 34% at 5 years. An objective response to this treatment occurred in 383 of 563 patients (68%), with a complete response in 109 (19%). Besides that, 5-year follow-up of patients treated with nivolumab and ipilimumab showed that overall survival in the group with the nivolumab-plus-ipilimumab combination was much longer (60.0 months) than single agent nivolumab (36.9 months) and ipilimumab groups (19.9 months). The rate of objective response among patients was 58%, 45% and 19% in the combined group, nivolumab group and ipilimumab group, respectively. The rate of complete response was 22%, 19%, and 6%, respectively [158, 169, 170]. Despite these successes, not all patients respond to immune checkpoint inhibitor therapy, and only 50% of patients can benefit from targeted therapies. The development of new melanoma therapies is predicated upon an in-depth understanding of the molecular mechanisms of tumor initiation, progression and metastasis development. Much of this knowledge has come from the development of preclinical models of melanoma, which have allowed the genetic drivers identified from next generation sequencing (NGS) studies to be validated along the entire continuum of cancer development [329].

A number of different animal models of melanoma have been developed including the mouse, *Xiphophorus* (Zebrafish), opossum and guinea pig. The most successful and widest used model has been the mouse, partially because of the relevance and similarity of mouse genetics to human. These syngeneic models have been supplemented with xenograft transplantation models, in

which human melanoma cells are grown in immune compromised mice. Of note, the human tumor xenograft models proved instrumental in the development and testing of targeted therapies such as the BRAF and MEK inhibitors. I will next review all the model systems in turn, outlining the strengths and weaknesses of each [330].

Cell line xenografts

These models use subcutaneously implanted human melanoma cell lines into immunocompromised mice which lack an adaptive immune system. This model system has many benefits including ease of use and the wide availability of multiple melanoma cell lines, often with different mutational profiles, varying levels of metastatic potential and drug sensitivity. Interestingly, not all melanoma cell lines derived from clinical metastases will form new metastases from primary tumors in xenograft models. As one example, the BRAF mutant melanoma cell lines WM164 and WM793 – which are derived from clinical metastases will only form new metastases in mice followed repeated passage through nude mice following tail vein injection. These results strongly suggest that these aggressive melanoma cells comprise multiple sub-populations of cells with only some of these able to form new metastases *in vivo*. For the cell lines which are not capable to spontaneously form the metastasis through subcutaneously injection in mice, the alternative strategy is experimental metastases from cancer cells directly injected into the tail-vein or via intracardiac injection. The method is very common and is convenient for the study of metastases into the lung, liver and even other organs or tissues. The weakness of this method is that it does not mimic the entire metastatic process from primary tumor to distant disease because the cancer cells are introduced directly into the bloodstream [331]. Another advantage of human cancer cell lines is that they tend to be genetically characterized, so cell lines can be selected with the desired mutational profiles.

This model system also has multiple disadvantages. First, the cells are often kept in culture for multiple passages and may drift from the original genetic state of the tumor. Establishment of cells in culture also introduces some selection bias, potentially reducing the heterogeneity of the tumors

that grow *in vivo*. In addition, it is likely that injection of millions of cancer cells does not mimic the natural process of primary tumor growth in which the cancer co-evolves with host cells. Due to the above reasons, the results of clinical trials based on the cell line xenograft models are often poorly predictive of outcome [331].

Patient-derived tumor xenografts

One strategy to overcome the problems associated with cell line models is the use of patient-derived xenografts (PDXs). This approach relies upon the growth and expansion of patient tumors in mice. As these tumors are never adapted to culture and are passage through mice, some of the selection bias associated with the use of cell lines is eliminated and the heterogeneity is maintained. Sequencing studies have shown that PDX models maintain the genetic profiles of the original patient tumors even after passage through multiple times through mice. A number of patient-derived treatment xenograft (PDTX) models have also been established in which tumors are derived from individuals failing on specific therapies (e.g. targeted therapy or immunotherapy). They have proven to be highly useful for studying drug resistance and identifying potential therapies to overcome resistance. Combination of these models with advanced genetic profiling allows for significant potential in developing better personalized therapies [331]. Although offering some advantages over cell line xenograft models, PDX models also have some drawbacks including a long time to tumor formation *in vivo,* no intact immune response and difficulties in performing modifications [331].

Syngeneic transplantation models

A lack of an immune response is a major drawback for all the human cancer cell xenograft models. One way to address this weakness is using mouse cancer cell lines grown as isografts in immune competent mice. These syngeneic transplantation models allow for the in-depth investigation of the interaction between melanoma cells with T-cells and B-cells of the adaptive immune system (a critical component of the microenvironment of human melanoma). For many years, the most widely used cell line was the B16 cell line, a mouse melanoma formed through chemical

carcinogenesis protocols in C57BL/6J mice. At this time, multiple B16 cell lines exist with different subclones showing distinct proliferation, migration and invasive phenotypes. Among them, the B16F1 and B16F10 variants are well-characterized subclones generated from *in vivo* passage experiments. The phenotype of these sub-clones is quite different, as detailed below. The B16F1 is much less aggressive with low potential for metastasis, while the B16F10 shows a stronger capacity for metastasis. The slow and moderate features of B16F1 allows for a more thorough investigation of primary tumor growth pattern while the high metastatic features of B16F10 allow us to explore the metastasis to distant organs *in vivo* like lung [331].

The B16 cells are known to have low expression of major histocompatibility complex class I (MHC I) which makes them less immunogenic due to poor recognition by cytotoxic CD8+ T-cells. However, the expression of some melanoma-associated antigens such as gp100 and tyrosinase related protein 2 (TRP2) are found to be very high in B16 cells and these represent potential immunotherapeutic targets. For example, mice vaccinated against the TRP-2 epitope can induce an immune response that blocks the growth of aggressive B16F10 cells, preventing the formation of lung metastases. Drawbacks associated with the B16F10 syngeneic transplantation model include the genetic background, which is not analogous to human melanoma, and the fact that mouse proteins are not always the same as their human counterparts. The recent years have seen the development of mouse melanoma cell lines from genetically engineered mouse (GEM) models that have superseded the B16 (see future discussion of GEM models) [331].

Genetically engineered mouse models

Genetically engineered mouse models (GEMMs) have been widely used to understand the genetic alterations which affects the melanoma tumor initiation, progression and metastasis. These models are more faithful to the process of melanoma development and allow study of tumor biology in an immune-competent setting. A number of melanoma GEMMs have been developed that harboring the same genetic changes known to drive melanoma tumor generation in humans. For example, the most frequent driver mutations in human melanoma BRAF and NRAS can be

induced in mouse skin melanocytes with Tamoxifen-inducible Cre allele driven by the Tyrosinase promoter. Using similar methods, the major tumor suppressors in melanoma, PTEN and CDKN2A can be specifically knocked out in melanocytes. Combinations of these alleles leads to melanoma development with varying penetrance and latency in mouse strains [331].

Because GEMMs harbor most of the major genetic changes found in human melanoma such as BRAF V600E, NRAS Q61R, PTEN loss and CDKN2A deletion, the models provide an excellent base to investigate the other potential candidate genes which might contribute to the melanoma formation. For example, the genes Dnmt3b, Akt, and Trp53 have been explored for melanoma progression in the GEMMs [332-335].

Although useful, traditional mouse modeling approaches have numerous drawbacks including high costs and the large time commitment required. One alternative method that overcomes both problems is the generation of embryonic stem cell-genetically engineered mouse models (ESC-GEMMs). This new approach is based upon the expression of the genes of interest in blastocyst-injected embryonic stem (ES) cells and can be used to generate new mice within 8 weeks after the modification of GEMM-derived ESCs *in vitro.* The alleles of the target gene of interest are expressed in the ESC-derived chimera tissues, thus enabling the use of chimeras as experimental mice. The use of ESC-GEMMs has been confirmed to be of great value in many cancers including breast, lung, and pancreatic cancers [336]. In melanoma, ESC-GEMMs several typical alleles are expressed, including melanocyte-specific, 4-Hydroxytamoxifen (4OHT)-inducible Cre recombinase allele (Tyr-CreERt2), a Cre-inducible Tet reverse transactivator (CAGs-LSL-rtTA3), and a homing cassette in the col1A1 locus (CHC) in ESCs for efficient genomic integration of expression constructs via recombination-mediated cassette exchange (RMCE). This allele combination enables Cre-inducible recombination of driver alleles that are activated by application of 4-OHT and Cre- and Doxycycline (Dox)-inducible regulation of genes of interest activated in melanocytes through a Dox diet given to the chimeras [336].

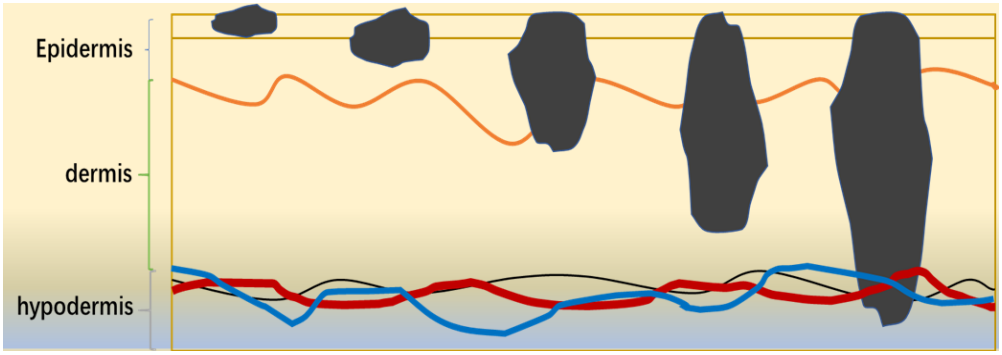

Figure 1. Skin architecture with melanoma. The skin consist of three layers as follows: epidermis, dermis and hypodermis. The squamous cells are in the superficial layer of epidermis. The basal cells can be found in the deep basal layers of epidermis. Melanoma raised from pigment producing melanocytes which can be found in the bottom layer of epidermis.

RESEARCH FOCUS

In this thesis, we are addressing the following questions:

1) To understand how melanoma is reprogrammed in response to the targeted therapy.
2) To determine how this shift and change contribute to the enhanced metastasis.
3) To investigate the major signaling that drives the phenotype switch.
4) To explore how the potential of these findings contribute to develop a novel and more effective therapy.

MATERIALS AND METHODS

Cell culture and generation of BRAF/MEK inhibitor resistance

The parental *BRAF(V600E)*-mutant human melanoma cell lines WM164, 1205Lu and SK-MEL-28 were kindly provided by Dr. Meenhard Herlyn (The Wistar Institute, Philadelphia, PA). The dual BRAF and MEK inhibitor–resistant (RR) cell lines 1205lu, SK-MEL-28 were established by chronic treatment with 1 μmol/L each vemurafenib and selumetinib for more than 6 months in our lab [327]. The Human Umbilical Vein Endothelial Cells (HUVEC) was purchased from Lonza. All the melanoma cells were cultured in RPMI 1640 with 5% FBS. The HUVECs was cultured in Endothelial Cell Growth Medium purchased from Sigma-Aldrich. HDAC8-modified cells were described in Emmons et al. (2019) [337].

3D cell culture on collagen

Type I Collagen Solution, 3 mg/ml (Bovine) was purchased from Advanced BioMatrix. The collagen solution was gently mixed with cold 10X PBS. The pH was adjusted to 7.0 after mixture by adding the sterile 0.1 M NaOH gradually. Then the 6-well plate was coated with the collagen/PBS mixture and incubated at 37°C for 2 hours to form the gel base.

Growth Inhibition Assay

4,000 cells were seeded in each well of a 96-well plate overnight. Each cell in single well was treated with vehicle (dimethyl sulfoxide, DMSO) and media containing inhibitors. After 3-day incubation, the Alamar Blue reagent was added to each well for measurement according to manufacturer's protocol (Invitrogen).

Colony Formation Assay

2×10^4 cells were plated in each well of a 6-well plate for overnight culture. Media with vehicle dimethyl sulfoxide (DMSO) or inhibitors were added next day. The medium was changed twice per week. After 4 weeks, the cells were counted after staining by crystal violet solution.

Inhibitors

Vemurafenib (PLX4032), selumetinib (AZD6244) and GDC-0941 were purchased from Selleck Chemicals.

Phosphoproteomic Analysis: Sample Processing

Mutant WM164 S897A and S897E cell lines were cultured in 10 x 15 cm tissue culture dishes. Each cell culture dish was washed with 10 mL ice-cold PBS with 1 mmol/L orthovanadate (Sigma Aldrich) once the cell confluence reached 70-80%. The cell lysis was processed by protein reduction, alkylation and trypsin digestion sequentially. After purification, the tryptic peptides were lyophilized and then enriched by immunoprecipitation with immobilized antibody p-Tyr-100 (Cell Signaling Technology). Flow-through from the immunoprecipitation was then further enriched for p-serine and p-threonine by SCX/IMAC enrichment approach. The enriched fractions were subjected to LC/MS-MS. The SEUQEST and MASCOT database were used to identify the phosphoproteins. In order to quantify intensities of the relative phospho-signal, MaxQuant was applied to measure the label-free protein of the mass spectrometry data. The analysis with GeneGo and KEGG database was performed to identify the highly correlated pathways.

Plasmid Construction and Transfection

The mutant S897A and S897E, and the mutant active Cdc42 and Rac1 plasmids were kindly provided from Dr. Elena Pasquale (Cancer Center, Sanford Burnham Prebys Medical Discovery

Institute, La Jolla, California). The pLenti CMV GFP plasmid was a gift from Dr. Lixin Wan (Moffit Cancer Center, Tampa, FL). Lentiviral constructs were co-transfected with essential plasmids for virus packaging into 293T cells. The media containing virus were collected and filtered for infection of targeted cell lines.

Western Blotting

The isolation of proteins and immunoblotting were performed as described in Fedorenko et al. (2014) [156]. The primary antibodies for EphA2, p-EphA2(S897), CDC42, RAC1, MLC2, p-MLC2(S19), GRB2 were purchased from Cell Signaling Technology. The antibody for GAPDH for loading control was from Sigma Aldrich.

RNA Interference

shRNA Lentiviral Particle targeting the 3'-UTR of endogenous EphA2 was purchased from Sigma Aldrich. siRNA targeting Cdc42 was purchased from Santa Cruz Biotechnology. Transfection was performed as described on the siRNA Transfection Protocol provided by Santa Cruz Biotechnology, Inc.

Transendothelial Cell Migration Assays

Human Umbilical Vein Endothelial Cells (HUVEC) were seeded into Transwell inserts to form the confluent monolayer overnight. DiI-labeled (a lipophilic membrane stain) melanoma cell lines were plated on the top of the HUVEC monolayer. After 2-4 hours migration, non-migrating melanoma cells were removed from the inside of the inserts by careful swabbing. The DiI-labeled migrating cells were imaged by EVOS imaging system and quantified by ImageJ.

Matrigel Invasion Assays

Cells were plated onto the bottoms of the inverted Transwell inserts which were coated with Matrigel (BD). After 24-48 hours invasion into the Matrigel, the cells were fixed and stained by phalloidin-AF594. To quantify the level of invasion, the fixed and stained cells were imaged by a Zeiss confocal microscope (20×) at 0 μm with 0.5 μm image slices taken throughout the distance of invasion.

Vascular Permeability Assays

This experiment was conducted by using the *In Vitro* Vascular Permeability Assay kit according to the manufacturer's guidelines (Sigma-Aldrich). 200,000 HUVECs were plated into the insert of the 24-well plate for overnight culture until confluent monolayer. 100,000 cells of each mutant WM164 melanoma cells (EphA2 S897A and EphA2 S897E) were seeded on the top of the monolayer for 24 hours co-culture. The media was removed after co-culture and the dextran-blue solution was carefully added into the inserts for 10-20 mins. The fluorescence from each well containing the dextran-blue was read with 485 nm and 535 nm (excitation and emission), respectively.

Shear Stress Assay

10,000 WM164 melanoma cells from each mutant (EphA2 S897A, EphA2 S897E, Cdc42 and Rac1) were plated on the u-slide chamber from Ibidi. The cells were cultured in media at 10 dyne/cm^2 fluid shear stress (FSS) by the Ibidi pump system. After 24 hours under shear stress, the cells were stained with calcein-AM and propidium iodide (PI) to identify live and dead cells. The images of the u-slide chambers were taken by EVOS imaging system. The green and red cells were quantified under each image with the same magnification from at least 3 different areas of the u-slide.

Adhesion Assay

10,000 HUVECs were seeded on the u-slide chamber from Ibidi to form a confluent monolayer overnight under static conditions. 4,000 GFP-tagged WM164 melanoma cells from each mutant (EphA2 S897A, EphA2 S897E, Cdc42 and Rac1) were plated on the top of the monolayer next day. After seeding the melanoma cells, the shear stress was set immediately at 10 dyne/cm^2 FSS through the Ibidi pump system. 30 mins later, the u-slide chambers were used for imaging and quantification of the GFP-tagged melanoma cells by EVOS imaging system.

CDC42 Activity Assay

This assay was performed by using the Cdc42 Activation Assay Kit according to the manufacturer's instructions (Abcam). Briefly, the activated form of Cdc42 was selectively isolated and pulled down by the PAK1 PBD Agarose beads from the cell lysates. Subsequently, the activated form of Cdc42 precipitated with the beads was detected by Western Blot.

RhoA Activity Assay

This assay was performed by using the RhoA Activation Assay Kit according to the manufacturer's instructions (Abcam). Briefly, the activated RhoA was selectively isolated and pulled down by the Rhotekin RBD Agarose beads from the cell lysates. Subsequently, the activated RhoA precipitated with the beads was detected by Western Blot.

In Vivo Lung Retention Assay

All animal work was conducted in accordance with the Institutional Animal Care and Use Committee guidelines. GFP-tagged WM164 S897A, S897E, CDC42 and RAC1 cells were cultured in 4 x 15 cm tissue culture dishes until 80% confluence. After collecting and counting the cells in PBS, the 8-week-old NSG mice (JAX) were injected with 8 x 10^5 cells in 100ul PBS via tail vein (5 mice per group). After that, mice were euthanized by CO_2 asphyxiation at two different

time points, 10 and 24 hours, and the whole lungs were collected. After fixation in 4% formaldehyde/PBS, the lungs were imaged through a Zeiss confocal microscope under a 20X objective with pinhole diameter set to 1 airy unit. Images were taken at a 512 × 512 resolution with randomly selected 5 fields per lung to detect and quantify the GFP-tagged cells arrested in lungs.

In Vivo Metastasis Study

All animal work was performed according to the Institutional Animal Care and Use Committee guidelines. WM164 S897A and S897E cells were cultured in 5 x 15 cm tissue culture dishes until 80% confluence. The NSG mice (JAX), aged between 6-8 weeks, were injected with 1×10^6 cells in 100ul PBS into the left ventricle (10 mice per group). 4 weeks after intracardiac injection, mice were euthanized by CO_2 asphyxiation and the main organs (brains, livers and lungs) were collected. After fixation in 4% formaldehyde/PBS, the main organs brains, livers and lungs were analyzed by IHC to identify potential metastatic lesions by H&E staining and staining for SOX10 and pAKT.

Genetically Engineered Mouse Models (GEMMs)

All animal work was performed according to the Institutional Animal Care and Use Committee guidelines. Transgenic mouse models of melanoma were generated by using a system based upon blastocyst-injected embryonic stem (ES) cells. This approach relies on GEMM-derived ESCs that are modified *in vitro* and then used to generate chimeras by blastocyst injection. We create four plasmids including EphA2 S897A and S897E, HDAC8 as well as GFP as control. These EphA2 isoforms were then introduced into an established genetically engineered mouse model harboring BRAFV600E, heterozygous PTEN deletion. Tumors were induced by 4-OHT application on the back of the mice after shaving. After tumor initiation and careful observation

for >1 year, mice were sacrificed and the brains, lungs, livers and other major organs were collected and fixed to analyze by IHC.

Cell Recovery/Viability Assay In Vivo

All animal work was performed according to the Institutional Animal Care and Use Committee guidelines. The intracardiac injections of the GFP-tagged WM164 EphA2 S897A and S897E cell lines were performed in NSG mice. The purpose of the study was to determine if mutant EphA2 increased survival of melanoma cells in the general circulation. Three experimental groups were used: S897A, S897E and S897E+PI3K inhibitor. Following cell injection, blood was harvested after 1 hour, 4 hours, 24 hours, 72 hours and 7 days. After the collection of the blood, viable melanoma cells were enumerated using flow cytometry.

Statistical Analysis

Data were analyzed by mean values through at least 3 repeats ± SEM. GraphPad Prism 7 software was used to calculate and determine the statistical significance among all the groups or conditions by performing the two-tailed unpaired t-test. And the p-values were described as follows: *$p \leq 0.05$, ** $p \leq 0.01$, *** $p \leq 0.001$, **** $p \leq 0.0001$.

RESULTS

An amoeboid phenotype in melanoma cells driven by non-canonical EphA2 signaling revealed through comprehensive proteomics.

With the aim of exploring the EphA2 function, two pairs of stable melanoma cell lines (WM164 and SK-MEL-28) expressing EphA2 mutants were generated. The EphA2-S897E mutant mimicked the phosphorylation at S897 which is constitutively activated. We also generated its counterpart, the inactivated EphA2-S897A mutant form, which cannot be phosphorylated. There was no significant difference in growth rate between the paired mutant cells (**Figure 2**). Next, multiple mass spectrometry-based proteomic platforms were employed for protein identification and quantification between the two WM164 mutant cell lines (EphA2 S897E VS EphA2 S897A). This comprehensive proteomics included the following aspects: 1) the total proteome 2) peptides phosphorylated on tyrosine residues 3) peptides phosphorylated on serine/threonine residues and 4) immunoprecipitations of the FLAG tag in the EphA2-S897E and EphA2-S897A mutants (**Figure 3**). Significant expression differences in proteins and phospho-proteins between the mutant WM164 cells expressing EphA2-S897E and EphA2-S897A were assessed. Potential targets were visualized in Volcano plots (**Figure 4**). Pathway analysis of these significantly upregulated and downregulated proteins by GeneGo suggested that EphA2-S897E was highly associated with a number of proteins involving cell adhesion, cell cycle, cell motility and cytoskeletal remodeling (**Figure 5 and 6**). These data indicated that EphA2 phosphorylation at S897 could play an important role in pathways and functions of regulating the axonal guidance, intermediate filaments and microtubules (**Figure 5 and 6**).

As these signaling pathways are highly correlated with cell motility and cytoskeletal organization, it is possible that EphA2-S897E could promote morphological transformation of the melanoma cells. Another consistent finding from the mapping of our proteomics data was the identification of a novel mesenchymal-to-amoeboid transition (MAT) phenotype (**Figure 7**). Of interest, we noticed the decrease in tyrosine phosphorylation of ACK1 which is known to inhibit the GTPase activity of Cdc42. At the same time, we noted increased expression of DOCK10, which is known to serve as a Guanine nucleotide-exchange factor (GEF) that can activate Cdc42 [245, 247]. On the other hand, the inhibition of Rac1, another member of the Rho-family GTPases, was also identified. Additional findings included a decrease in the total expression and tyrosine phosphorylation of FAK [338], which is known to facilitate the activation of Rac1 (**Figure 7**). Altogether, the proteomics data strongly suggested that EphA2-S897E led to the adoption of an amoeboid phenotype that could result from a signaling switch from Rac1 to Cdc42.

In order to validate our predictions from the proteomic analysis, we performed 3D culture on collagen with both WM164 and SK-MEL-28 cell lines expressing EphA2 mutants. We observed that the EphA2-S897E was highly associated with the amoeboid phenotype, whereas the EphA2-S897A expressing cells showed a more mesenchymal state in both cell lines (**Figure 8 and 9**). It is known that MLC2 is a major MAT regulator through its regulation of actomyosin contractility [339]. In accordance with this, the increased phosphorylation of MLC2 at S19 was detected in both cell lines with expression of EphA2-S897E but not in those with EphA2-S897A (**Figure 10**). The knockdown of endogenous EphA2 expression by shRNA targeting 3'-UTR verified that the endogenous EphA2 level did not change the original phenotype in both cell lines expressing EphA2 mutants (**Figure 11 and 12**).

EphA2-S897E associated with the invasive phenotype in melanoma cell lines and is driven by the switch from Rac1 to Cdc42.

We noticed that the EphA2-S897E expressing cells showed increased invasive ability into the 3D Matrigel Matrix (**Figure 13 and 14**). It was also confirmed that the endogenous level of EphA2 did not affect the initial ability for invasion (**Figure 15**).

Our proteomics analysis suggested that Cdc42 activation was a potential mediator of cytoskeletal reorganization and the adoption of an amoeboid phenotype. We noted an increased binding of EphA2 to Cdc42 in EphA2-S897E cells following co-immunoprecipitation, whereas Rac1 showed an increased binding to EphA2 in the EphA2-S897A (**Figure 16**). Furthermore, increased expression of GTP-bound Cdc42 (activated form) was detected in EphA2-S897E cells compared to the EphA2-S897A cells. However, the GTP-bound Rac1 (activated form) showed the reversed expression in these paired cell lines (**Figure 17**). Taken together, the above data suggested that the phosphomimic S897E mutation led to the enhanced interaction of EphA2 with active Cdc42 and not Rac1. The increased expression of active RhoA was also confirmed in EphA2-S897E cells compared to EphA2-S897A cells, which again agreed with the signaling mapping from the proteomics data (**Figure 18**).

To further validate that the active Cdc42 but not Rac1 contributed to the MAT phenotype, and then promote the invasive ability in melanoma cells, we transfected constitutively activated mutants of Cdc42 and Rac1 into WM164 cell lines. It was demonstrated that the active Cdc42 led to the increased phosphorylation of MLC2, which in consistent with the amoeboid phenotype of WM164 cells expressing constitutively activated Cdc42 from 3D culture on collagen (**Figure 19 and 20**). Moreover, the WM164-Cdc42 cells displayed a stronger ability to invade into 3D Matrigel Matrix (**Figure 21**). In contrast with the above observation, the active Rac1 was correlated with the mesenchymal shape and decreased invasive ability (**Figure 20 and 21**).

The major functions of the active Cdc42 signaling in driving this invasive MAT phenotype were further demonstrated by siRNA knockdown and overexpression of Cdc42 in WM164 EphA2-

S897E and EphA2-S897A cell lines, respectively. After Cdc42 silencing in WM164 EphA2-S897E cells, they exhibited reduced phosphorylation of MLC2 (**Figure 22**), the reversed elongated shape from amoeboid state and less invasive ability into 3D Matrigel Matrix (**Figure 23 and 24**). Nevertheless, the introduction of Cdc42 into WM164 EphA2-S897A cells led to the amoeboid phenotype and improved invasive ability (**Figure 25 and 26**).

EphA2-S897E in melanoma cells enhanced the survival ability under shear stress and interaction with endothelial cells in adhesion and transmigration.

Successful metastatic dissemination is a multi-step process. To evaluate whether EphA2-S897E promoted the metastatic potential, we next focused on each individual step in the metastatic cascade. First, we tested the cell survival ability under shear stress to mimic the melanoma cells in the blood circulation. The cells were stained with calcein-AM (green) and propidium iodide (red) to identify live and dead cells after 24 hours circulating in the continuous unidirectional flow by the Ibidi automated perfusion pump system. Notably, more EphA2-S897E cells than EphA2-S897A cells survived and remained attached on the Ibidi chamber slide (**Figure 27**). We found EphA2-S897E to be associated with an increase in expression of multiple mediators of cell structure and membrane integrity (**Table 1**). We repeated the same shear stress experiment comparing WM164 cell lines expressing either constitutively active Cdc42 or Rac1. We noticed that more viable EphA2-Cdc42 cells were retained on the chamber slide compared to the EphA2-Rac1 cells (**Figure 28**).

Next, the surviving circulating cancer cells would be able to attach to the blood vessel and extravasate out of the endothelial layer. We then explored if EphA2-S897E contributed to this process and used GFP-tagged WM164 mutant cell lines in co-culture with endothelial cells. Under continuous unidirectional flow conditions (provided by Ibidi pump system), the EphA2-S897E cells presented stronger adhesion to the endothelial monolayer than EphA2-S897A cells (**Figure 29**). We also noted similar findings (e.g., faster and stronger adhesion to endothelial cells) in WM164

cells expressing active Cdc42 but not Rac1 (**Figure 30**). In addition, both the DiI-labeled EphA2-S897E and Cdc42 cells exhibited increased motile behavior in transmigration assay, in which melanoma cells were allowed to migrate through confluent endothelial monolayers, compared to their counterparts (**Figure 31 and 32**).

Finally, after co-culture of WM164 mutant cells on top of confluent endothelial cell monolayers, it was noted that EphA2-S897E led to the increased permeability of the endothelial cell monolayers (**Figure 33**). This suggested that this non-canonical EphA2 signaling in melanoma cells potentially enhanced the interaction with endothelial cells and that this then disrupted the integrity of the endothelial monolayers for further migration. A further analysis of our proteomic data supported these findings and demonstrated that introduction of EpA2-S897A was associated with suppression of multiple pathways involved in the metastatic cascade including transendothelial migration, N-cadherin signaling and αVβ3 integrin signaling (**Figure 34, Table 2**). By contrast, introduction of EphA2-S897E was associated with suppression of negative regulators of RhoA signaling and drivers of EMT (**Figure 35, Table 2**).

EphA2-S897E promoted the metastatic potential of melanoma cells in vivo.

We next investigated whether the invasive amoeboid phenotype driven by EphA2-S897E in melanoma cells led to increased metastatic potential *in vivo.* We carried out the lung retention assay in a xenograft model. GFP-tagged WM164 mutant cell lines were seeded into immunodeficient NSG mice through tail vein injection (**Figure 36**). 10 and 24 hours after injection, the lungs were collected and analyzed under the confocal microscopy. It was found that a significantly greater number of EphA2-S897E cells were retained in the lungs compared to the EphA2-S897A cells from both time points at 10 and 24 hours. Similarly, more Cdc42-expressing cells were able to arrest in the lungs than their Rac1 expressing counterparts (**Figure 37-40**). The clinical relevance of these findings was suggested by immunohistochemical analysis of lung metastasis resections from human melanoma patients, which showed EphA2-positive melanoma

cells interacting with endothelial cells lining the blood vessels in the lung parenchyma (**Figure 41**). These findings were consistent with our previous observation that the EphA2-S897E expression was significantly higher in metastatic lesions compared to the paired primaries in melanoma patient specimens [327].

Next, we carried out the intracardiac injection of either EphA2-S897E or EphA2-S897A cells in NSG mice. 4 weeks after injection, the major organs including brain, liver and lung were collected to analyze patterns of metastasis. Analysis of liver and lung samples by immunohistochemistry (H&E staining) showed no differences between the groups injected with EphA2-S897E and EphA2-S897A cells (**Figure 42**). Surprisingly, when we investigated brain samples, immunohistochemistry analysis showed that almost 90% mice injected with EphA2-S897E cells developed metastasis whereas less than 30% mice injected with EphA2-S897A cells found tumor burdens based on the SOX10 staining (**Figure 43**). These findings suggested that EphA2-S897E might preferentially promote the melanoma cells homing to the brain.

Development of transgenic mouse melanoma models of EphA2-driven tumor progression.

To investigate whether EphA2-S897E promoted melanoma formation and development, we generated an embryonic stem cell-based genetically engineered mouse model (ESC-GEMM). These genetically engineered mice harbor the background of Braf-V600E mutation and Pten heterozygous deletion in melanocytes, which mimic the prevalent driver mutations found in malignant melanoma. In addition to this we cloned the EphA2-S897E and EphA2-S897A mutants into dox-inducible targeting vectors for ESC-GEMM generation. The genes of interest were delivered into the mice through embryonic stem cell injection. The chimeras were first shaved on the back followed by administration of 25 mg/mL 4-Hydroxytamoxifen (4OHT) dissolved in DMSO on the shaved back skin on 2 consecutive days. 4OHT activates the background of Braf-V600E mutation and Pten heterozygous deletion. Mice were then fed chow containing 200 mg/kg doxycycline to continuously activate the target genes (EphA2-S897E and EphA2-S897A). Tumor

formation and development were carefully monitored. The Kaplan–Meier survival analysis suggested that the EphA2-S897E potentially induced tumor growth faster and that these tumors were more aggressive than EphA2-S897A (**Figure 44**). In addition, we also collected the major organs including brain, liver and lung for metastatic analysis at the end point from GEMM. However, we did not observe any apparent tumor possibly due to the short period of time.

PI3K/AKT potentially mediated this invasive amoeboid phenotype in EphA2-S897E cells and BRAF inhibitor resistant cell lines.

It was demonstrated that EphA2 S897 phosphorylation can be mediated by the PI3K/AKT pathway [327]. We confirmed that the level of AKT activity was higher in EphA2-S897E cells by pulling down the GSK-3α, a downstream target of AKT (**Figure 45**). Additionally, the increase in MLC2 S19 phosphorylation driven by the EphA2-S897E signaling was reversed by the presence of a PI3K inhibitor (GDC-0941) (**Figure 46**). The use of the PI3K inhibitor also drove an amoeboid to mesenchymal transition in EphA2-S897E cells (**Figure 47 and 48**). The strong transmigration ability of EphA2-S897E cells was also found to be abrogated after inhibition of PI3K pathway by the trans-endothelial migration assay (**Figure 49 and 50**).

It is known that BRAF-inhibitor resistant melanoma cells have high expression of EphA2 and its S897 phosphorylation [327]. Next, we investigated if melanoma cell lines with acquired resistance to BRAF-inhibitor also adopted an aggressive MAT phenotype. Two pairs of drug-naïve and BRAF inhibitor-resistant cell lines (1205LU and SK-MEL-28) were first seeded on each well of the 6-well plate coating with collagen. We noted that the resistant cell lines exhibited a round, amoeboid-like morphology; conversely, the elongated shape was found mostly in paired drug-naïve cells (**Figure 51**). In accordance with the observation in EphA2-S897E cells, we further found that the BRAF inhibitor resistant cells exhibited increased MLC2 phosphorylation, enhanced Cdc42 activity, greater invasion into the 3D Matrigel Matrix and stronger migration through the endothelial monolayers (**Figure 52-55**). These findings led us to believe that acquired BRAF-inhibitor

resistance promoted the MAT phenotype. In agreement with this, use of the PI3K inhibitor GDC-0941 was able to reverse the amoeboid phenotype in the resistant cells (**Figure 56**).

The metastatic phenotype in resistant cell lines driven by non-canonical EphA2 signaling dependent upon HDAC8.

Previous studies from our group suggested that the drug-resistant transcriptional state was maintained in part by the histone deacetylase 8 (HDAC8) [337]. We next asked whether the non-canonical EphA2 signaling was also mediated by HDAC8 and in turn whether this contributed to the enhanced communication with endothelial cells. The gene set enrichment analysis (GSEA) comparing 1205Lu cells overexpressing HDAC8 vs empty vector showed an association of EphA2 gene signature upregulation with overexpression of HDAC8 (**Figure 57**). Meanwhile, the knockdown of HDAC8 by shRNA in BRAF inhibitor resistant cells led to the decreased phosphorylation of AKT S473 and EphA2 S897 (**Figure 58**). The invasive ability into Matrigel was largely attenuated in WM164 BRAF inhibitor resistant cells after HDAC8 silencing (**Figure 59**). In addition, HDAC8 overexpression in 1205LU drug-naïve cells induced the amoeboid phenotype transition, whereas silencing of HDAC8 in the same cells led to the elongated shape from 3D culture on collagen (**Figure 60**). Moreover, HDAC8 overexpression also promoted the adhesion of drug-naïve melanoma cells to the endothelial cell monolayers under the shear stress compared to those with empty vector and shRNA targeting HDAC8 (**Figure 61**). Similarly, we also investigated the oncogenic properties of HDAC8 in the GEMM model since HDAC8 activation is known to control and regulate the expression of EphA2. As expected, the Kaplan–Meier survival analysis showed that the high levels of HDAC8 potentially contributed to the worse overall survival (**Figure 62**). These data revealed that non-canonical EphA2 signaling may be one feature of the broader HDAC8-driven program that is potentially associated with a switch to an MITF-low/Axl-high transcriptional phenotype [163].

Table 1: Expression proteomics associated with membrane integrity.

id	Uniprot ID (Rep)	Uniprot Accession (Rep.)	fold change (S897E/S897A)	p-value (S897E/S897A)	p-value (neglog10)	Sig. Up	Sig. Down	Function
1343	CAPG_HUMAN	P40121	0.544769033	0.00323469	2.490167033	YES	NO	Actin filament regulation
4518	TPX2_HUMAN	Q9ULW0	0.454673723	0.01708692	1.767336264	YES	NO	Spindle/microtubule regulation
2065	MGAT2_HUMAN	Q10469	0.429107363	0.00064267	3.192013885	YES	NO	ER/Golgi integrity
4070	JPH1_HUMAN	Q9HDC5	0.398632913	0.03652298	1.437433827	YES	NO	Regulation of junctional membrane complexes
3621	SEPT5_HUMAN	Q99719	-0.676582525	0.04267771	1.369798847	NO	YES	Cytoskeleton regulation

Table 2: Genes found in proteomic dataset matching the GSEA enrichment pathway.

Down-regulated in S897A			
		N cadherin pathway	AVB3 Integrin
ENRICHED PROTEINS	ARHGAP5 CTNNB1 CTNND1 MAP2K1 PTPN11 RAC1 VCL	CTNNB1 CTNND1 PTPN11 RAC1	CBL ILK MAP2K1 PTPN11 RAC1 VCL
TOTAL PROTEINS	27	16	24
NES	-2.17	-2.11	-2.09
P-VALUE	0	0	0
FDR	0.03	0.04	0.05

Down-regulated in S897E			
	cell-cell communication	RHOA regulation	EMT_down genes
ENRICHED PROTEINS	F11R FLNA LIMS1 NCK1 PARVA PLEC PTK2 PXN SPTAN1 SPTBN1	ARAP3 ARHGAP35 ARHGEF2 ARHGEF17 ARHGEF18 FARP1	ATP1A1 FLNA MYH9
TOTAL PROTEINS	39	15	15
NES	-2.14	-1.88	-1.89
P-VALUE	0	0.02	0.004
FDR	0.03	0.02	0.004

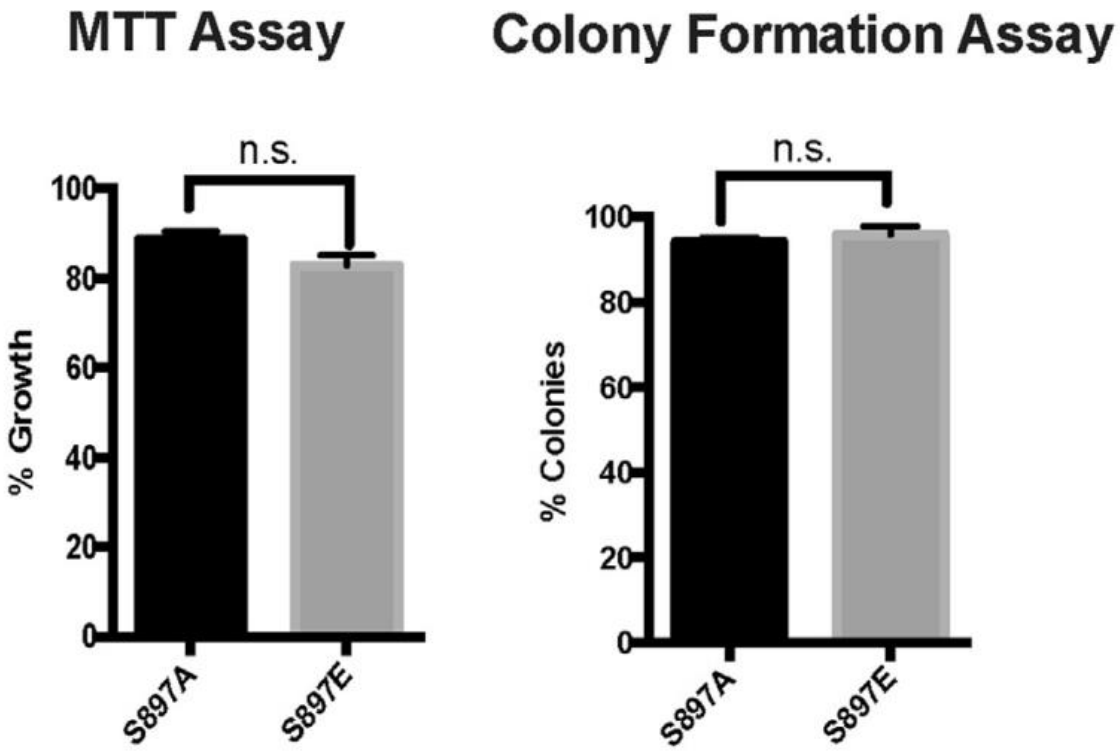

Figure 2. No growth difference between the EphA2 mutants. No significant difference of growth rate was observed between the WM164 EphA2-S897A and EphA2-S897E melanoma cell lines by MTT assay and colony formation assay. MTT, 3-(4,5-Dimethylthiazol-2-yl)-2,5-diphenyltetrazolium bromide; n.s., not significant.

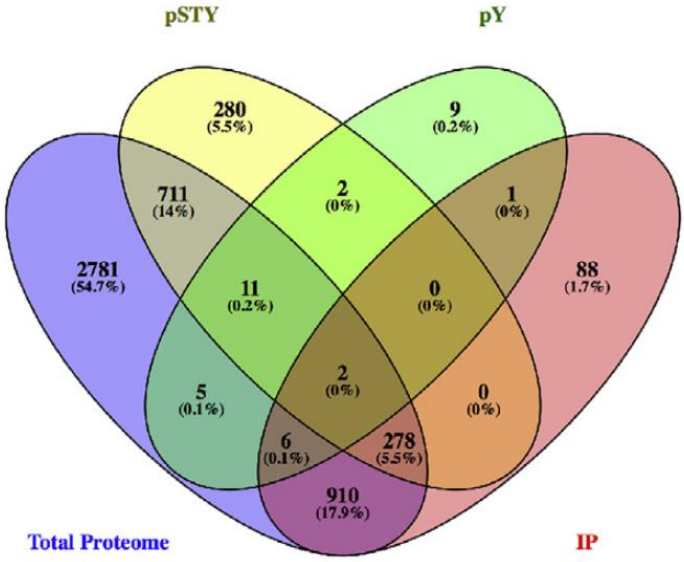

Figure 3. The number of proteins differentially expressed/phosphorylated were detected by comprehensive phosphoproteomics. Venn diagram showing the number of proteins differentially expressed/phosphorylated in the WM164 EphA2-S897A/S897E melanoma cells. pSTY, phosphorylated serine/threonine/tyrosine; pY, phosphotyrosine; IP, immunoprecipitation.

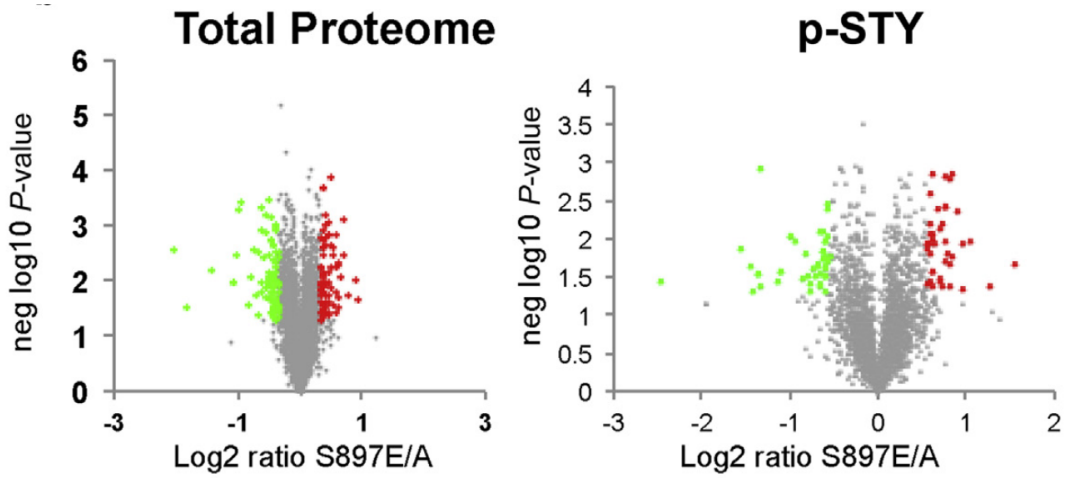

Figure 4. Upregulation and downregulation of proteins were identified by volcano plots. Volcano plots showing significant upregulation and downregulation of proteins in the WM164 EphA2-S897A/S897E melanoma cells. neg, negative; pSTY, phosphorylated serine/threonine/tyrosine; pY, phosphotyrosine.

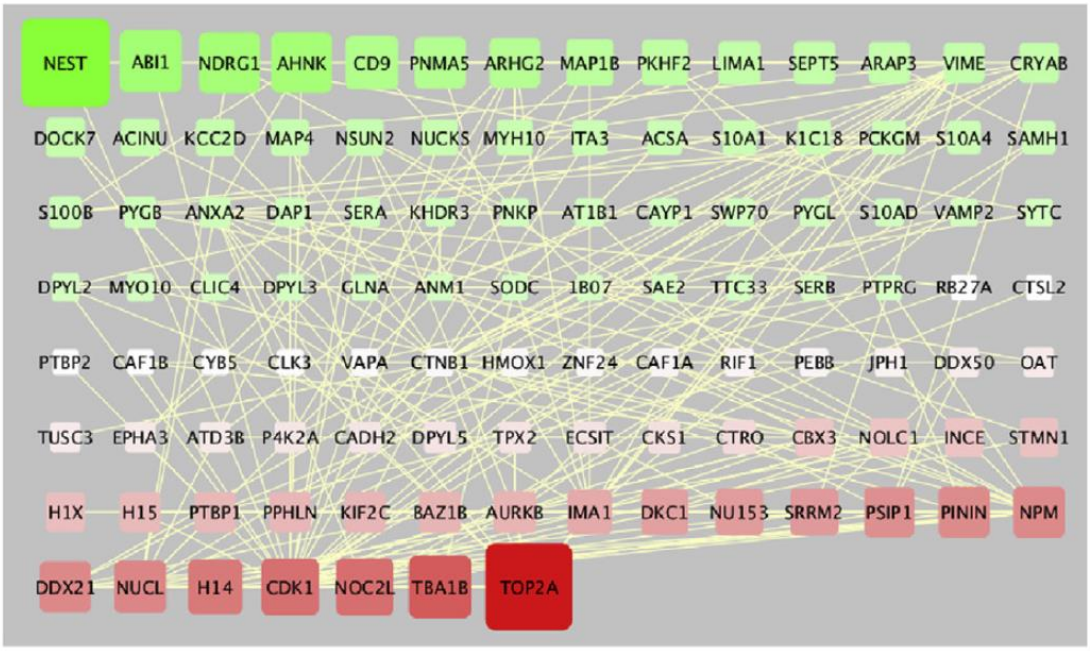

Figure 5. An inter-connected network was involved in cytoskeleton remodeling and adhesion. Upregulated and downregulated proteins form an inter-connected network involved in cytoskeleton remodeling and adhesion.

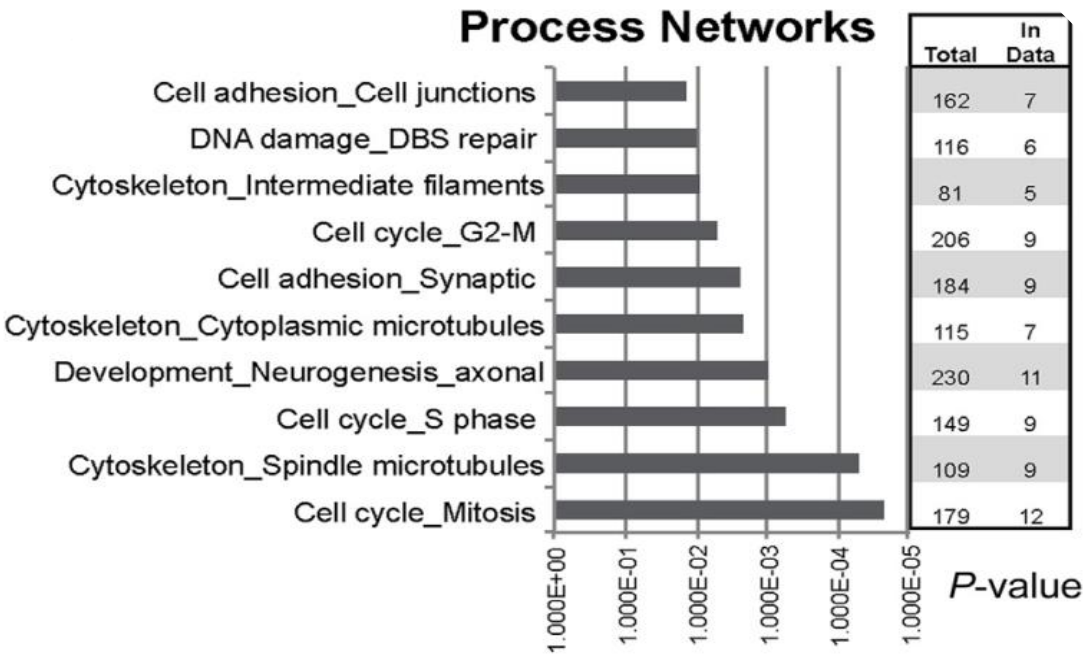

Figure 6. EphA2-S897E was involved in cell adhesion, cell cycle, and cytoskeletal remodeling. GeneGo enrichment analysis reveals pathways (–log P-value >2) associated with EphA2 signaling. DBS, double strand.

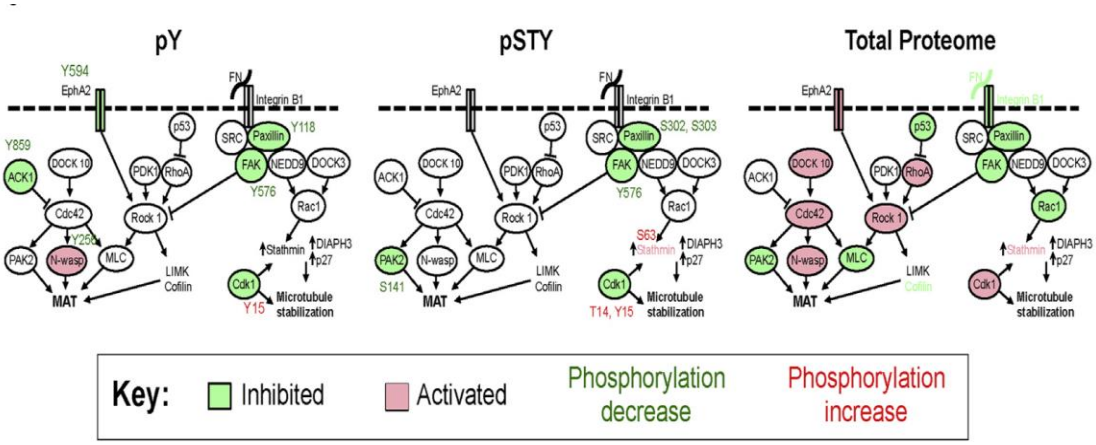

Figure 7. EphA2-S897E promoted the MAT by proteomics data. Integration of proteomic analyses into signaling maps of MAT switching. Eph, ephrin receptor; MAT, mesenchymal-to-amoeboid transition; p-MLC2, phosphorylated MLC2; pSTY, phosphorylated serine/threonine/tyrosine; pY, phosphotyrosine.

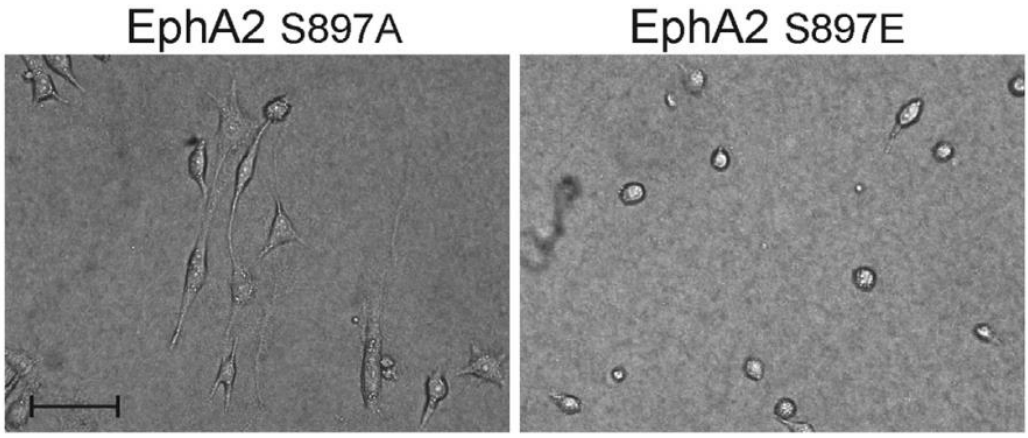

Figure 8. Amoeboid phenotype was driven by EphA2-S897E. Brightfield images of WM164 EphA2-S897A/S897E cells in 3D culture on collagen matrix. Scale bar = 100μm. 3D, three-dimensional; MAT, mesenchymal-to-amoeboid transition.

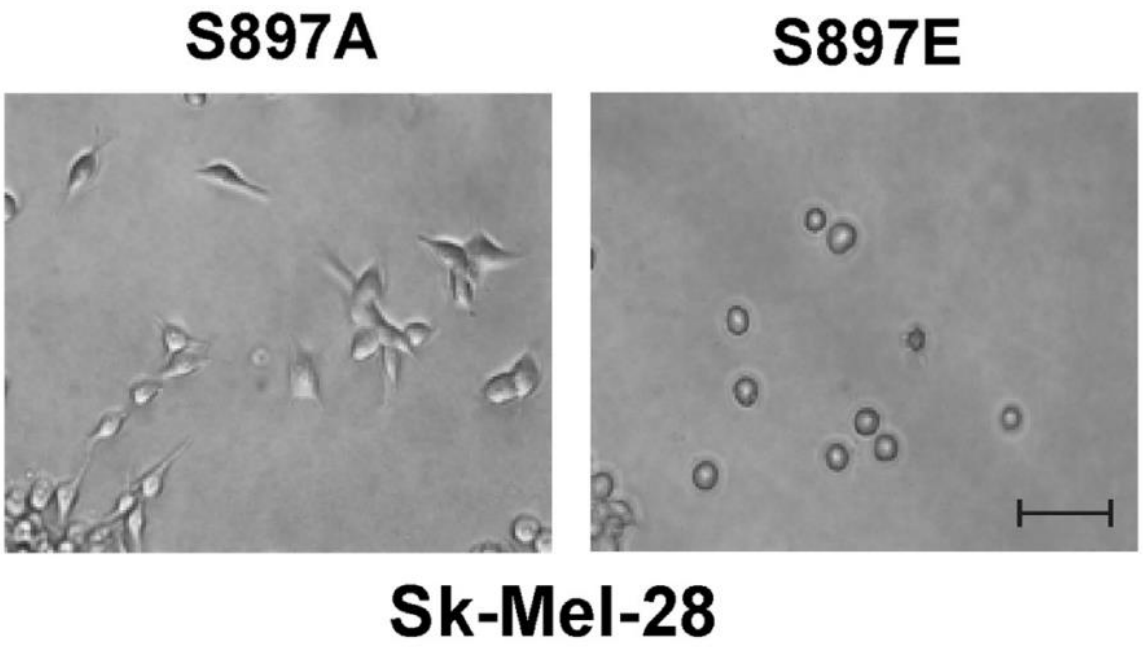

Figure 9. Mesenchymal-to-amoeboid transition was driven by EphA2-S897E. Brightfield images of Sk-Mel-28 EphA2-S897A and S897E cell lines in 3D culture on collagen matrix. 3D, three-dimensional; MAT, mesenchymal-to-amoeboid transition.

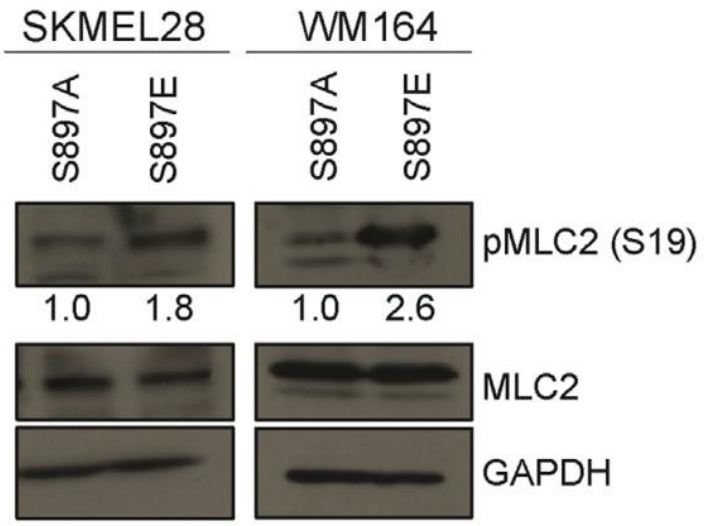

Figure 10. EphA2-S897E promoted the MLC2 phosphorylation. Western blot of phospho-MLC2 from EphA2-S897E versus S897A-lysates of WM164 and SK-MEL-28 melanoma cells. MAT, mesenchymal-to-amoeboid transition; p-MLC2, phosphorylated MLC2.

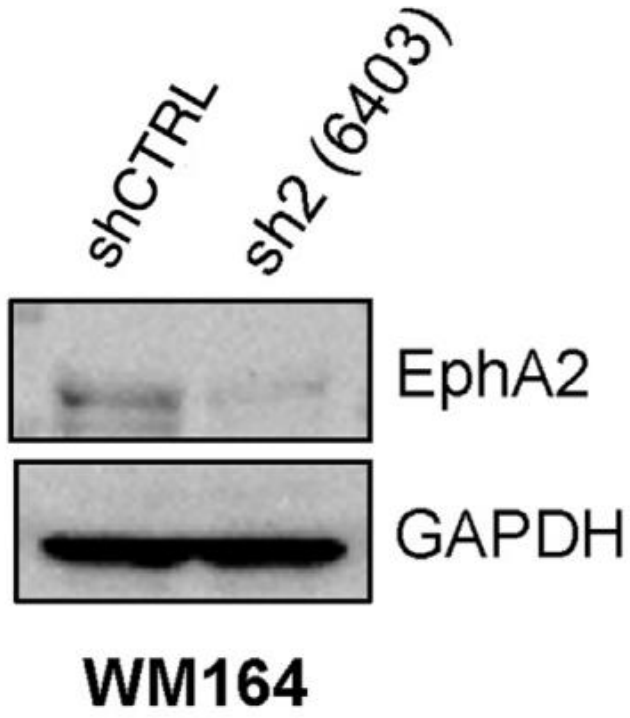

Figure 11. Knock down of endogenous EphA2 by shRNA. Western blot analysis showing the knock down of endogenous EphA2 expression by shRNA targeting the EphA2-3'UTR compared to shRNA control. Bar = 100 μm. 3′UTR, 3′ untranslated region; shCTRL, short hairpin control; shRNA, short hairpin RNA.

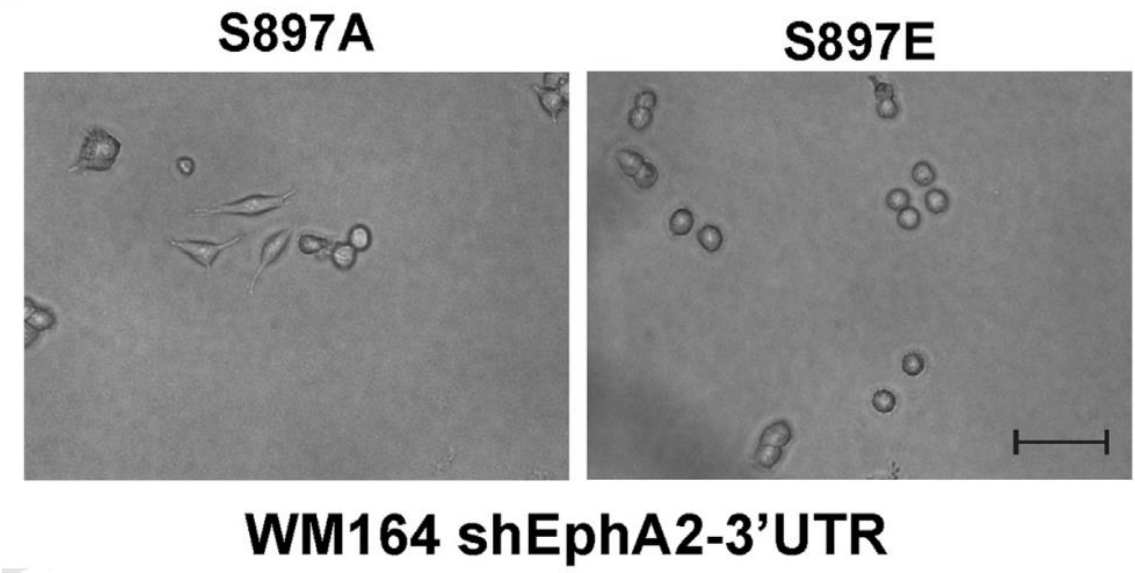

Figure 12. Knockdown of endogenous EphA2 did not affect the original phenotype. 3D culture on collagen revealed that the amoeboid (EphA2 S897E) and mesenchymal (EphA2 S897A) morphology were not affected by the knockdown of endogenous EphA2 expression in these two mutant WM164 melanoma cell lines. Scale bar = 100μm. Bar = 100 μm. 3D, three-dimensional; 3′UTR, 3′ untranslated region; shRNA, short hairpin RNA.

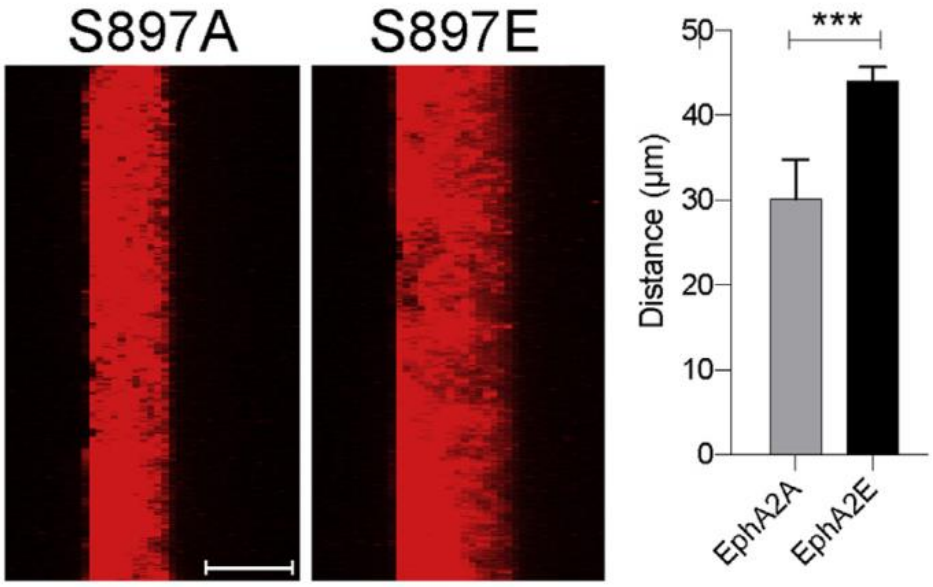

Figure 13. EphA2-S897E increased invasive ability. Invasion assays using WM164 EphA2-S897A or -S897E. Bars = 25 μm (white) and 100 μm (black).

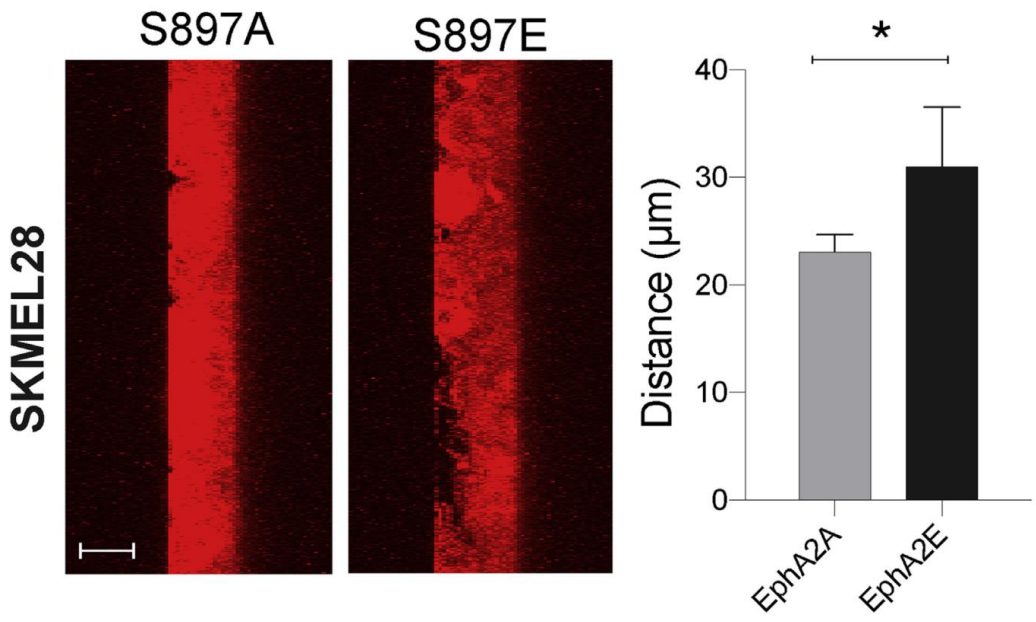

Figure 14. EphA2-S897E promoted the Matrigel invasion. Matrigel invasion assay confirmed that the stronger invasive phenotype driven by the EphA2 S897E compared to EphA2 S897A was not influenced by the knockdown of endogenous EphA2 expression in SKMEL28 melanoma cell line. Bar = 25 µm.

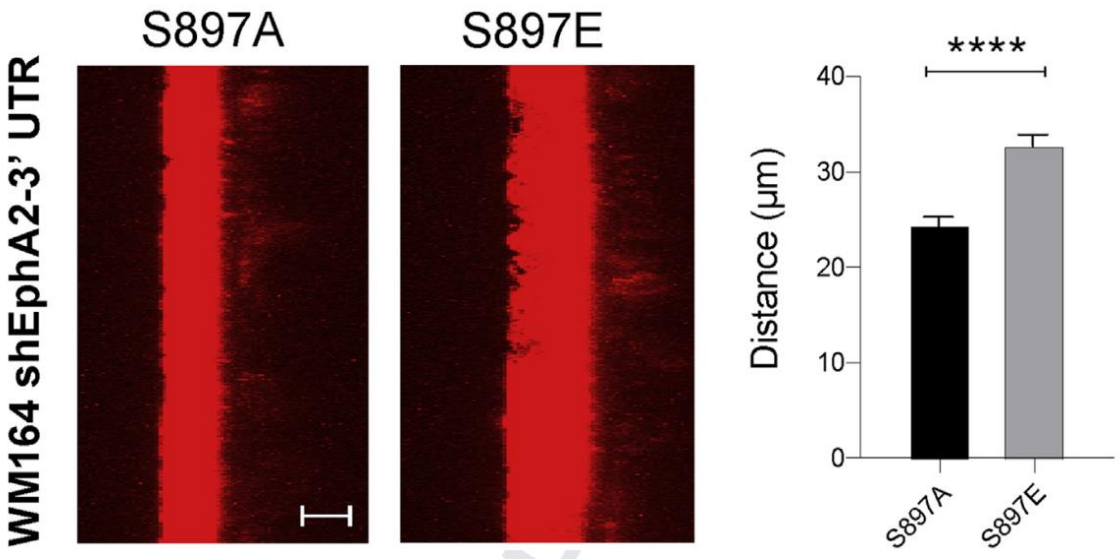

Figure 15. Knockdown of endogenous EphA2 did not affect Invasive ability. Matrigel invasion assay validated that the aggressive invasion driven by the EphA2 S897E compared to EphA2 S897A was not impacted by the knockdown of endogenous EphA2 expression in the WM164 melanoma cell lines. Bar = 25 μm. 3′UTR, 3′ untranslated region.

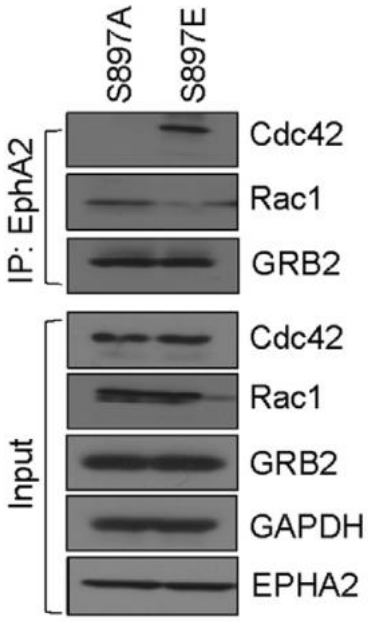

Figure 16. Increased binding of EphA2 to Cdc42 in EphA2-S897E cells. EphA2 immunoprecipitation and western blot for Cdc42 and Rac1 (WM164). IP, immunoprecipitation; p-MLC2, phosphorylated MLC2.

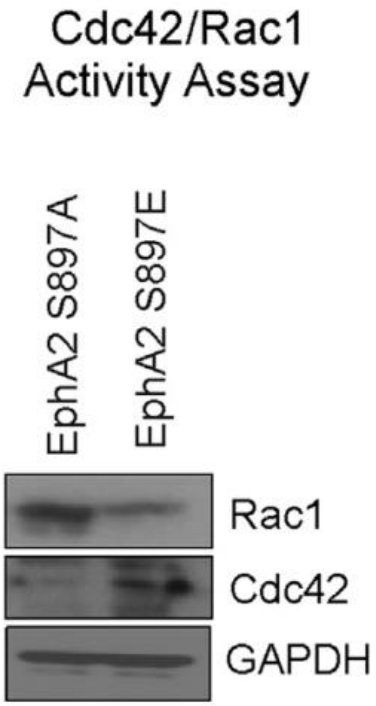

Figure 17. Increased Cdc42 activity was found in EphA2-S897E cells. Cdc42/Rac1 activity assays using WM164 EphA2-S897A or -S897E cells on collagen.

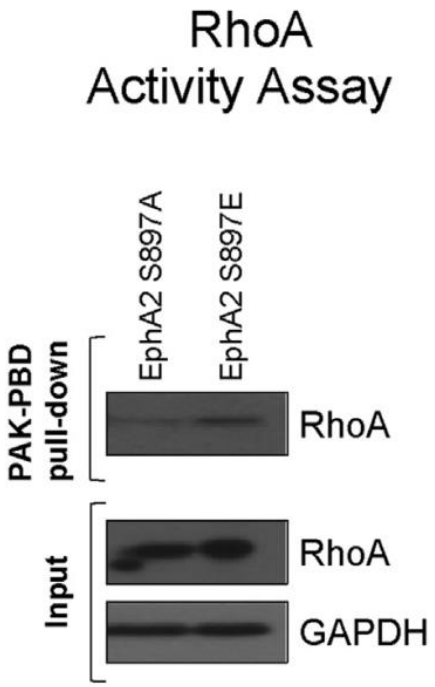

Figure 18. Increased RhoA activity was detected in EphA2-S897E cells. RhoA activity assay on WM164 EphA2-S897A and -S897E melanoma cell lines grown in 3D culture on collagen Bar = 25 μm. PAK-PBD, Rac/Cdc42 (p21) binding domain of the human p21 activated kinase 1 protein.

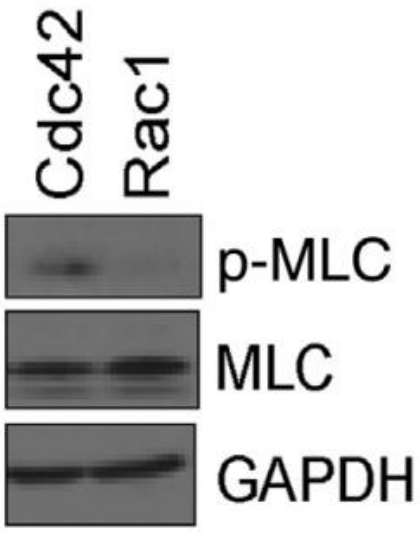

Figure 19. Active Cdc42 increased MLC2 phosphorylation. Western blot of cells with activated forms of Cdc42/Rac1 (WM164). p-MLC, phosphorylated MLC.

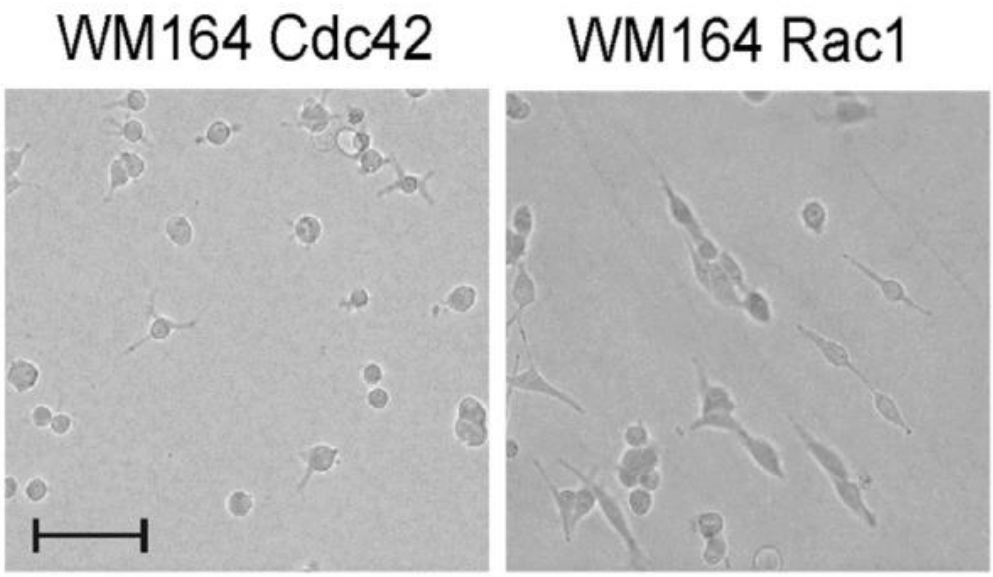

Figure 20. Active Cdc42 led to the amoeboid phenotype. WM164 cells transfected with active Cdc42 or Rac1 on collagen. Scale bar=100μm. Bars = 25 μm (white) and 100 μm (black).

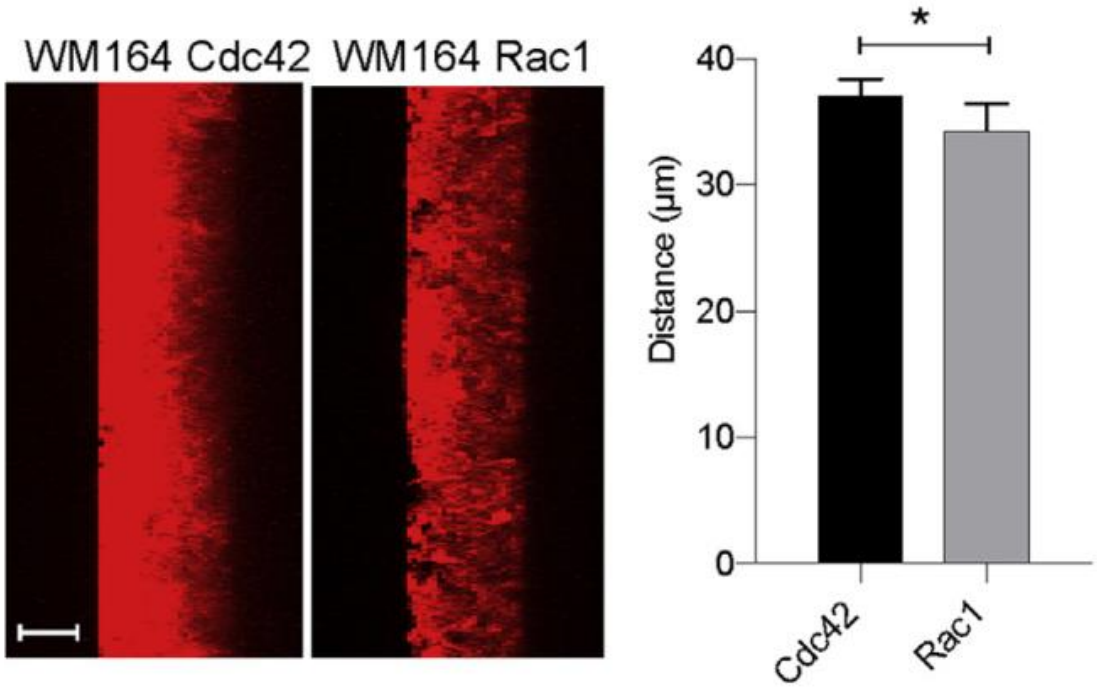

Figure 21. Active Cdc42 led to the increased invasive ability. Invasion assays of cells transfected with active Cdc42 or Rac1. Bars = 25 μm (white) and 100 μm (black).

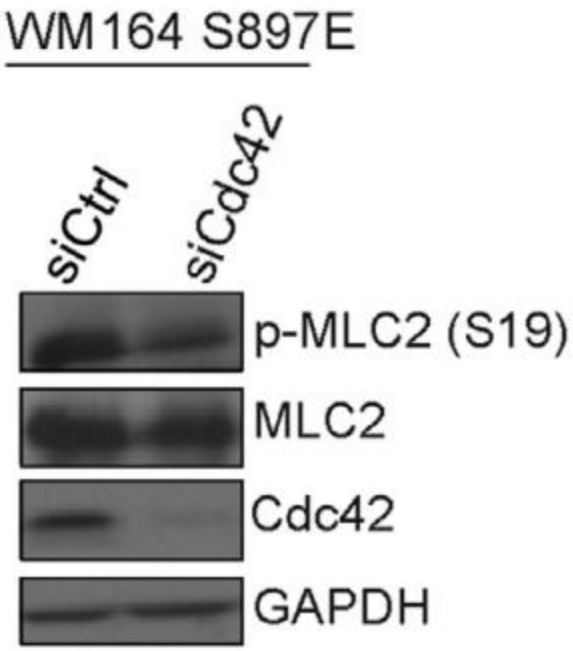

Figure 22. Cdc42 silencing decreased MLC2 phosphorylation. Western blot of WM164 EphA2-S897E cells with siRNA for Cdc2. Bars = 25 μm (white) and 100 μm (black). p-MLC2, phosphorylated MLC2; siCdc42, small interfering Cdc42; siCtrl, small interfering Ctrl; siRNA, small interfering RNA.

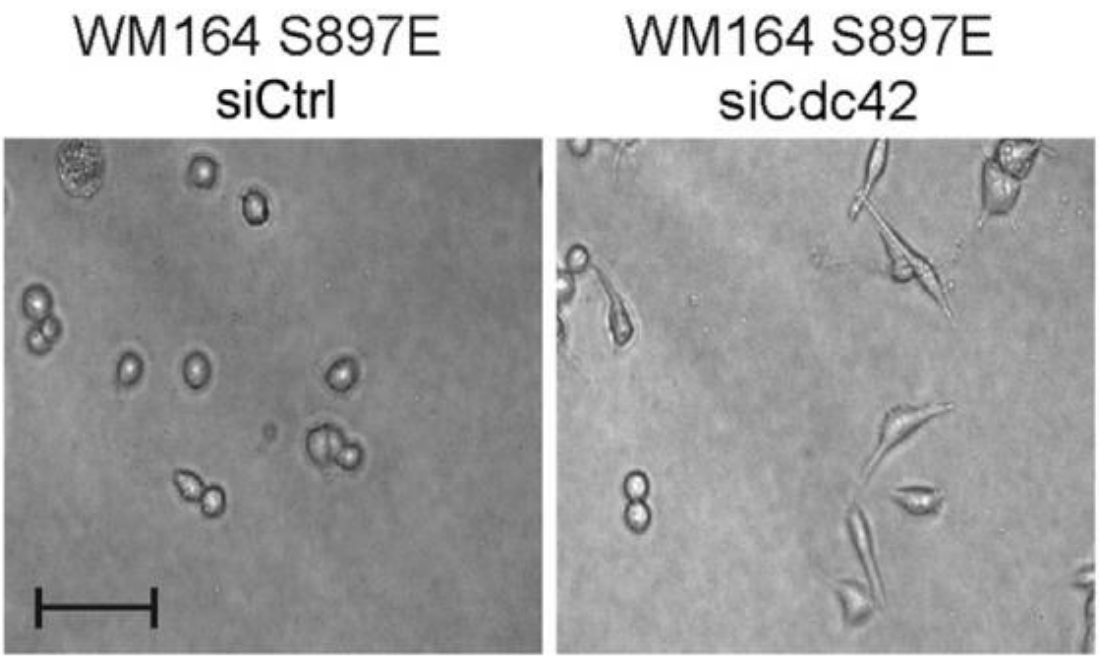

Figure 23. Cdc42 silencing reversed amoeboid to mesenchymal state. EphA2-S897E cells with siRNA for Cdc42 on collagen. Bars = 25 μm (white) and 100 μm (black). siCdc42, small interfering Cdc42; siCtrl, small interfering Ctrl; siRNA, small interfering RNA.

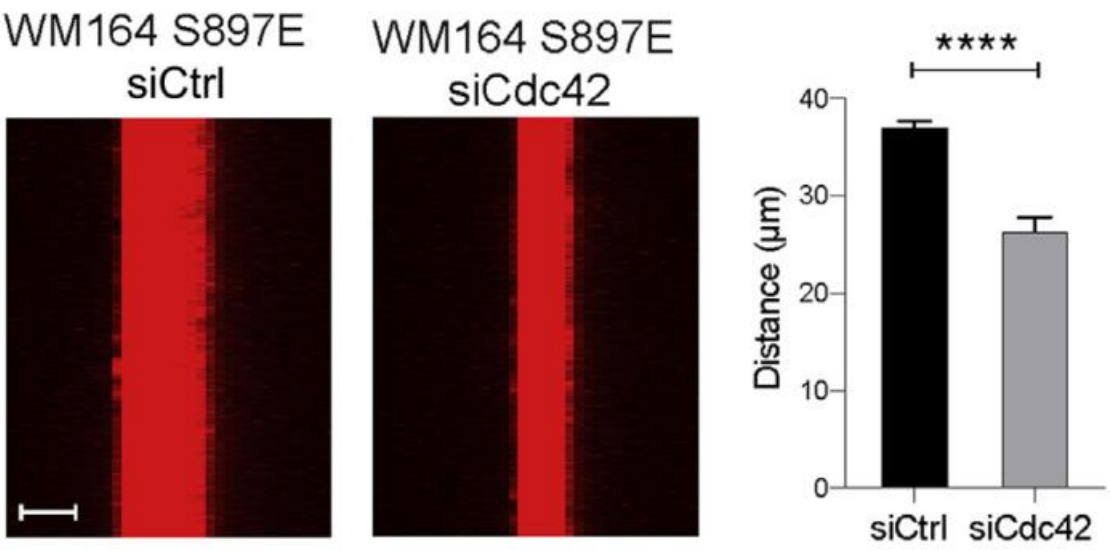

Figure 24. Cdc42 silencing decreased Matrigel invasion. Invasion assays of EphA2-S897E cells with siCtrl and siRNA for Cdc42 from cell culture on collagen. Bars = 25 µm (white) and 100 µm (black). siCdc42, small interfering Cdc42; siCtrl, small interfering Ctrl; siRNA, small interfering RNA.

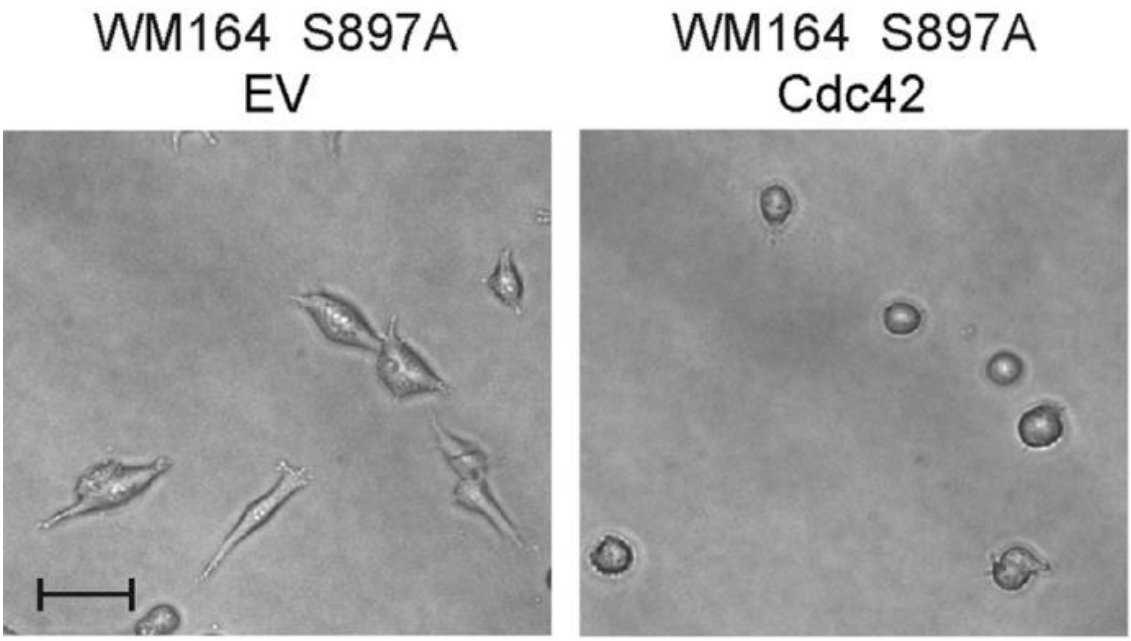

Figure 25. Cdc42 overexpression led to amoeboid phenotype. EphA2-S897A cells with EV and active Cdc42 on collagen. Bars = 25 μm (white) and 100 μm (black). EV, empty vector.

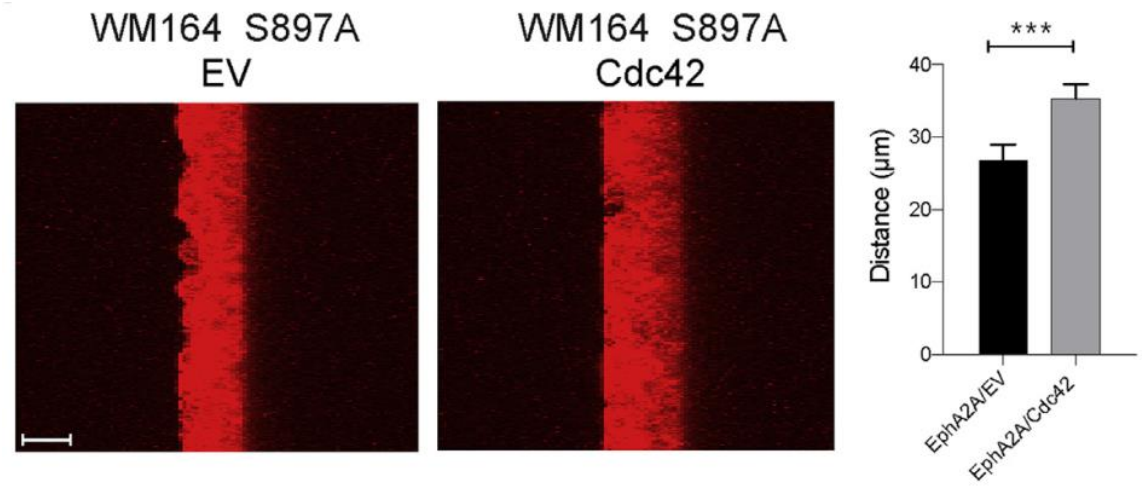

Figure 26. Cdc42 overexpression increased Matrigel invasion. Invasion assays of EphA2-S897A cells with EV and active Cdc42 on collagen. Bars = 25 μm (white) and 100 μm (black). EV, empty vector.

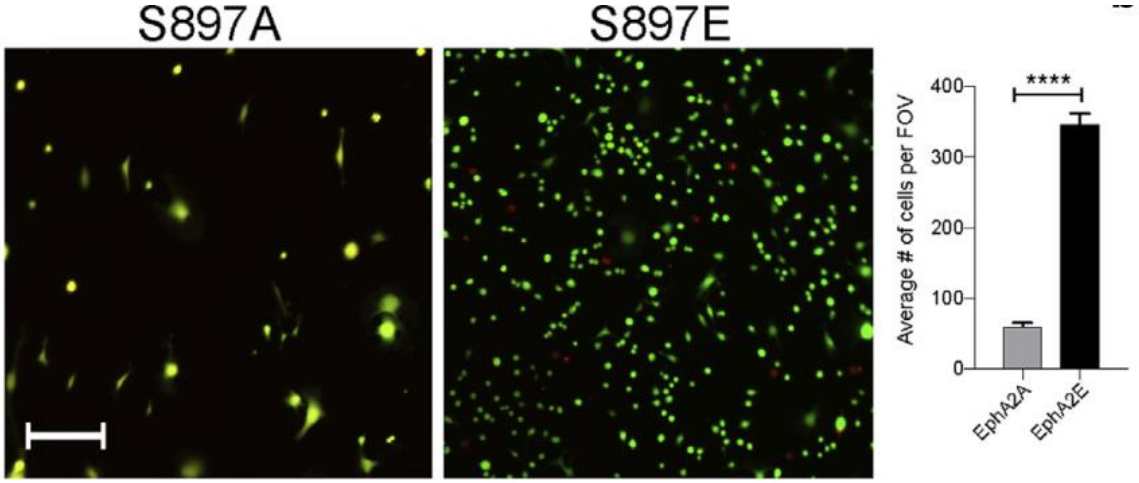

Figure 27. EphA2-S897E promoted cell survival under shear stress. Quantification of live and dead EphA2-S897A or -S897E cells in 10 dyne/cm^2 fluid shear stress (FSS; WM164, overnight). Bars = 250 μm. FOV, field of view; FSS, fluid shear stress.

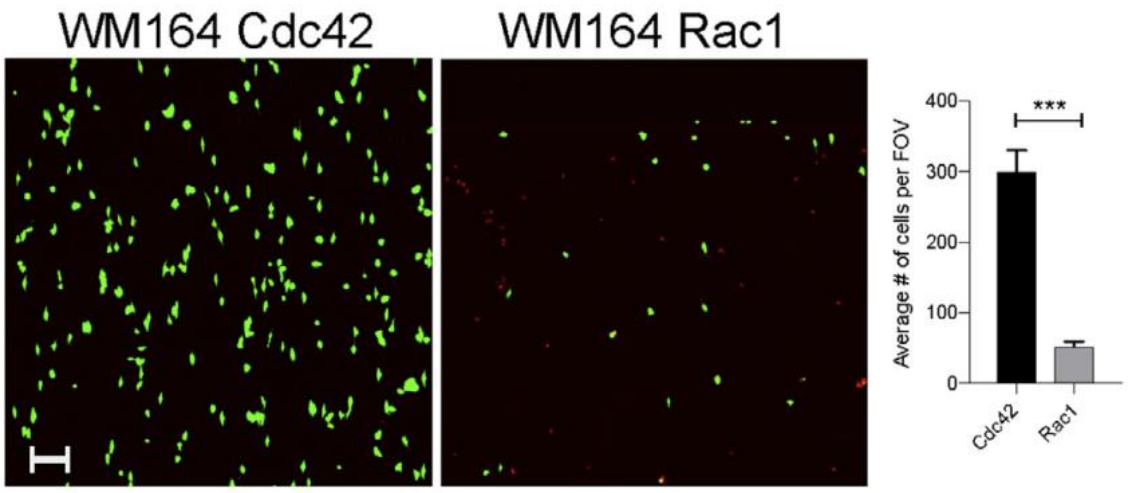

Figure 28. Active Cdc42 promoted cell viability under shear stress. Quantification of live and dead Cdc42 or Rac1 cells in 10 dyne/cm^2 FSS (WM164, overnight). Bars = 250 μm. FOV, field of view; FSS, fluid shear stress.

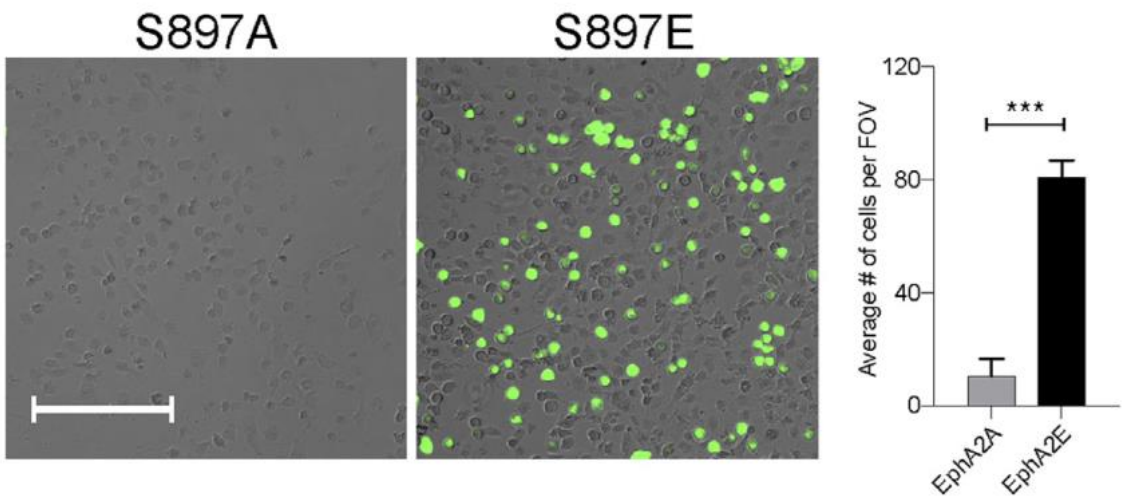

Figure 29. EphA2-S897E promoted cell adhesion under shear stress. Attachment of EphA2-S897A or -S897E cells to HUVECs at 10 dyne/cm^2 fluid shear stress (WM164, 30min). Bars = 250 μm. FOV, field of view; FSS, fluid shear stress; HUVEC, human umbilical vein endothelial cell.

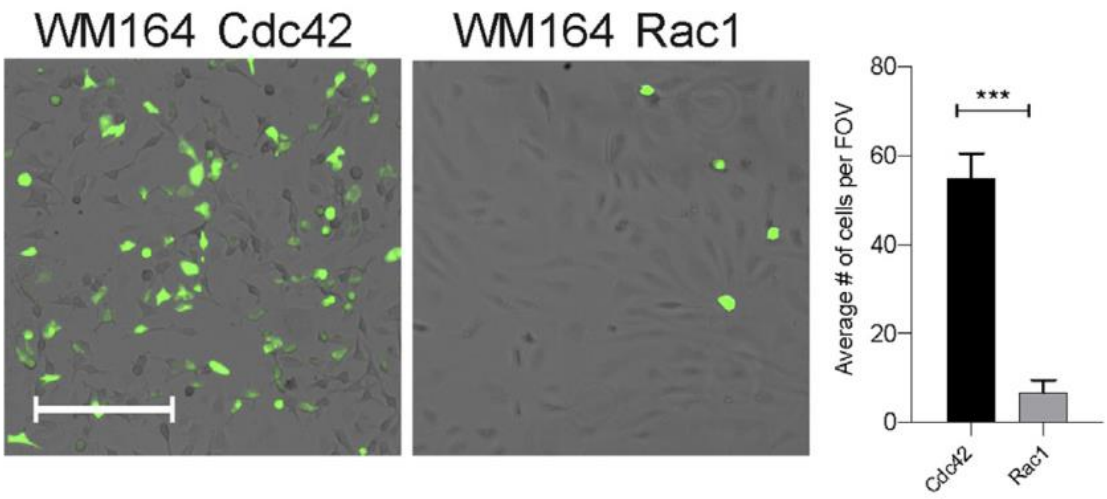

Figure 30. Active Cdc42 led to increased adhesion under shear stress. Attachment of WM164 with active Rac1 or Cdc42 cells to HUVECs at 10 dyne/cm^2 fluid shear stress (30min). Bars = 250 μm. FOV, field of view; FSS, fluid shear stress; HUVEC, human umbilical vein endothelial cell.

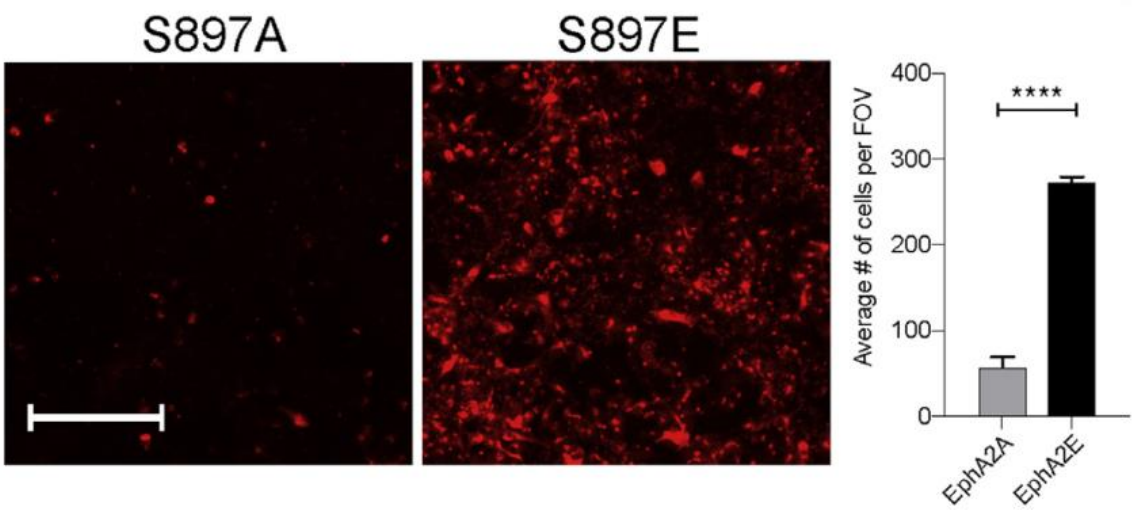

Figure 31. EphA2-S897E promoted transendothelial migration. Transendothelial migration assay of WM164 EphA2-S897A or -S897E cells. Bars = 250 μm. FOV, field of view.

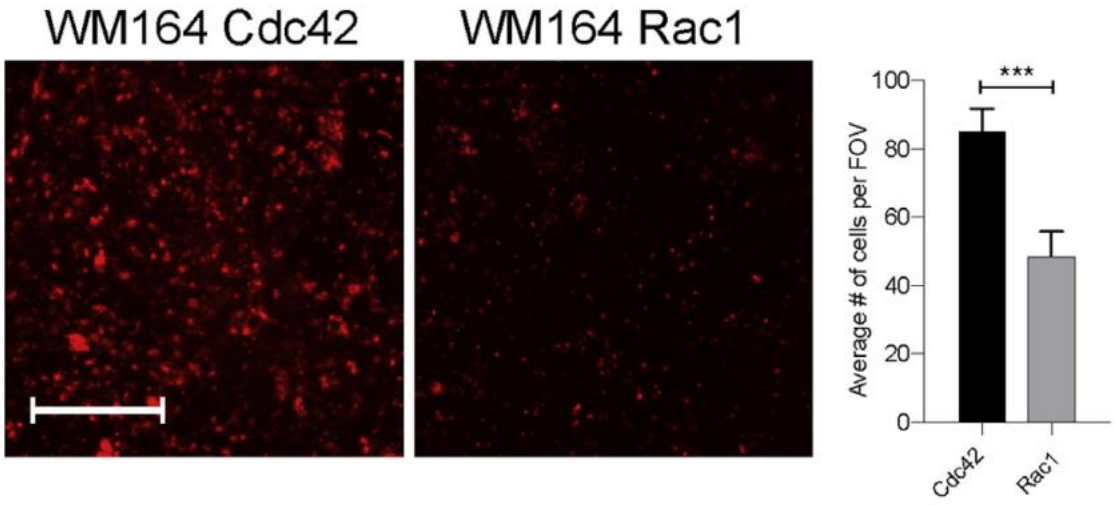

Figure 32. Active Cdc42 led to increased trans-migration ability. Transendothelial migration assay of WM164 cells with active Cdc42 or Rac1. Bars = 250 μm. FOV, field of view.

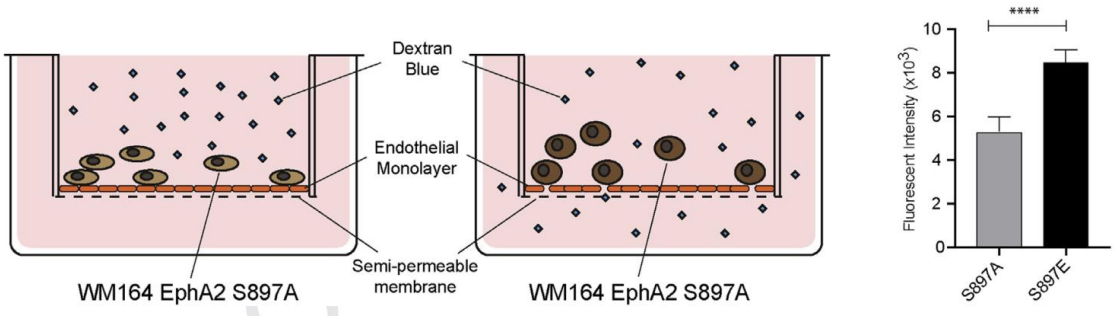

Figure 33. EphA2-S897E abrogated the membrane integrity. Diagram showing vascular permeability assay using spectrometric assessment of dextran blue dye penetration (left). Quantification of the permeability of a HUVEC monolayer after 24 hours of co-culture with WM164 EpHA2-S897A or S897E mutant cell lines (right). Scale bars=250μm. HUVEC, human umbilical vein endothelial cell.

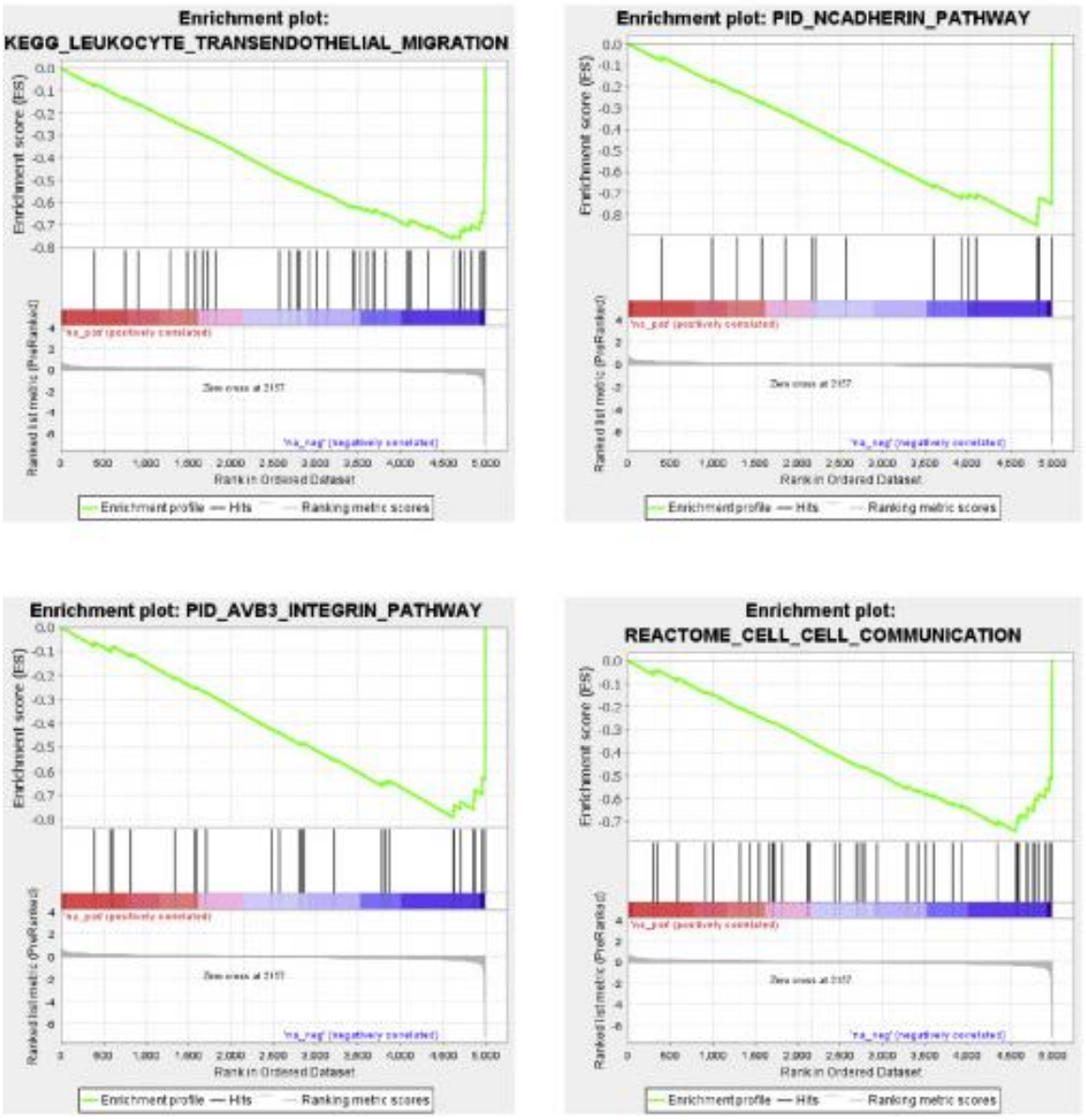

Figure 34. EphA2-S897A was associated with suppression of metastatic cascade. GSEA analysis shows pathways involved in transendothelial migration, cell-cell communication, N-Cadherin and Integrin αVβ3 signaling are downregulated in melanoma cells expressing EphA2-S897A. GSEA, Gene Set Enrichment Analysis; KEGG, Kyoto Encyclopedia of Genes and Genomes.

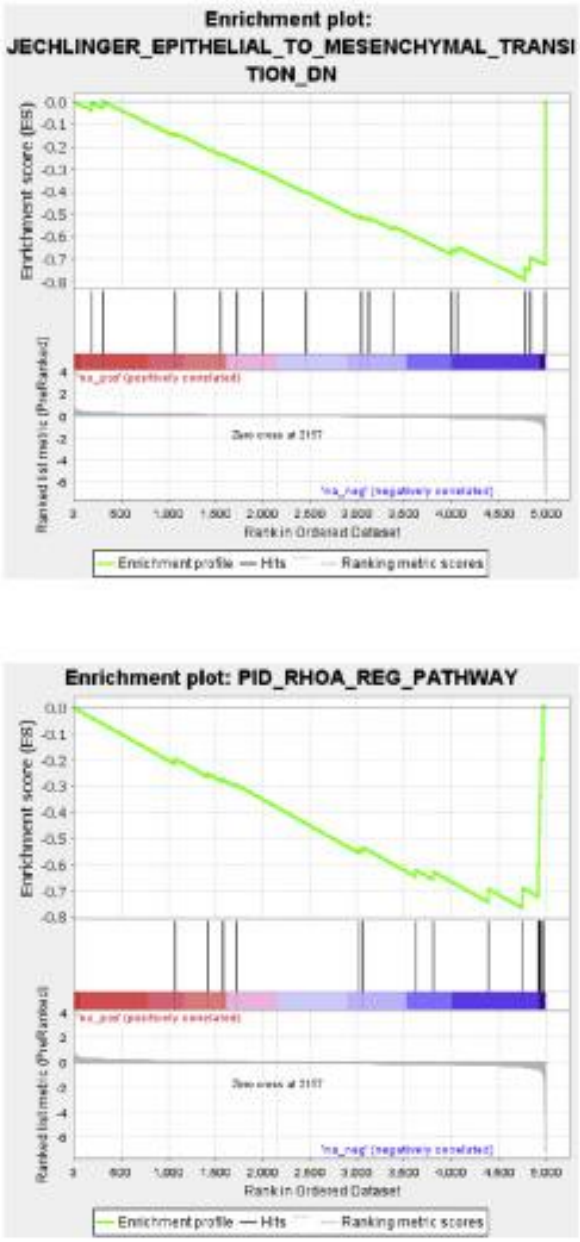

Figure 35. EphA2-S897E was associated with suppression of negative regulators. GSEA analysis shows pathways involved in EMT and RhoA signaling are downregulated in melanoma cells expressing EphA2-S897E. EMT, epithelial–mesenchymal transition; GSEA, Gene Set Enrichment Analysis; KEGG, Kyoto Encyclopedia of Genes and Genomes.

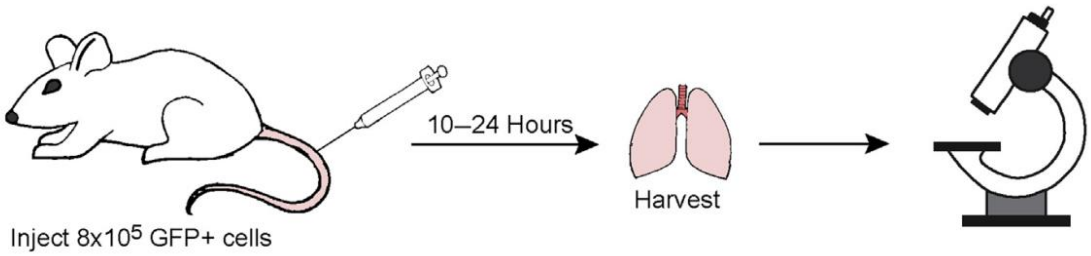

Figure 36. GFP-tagged WM164 mutant cell lines were used for lung retention analysis. Lung retention experiments using GFP-tagged WM164 cells injected into tail vein of NSG mice. After 10 and 24 hours, the lungs were harvested. Cells were quantified by confocal imaging.

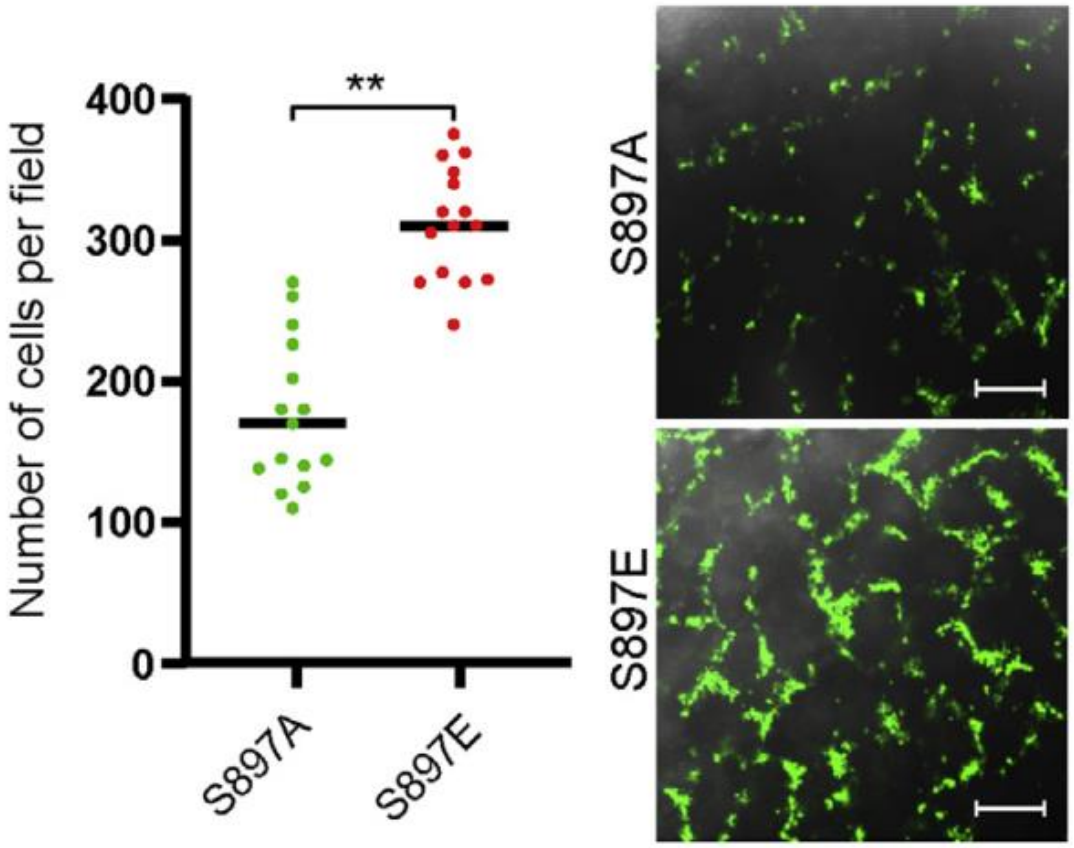

Figure 37. More EphA2-S897E cells arrested in the lung after 10 hours. Lung retention of EphA2-S897A or -S897E cells after 10 hours. Bars = 200 μm (white) and 25 μm (black).

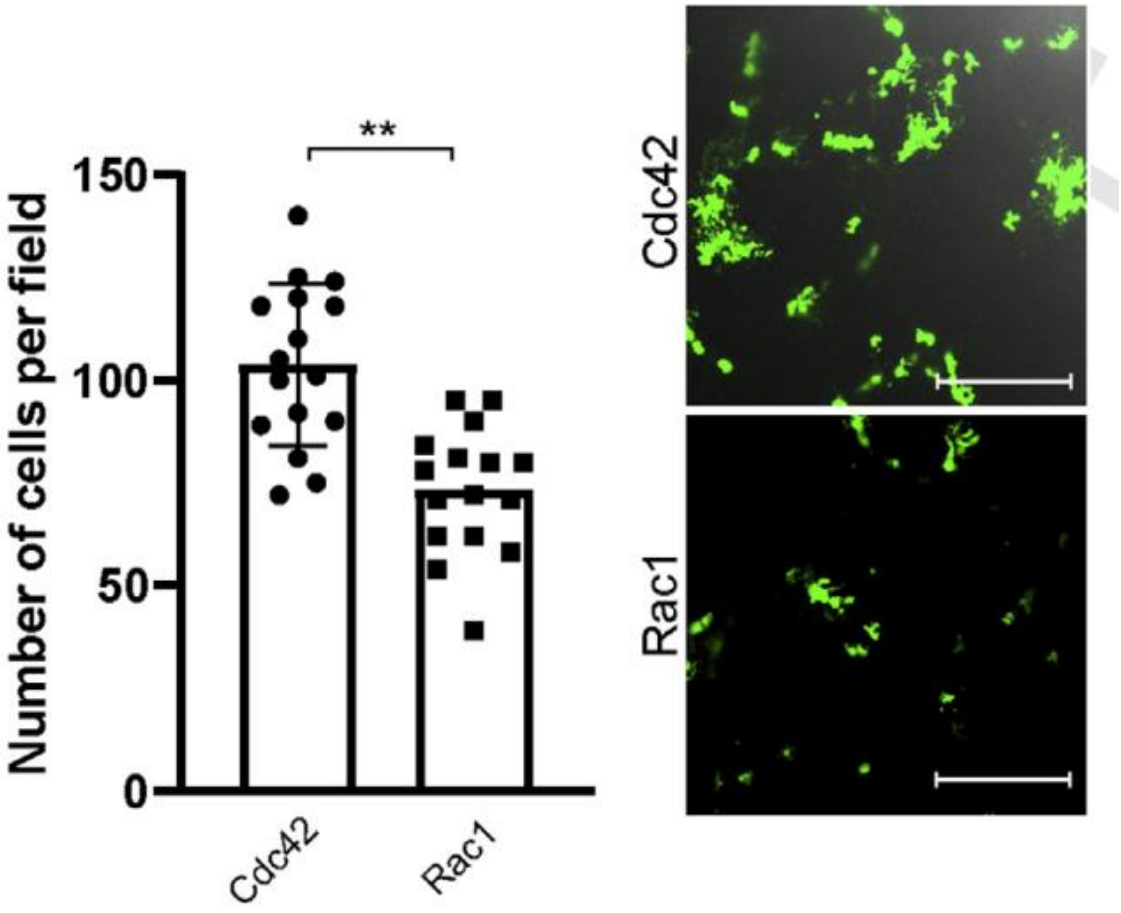

Figure 38. More cells expressing active Cdc42 arrested in the lung after 10 hours. Lung retention of WM164 cells with active Cdc42 or Rac1 after 10 hours. Bars = 200 μm (white) and 25 μm (black).

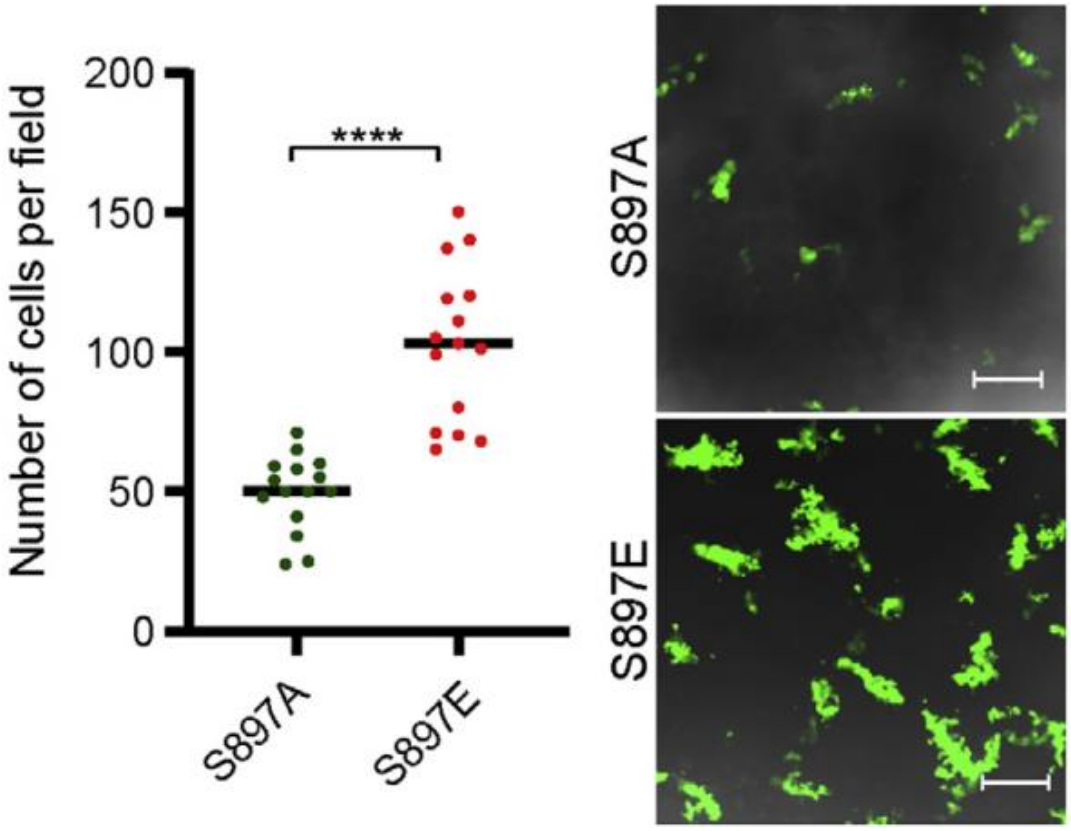

Figure 39. EphA2-S897E increased lung retention after 24 hours. Lung retention of EphA2-S897A or -S897E cells after 24 hours. Bars = 200 μm (white) and 25 μm (black).

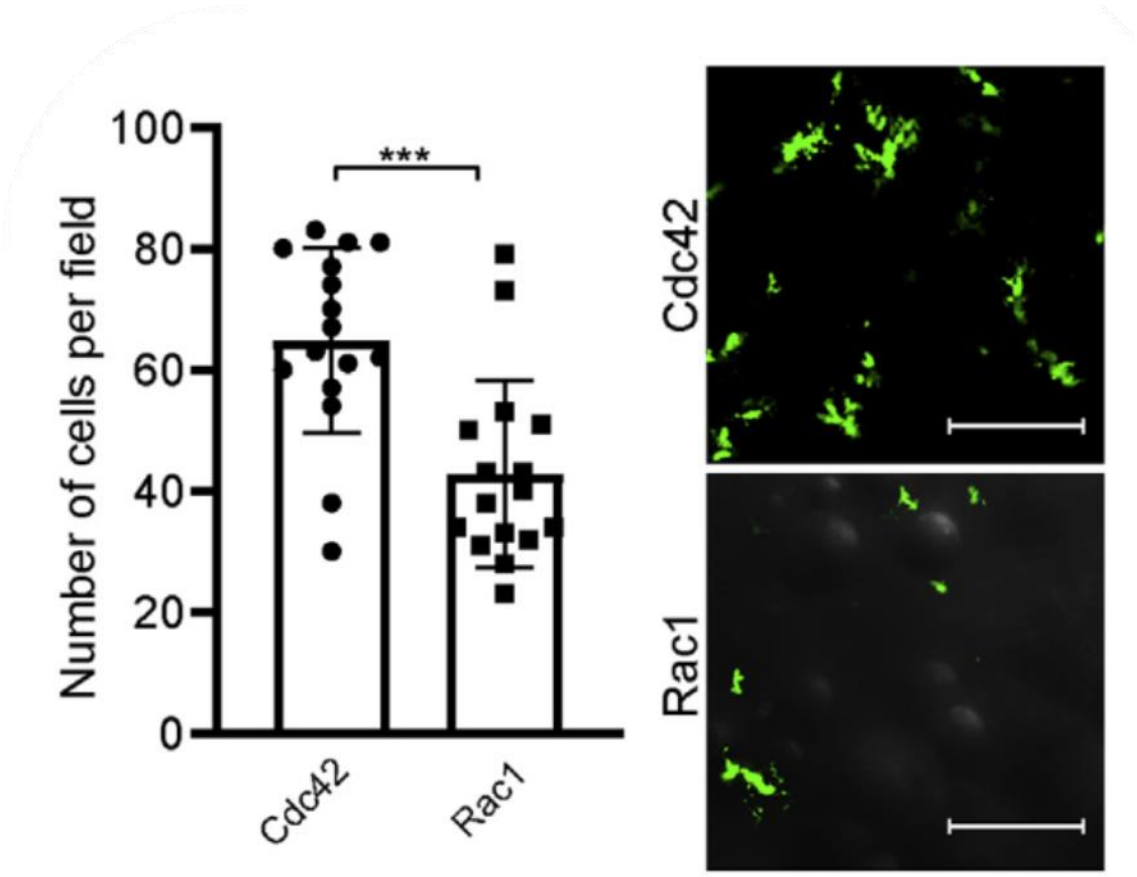

Figure 40. Active Cdc42 increased lung retention after 24 hours. Lung retention of WM164 with active Cdc42 or Rac1 after 24 hours. Bars = 200 μm (white) and 25 μm (black).

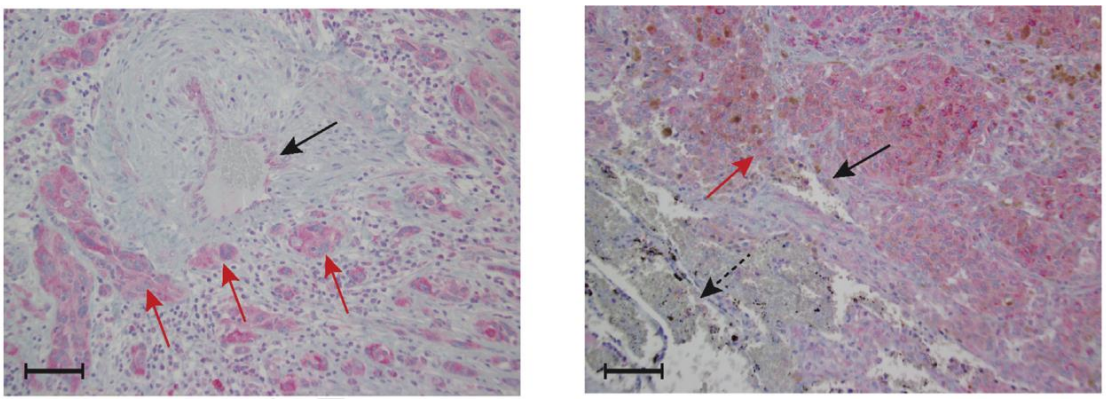

Figure 41. IHC of EphA2 confirmed the interaction in patient samples. Immunohistochemistry in human melanoma specimens shows EphA2-positive (Redkit) melanoma cells (red arrow) interacting with endothelial cells (black arrow) in the lung parenchyma (dashed black arrow) of two patients (left: 200x, right: 100x). Scale bars: white = 200µm, black=25µm.

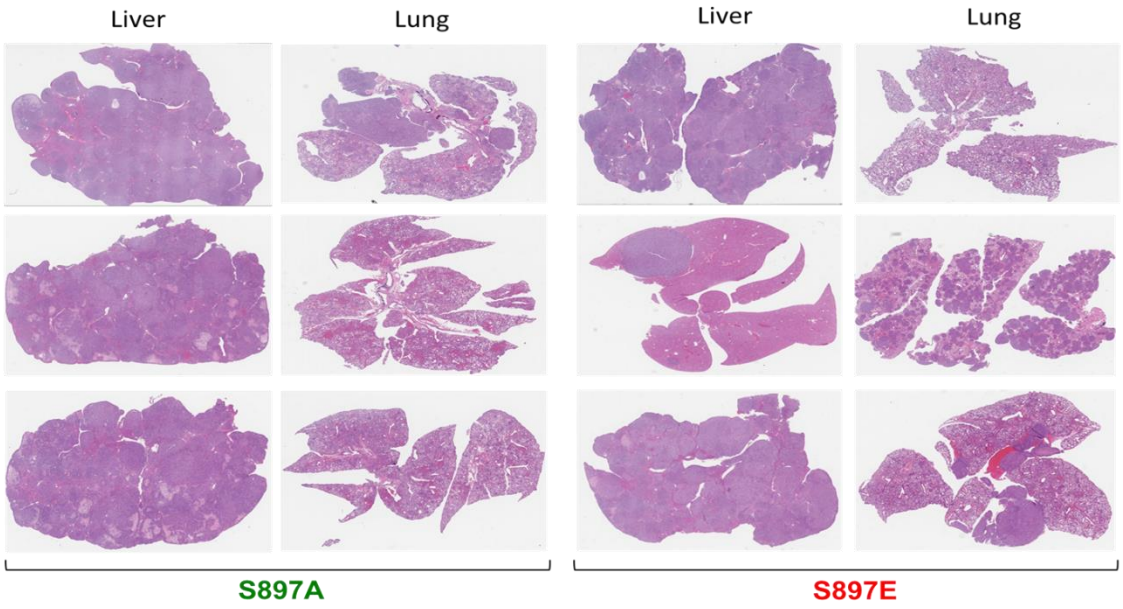

Figure 42. No metastatic difference in liver and lung between groups of EphA2 mutants. H&E staining of tissues including liver and lung showed all melanoma metastatic tumor burdens from NSG mice injected with WM164 EphA2-S897E or -S897A cells. Total number of mice with EphA2-S897E or -S897A cells were 9 and 7, respectively.

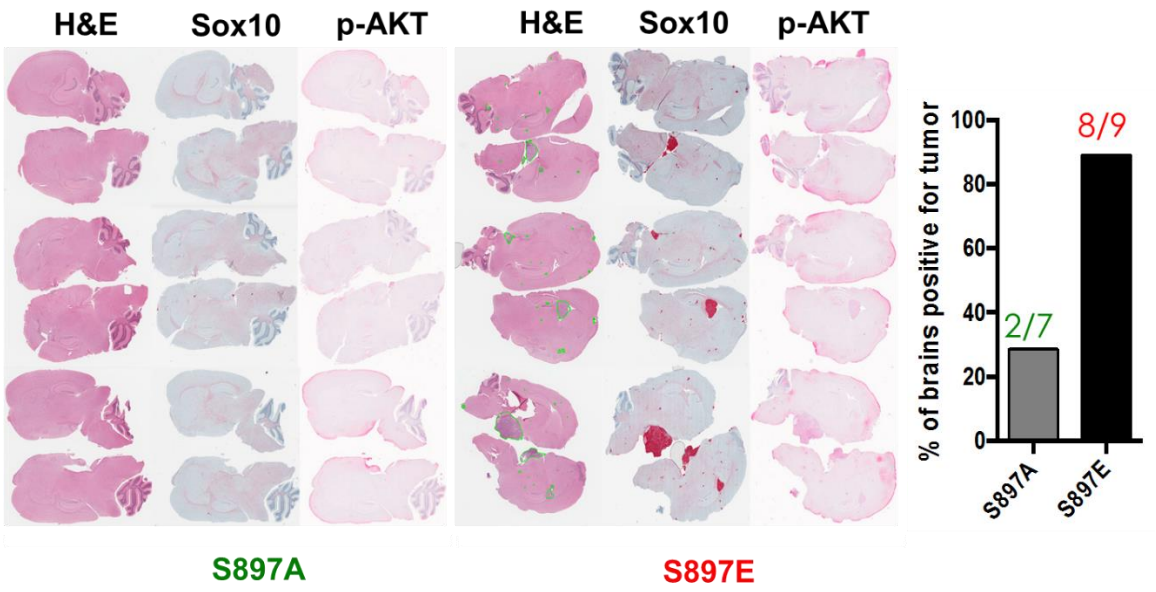

Figure 43. EphA2-S897E promoted the brain metastasis. IHC of SOX10 and p-AKT staining for identification of metastasis in brain from NSG mice. Total number of mice with EphA2-S897E or -S897A cells were 9 and 7, respectively.

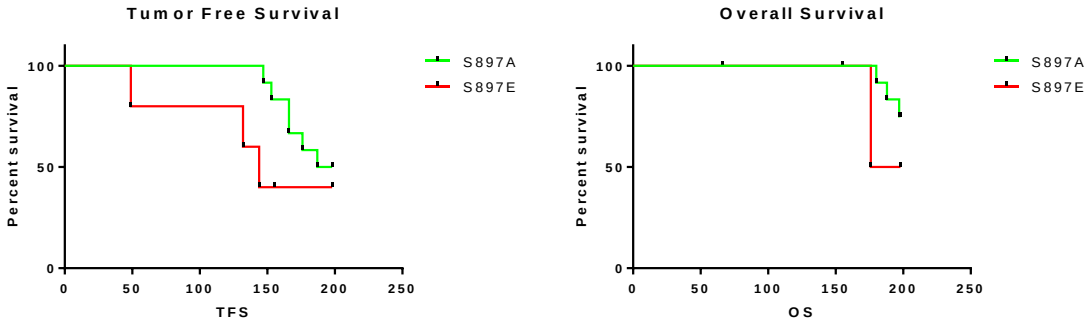

Figure 44. EphA2-S897E was associated with worse survival rate. Kaplan–Meier survival analysis of chimeric EphA2 s897A and EphA2 S897E mice. Total number >10 in each type of mice.

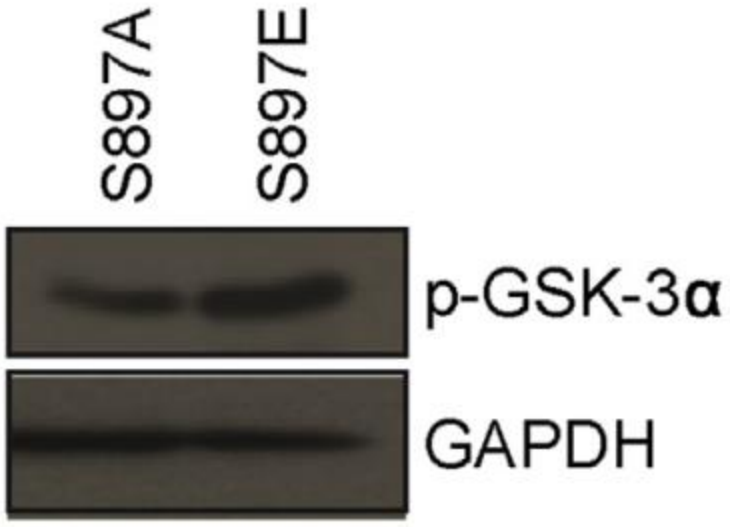

Figure 45. EphA2-S897E linked to increased AKT activity. AKT activity assays in WM164 EphA2-S897A or -S897E cells. Akt, protein kinase B; p-GSK-3α, phosphorylated GSK-3α.

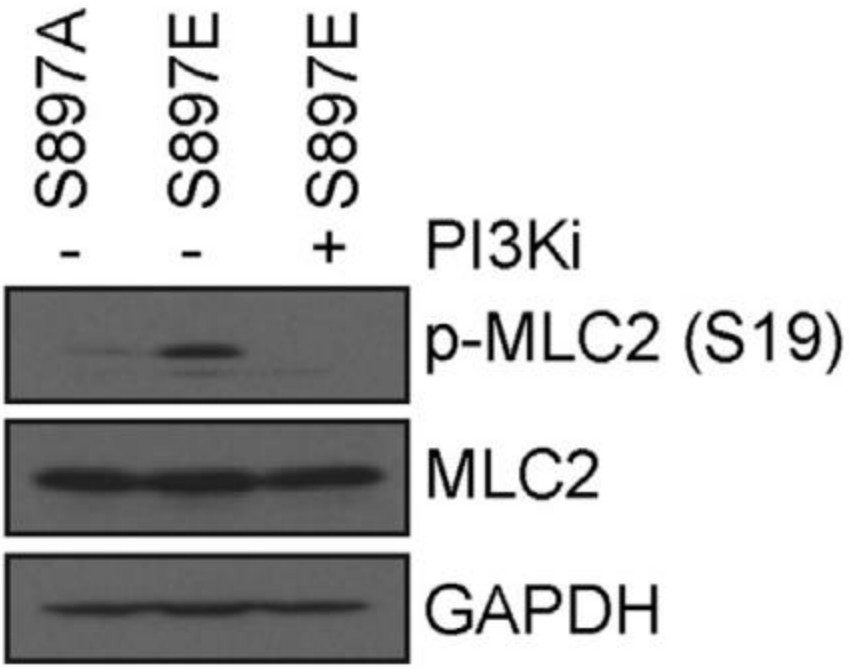

Figure 46. PI3K inhibition led to decreased MLC2 phosphorylation. Western blot of WM164 EphA2 S897E cells with or without GDC-0941 (3 μM, 72 hours). PI3k, phosphoinositide-3 kinase; PI3ki, PI3k inhibitor; p-MLC2, phosphorylated MLC2.

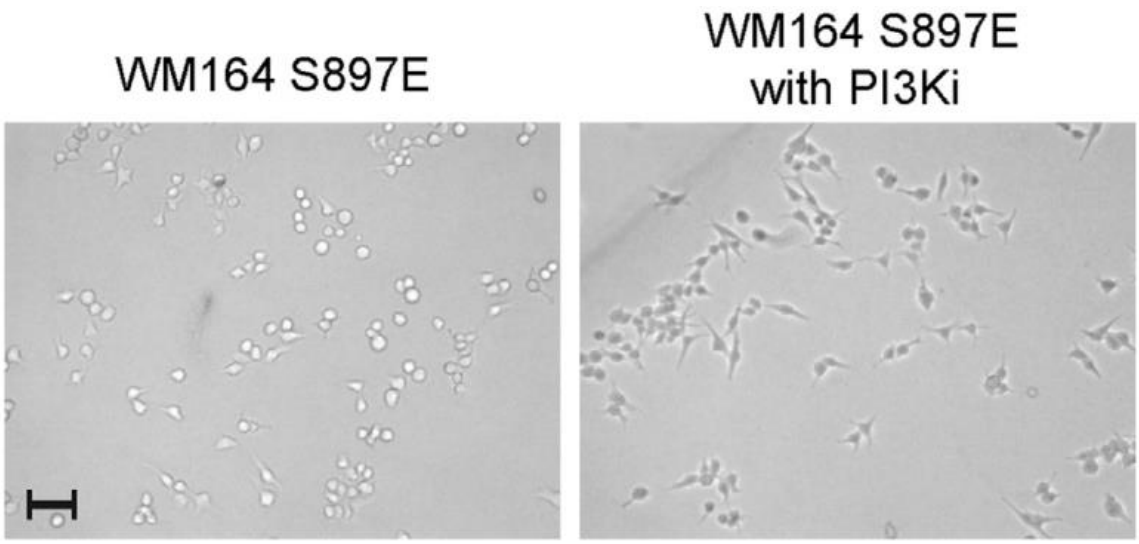

Figure 47. PI3K inhibition reversed the amoeboid phenotype. 3D culture of EphA2-S897E cells on collagen with or without GDC-0941 (10x, 3 μM, 72 hours). Bars = 25 μm (white), 100 μm (black), and 200 μm (blue). 3D, three-dimensional; PI3k, phosphoinositide-3 kinase; PI3ki, PI3k inhibitor.

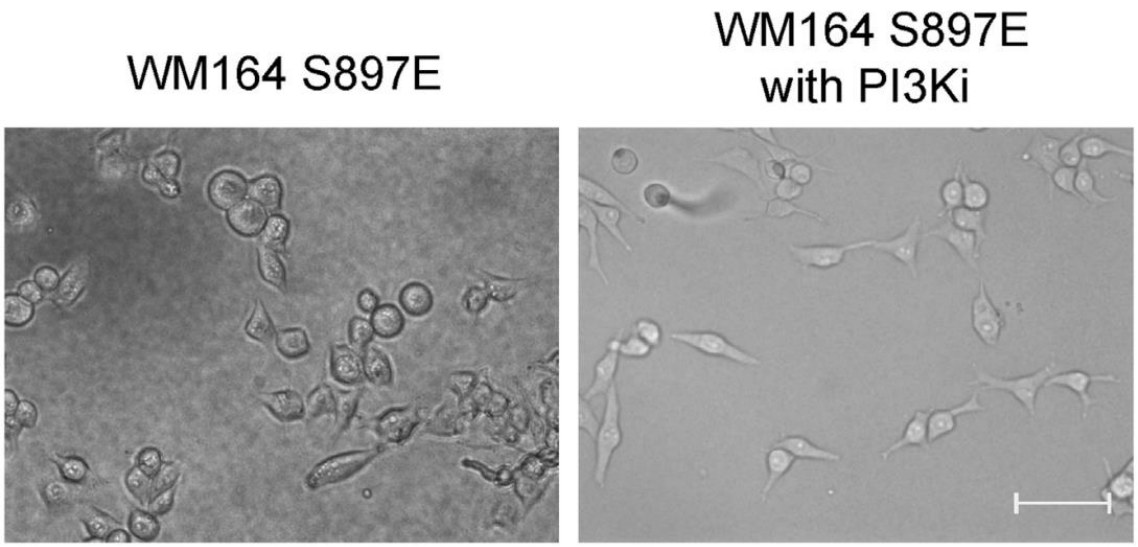

Figure 48. PI3K inhibition led to the elongated phenotype. Brightfield images (20X) of WM164 EphA2-S897E cells treated with vehicle control or GDC-0941 (3μM, 72 hours) in 3D culture on collagen matrix shows a reduction of amoeboid morphology. Bar = 100 μm. 3D, three-dimensional; PI3k, phosphoinositide-3 kinase; PI3Ki, phosphoinositide-3 kinase inhibitor.

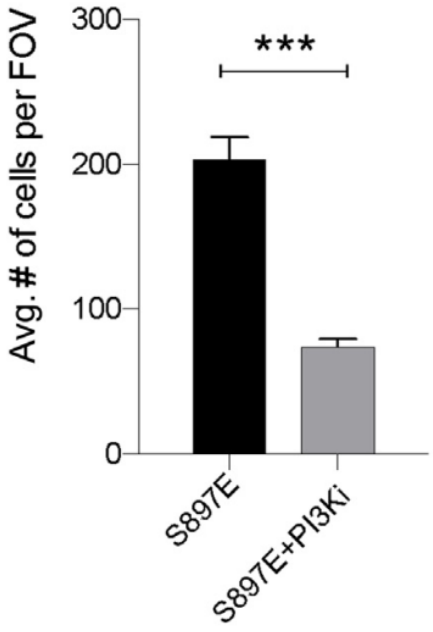

Figure 49. Quantification showed less cells can migrate after PI3K inhibition. Transendothelial migration of WM164 EphA2-S897E cells with or without GDC-0941. Avg, average; FOV, field of view; PI3k, phosphoinositide-3 kinase; PI3ki, PI3k inhibitor.

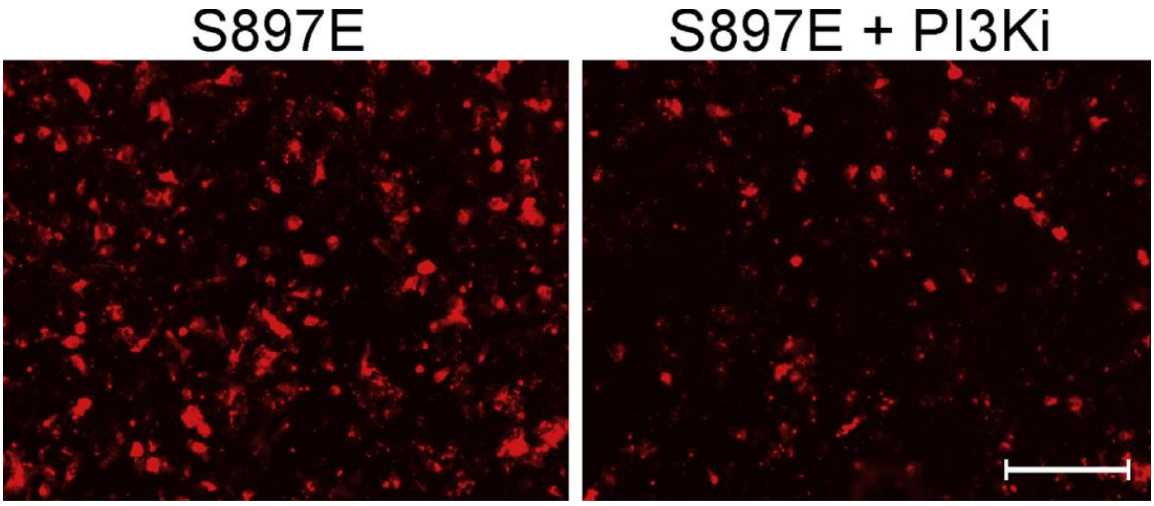

Figure 50. PI3K inhibition decreased the trans-migration ability. Transendothelial migration assay showing the number of DiI-labeled WM164 EphA2-S897E melanoma cells migrated through a HUVEC monolayer after 2-4 hours in presence of vehicle control or GDC-0941. Scale bar = 100μm. HUVEC, human umbilical vein endothelial cell; PI3Ki, phosphoinositide-3 kinase inhibitor.

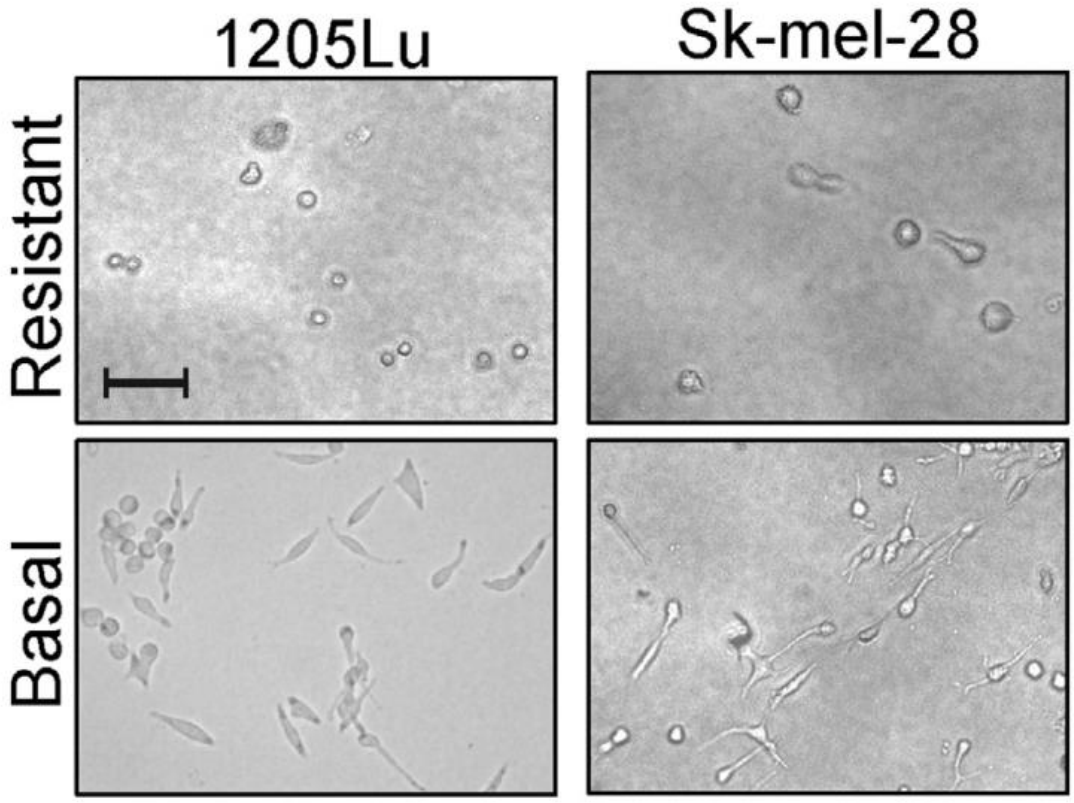

Figure 51. Resistant cells adopted amoeboid phenotype. 3D culture on collagen of treatment-naïve and -resistant melanoma cells. Bars = 25 μm (white), 100 μm (black), and 200 μm (blue). 3D, three-dimensional.

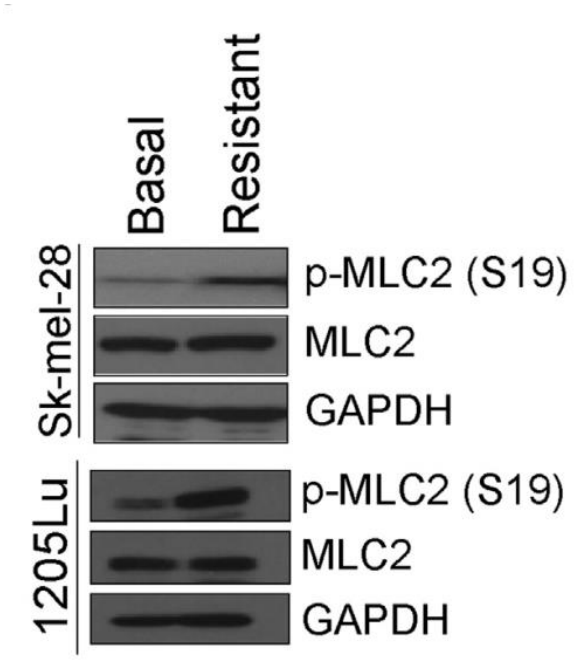

Figure 52. Resistant cells were associated with increased phosphorylation of MLC2. Western blot of treatment-naïve and -resistant melanoma cells. PI3k, phosphoinositide-3 kinase; p-MLC2, phosphorylated MLC2.

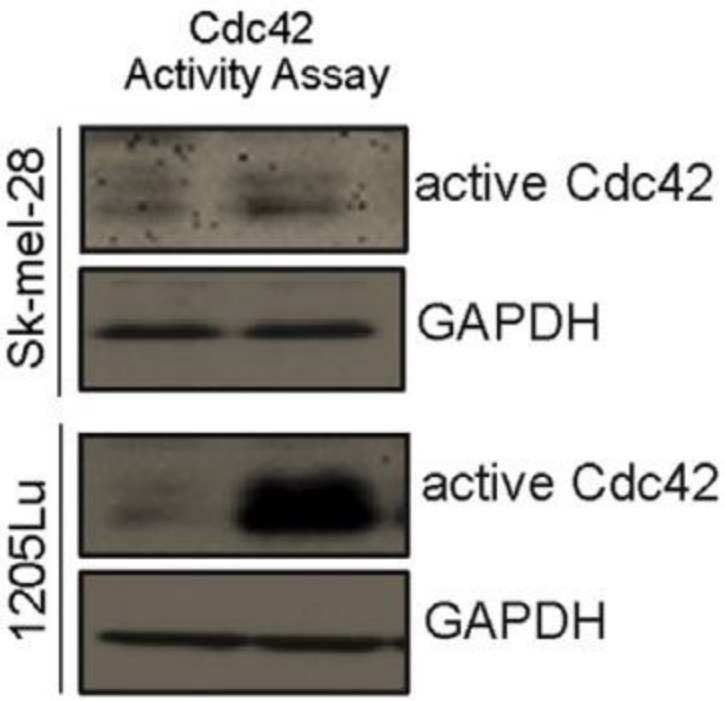

Figure 53. Resistant cells showed increased Cdc42 activity. Cdc42 activity assays of treatment-naïve and -resistant 1205Lu and SKMEL28 cells. PI3k, phosphoinositide-3 kinase.

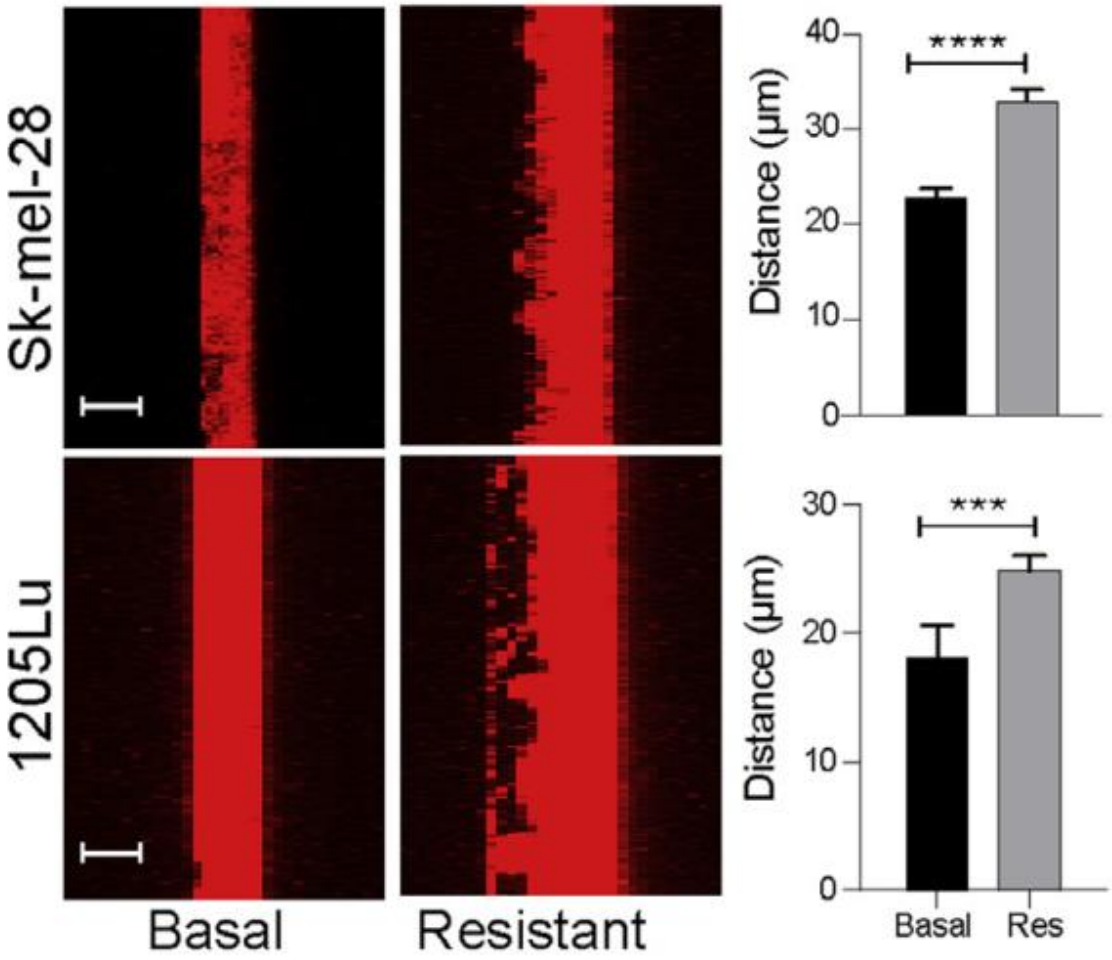

Figure 54. Resistant cells displayed stronger invasive ability. Matrigel invasion assays of treatment-naïve and -resistant melanoma cells. Bars = 25 μm (white), 100 μm (black), and 200 μm (blue). PI3k, phosphoinositide-3 kinase; Res, resistant.

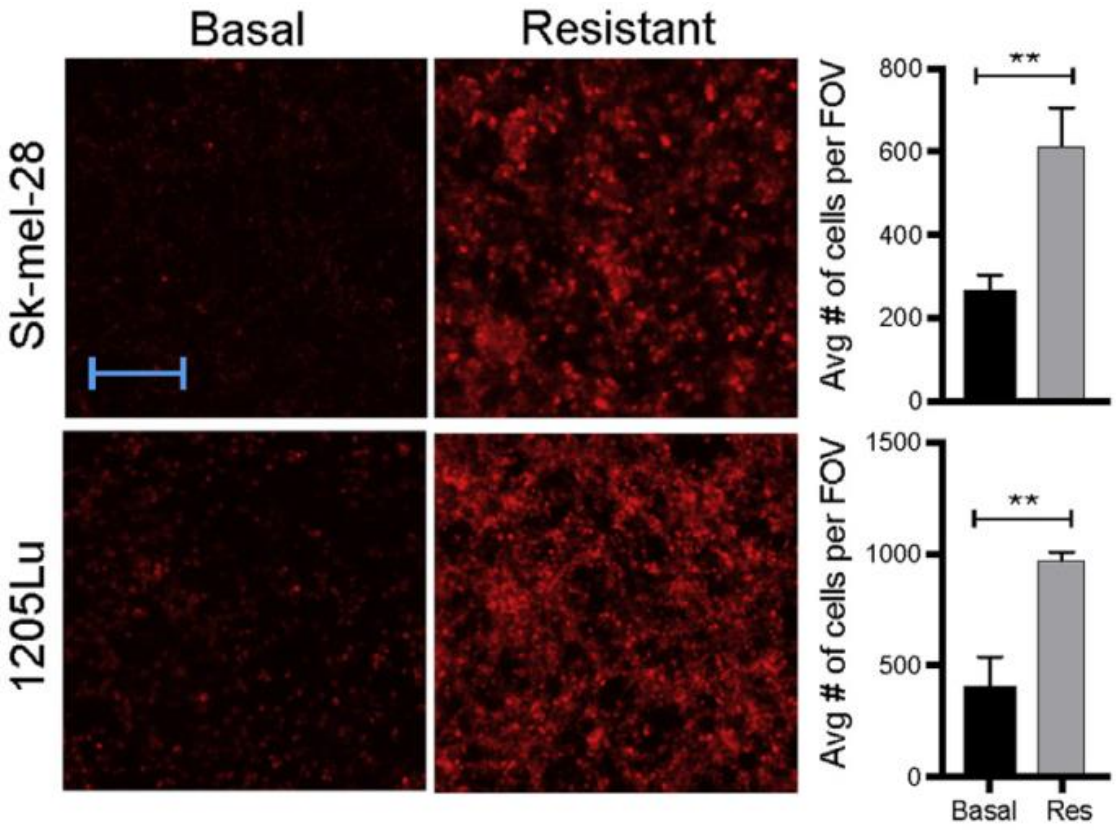

Figure 55. More resistant cells migrated though endothelial monolayers. Transendothelial migration assays of treatment-naïve and -resistant melanoma cells. Bars = 25 μm (white), 100 μm (black), and 200 μm (blue). Avg, average; FOV, field of view; PI3k, phosphoinositide-3 kinase; Res, resistant.

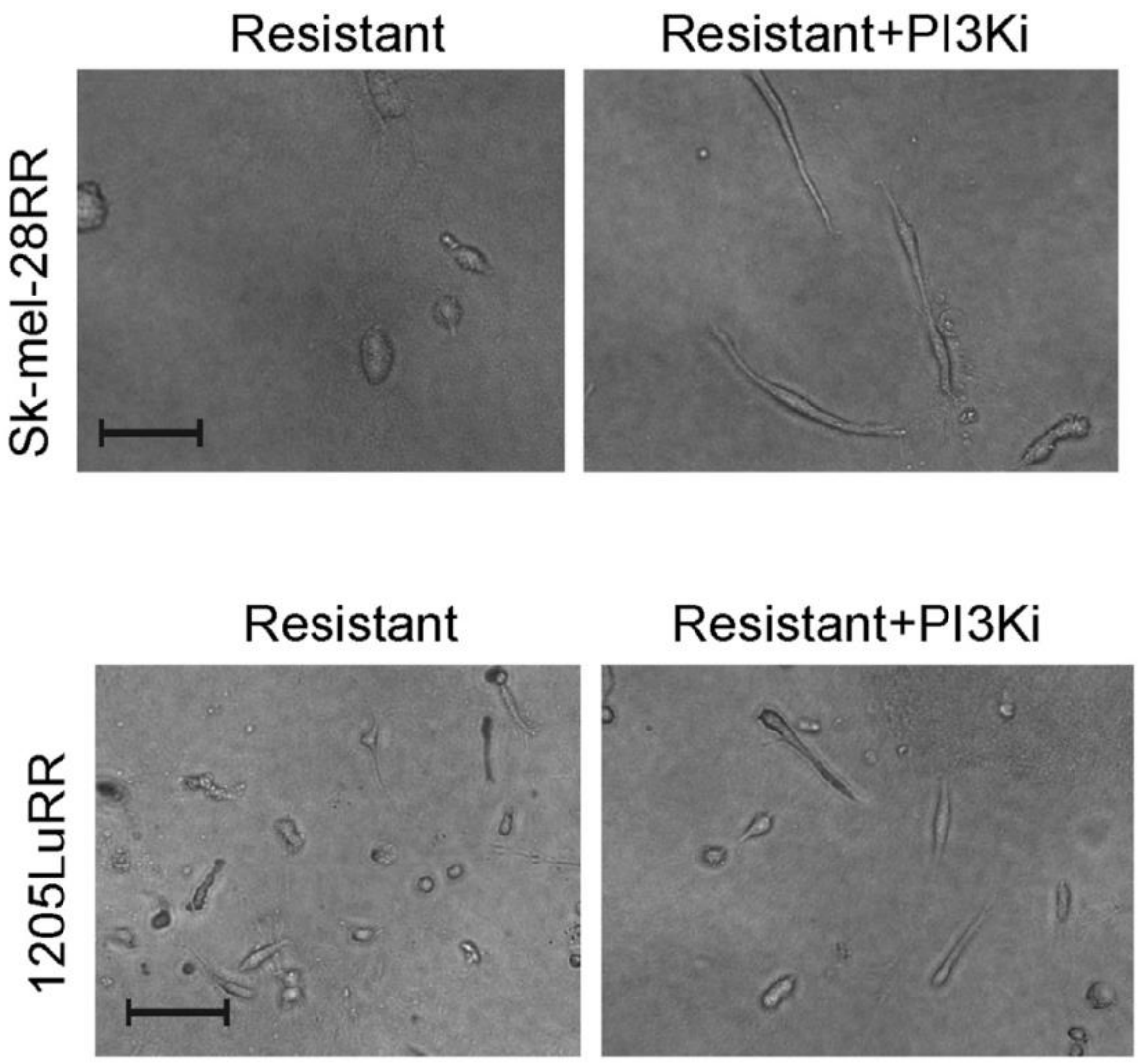

Figure 56. PI3K inhibition reversed amoeboid phenotype of resistant cells. GDC-0941 reverses the amoeboid phenotype in BRAF inhibitor-resistant 1205Lu and SKMEL28 BRAF mutant cell lines (3 μM, 72 hours). Bars = 25 μm (white), 100 μm (black), and 200 μm (blue). PI3k, phosphoinositide-3 kinase; PI3ki, PI3k inhibitor.

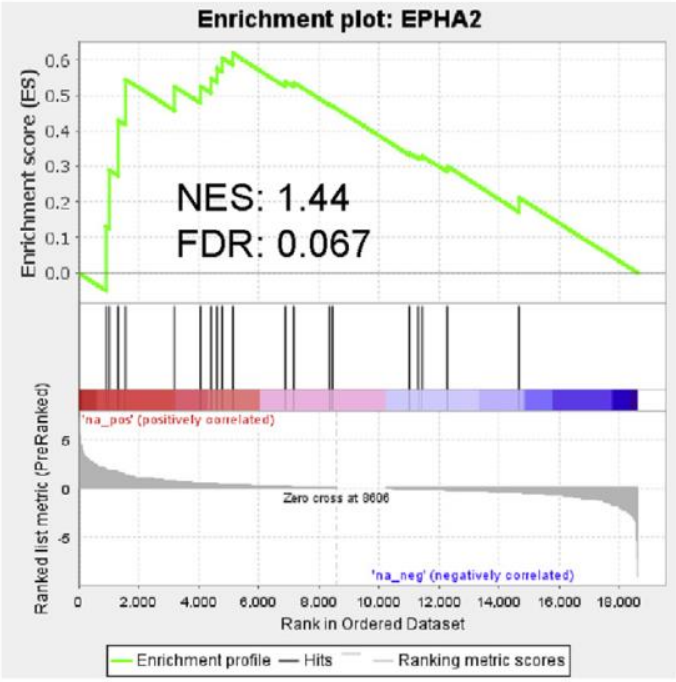

Figure 57. Upregulation of EphA2 gene signature was associated with HDAC8 overexpression. GSEA analysis shows that an EphA2 gene signature is upregulated in melanoma cells expressing HDAC8. FDR, false discovery rate; GSEA, Gene Set Enrichment Analysis; HDAC8, histone deacetylase 8; MAT, mesenchymal-to-amoeboid transition; NES, normalized enrichment score.

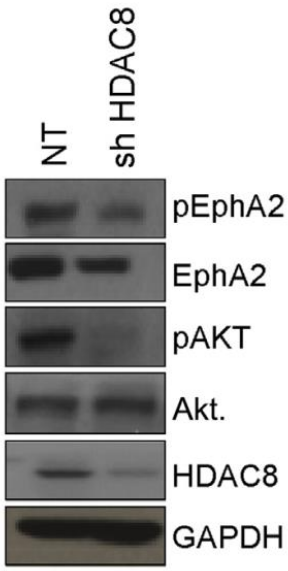

Figure 58. HDAC8 silencing decreased phosphorylation of EphA2 and AKT. Western blot following shRNA-mediated knockdown of HDAC8 (WM164RR). HDAC8, histone deacetylase 8; MAT, mesenchymal-to-amoeboid transition; NT, non-targeting; pAkt, phosphorylated Akt; pEphA2, phosphorylated EphA2; shHDAC8, short hairpin HDAC8; shRNA, short hairpin RNA.

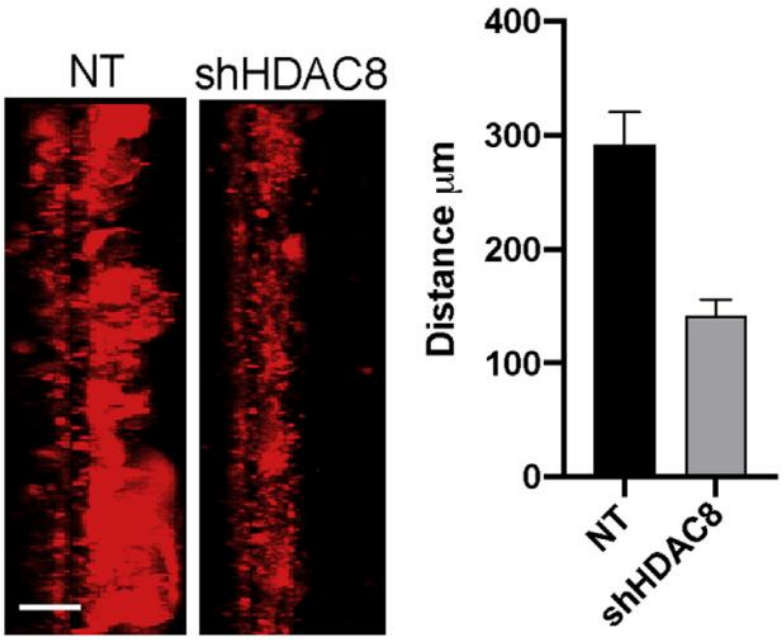

Figure 59. HDAC8 silencing decreased Matrigel invasion. Matrigel invasion assays of WM164RR cells following transfection with shRNA targeting HDAC8. Bar = 100 μm. HDAC8, histone deacetylase 8; MAT, mesenchymal-to-amoeboid transition; NT, non-targeting; shHDAC8, short hairpin HDAC8; shRNA, short hairpin RNA.

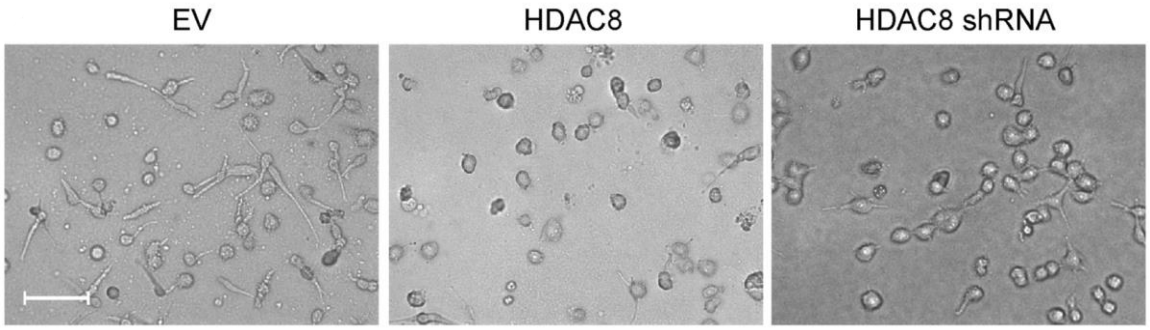

Figure 60. HDAC8 overexpression led to amoeboid phenotype. 1205Lu melanoma cells transfected with empty vector (EV), HDAC8 expression vector (HDAC8) or shRNA targeting HDAC8 (HDAC8 shRNA) in 3D culture on collagen. Bar = 100 μm. 3D, three-dimensional; EV, empty vector; HDAC8, histone deacetylase 8; MAT, mesenchymal-to-amoeboid transition; shRNA, short hairpin RNA.

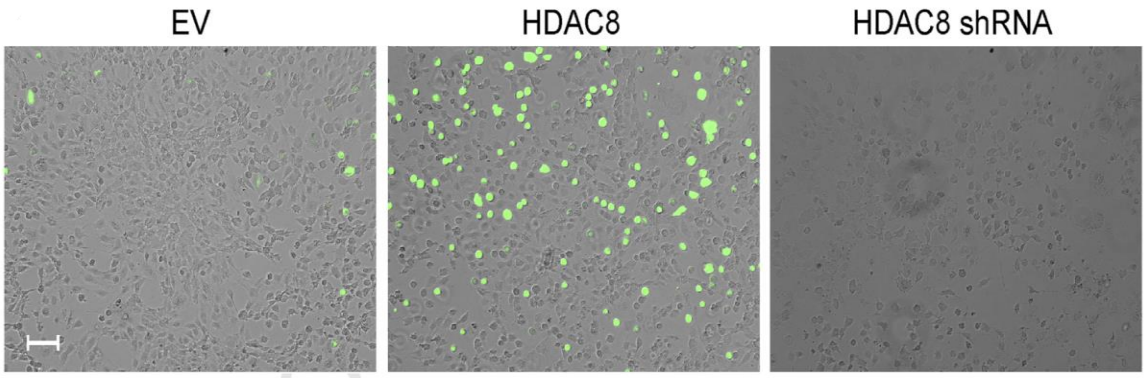

Figure 61. HDAC8 overexpression increased cell adhesion under shear stress. Attachment of melanoma cells transfected with empty vector (EV), HDAC8 expression vector (HDAC8) or shRNA targeting HDAC8 (HDAC8 shRNA) cells to HUVECs at 10 dyne/cm^2 fluid shear stress (1205Lu, 30min). Scale bar=100μm. EV, empty vector; FSS, fluid shear stress; HDAC8, histone deacetylase 8; HUVEC, human umbilical vein endothelial cell; MAT, mesenchymal-to-amoeboid transition; shRNA, short hairpin RNA.

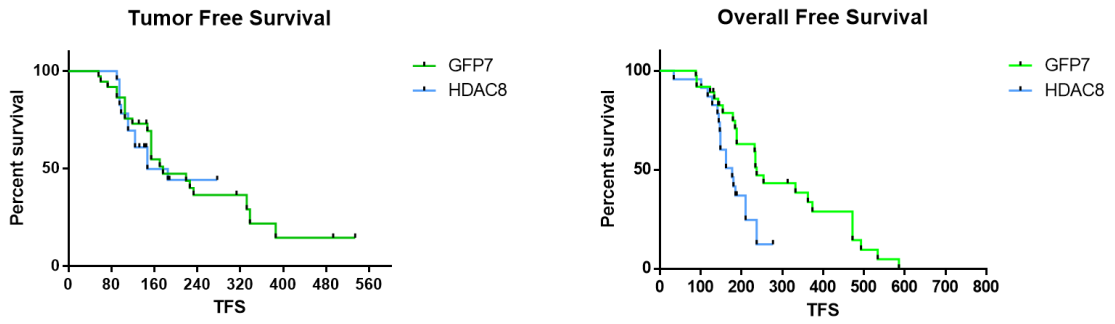

Figure 62. High levels of HDAC8 were associated with worse overall survival. Kaplan–Meier survival analysis of chimeric HDAC8 and GFP mice. The total number >10 in each type of mice. HDAC8, histone deacetylase 8; GFP, green fluorescent protein; MAT, mesenchymal-to-amoeboid transition.

DISCUSSION

Metastatic spread and distal invasion remain huge challenges in the treatment of late-stage melanoma patients [340, 341]. These processes are frequently associated with poor survival and responsible for most deaths [340]. The development of distant metastases is a complex, multi-step process that involves the escape of cells from the initial tumor, their intravasation into the blood circulation, arrest of the cells in a capillary bed, extravasation, and the establishment of new tumor cell colonies at the distant site [342]. Because of their high plasticity, melanoma cells can adopt multiple strategies for migration and invasion [239]. These morphological changes largely occur as adaptations to changes in the microenvironment. Amoeboid migration occurs in the absence of extracellular proteolysis and is associated with contraction of the cell body, allowing the cell to squeeze through the extracellular matrix [239]. Mechanistically, the round shape of the amoeboid cells is maintained due to RhoA/ROCK-mediated contraction of cortical actin, which depends on the phosphorylation of myosin light chain (MLC2) [245]. In accordance with this idea, we also detected high activity of RhoA in EphA2-S897E cells. Importantly, we found that a novel noncanonical EphA2-Cdc42-MLC2 pathways drives this amoeboid phenotype transition in melanoma cells.

Switching between the mesenchymal and amoeboid phenotypes is regulated through the activity of small GTPases. Rac1 plays a key role in mesenchymal movement by regulating actin assembly [243, 343]. RhoA activates downstream ROCK family kinases leading to cortical actin assembly and increased actomyosin contractility [237, 344, 345]. Cdc42 can induce the amoeboid phenotype in melanoma cells following its activation by DOCK10 [247]. Ameboid melanoma cells can utilize a variety of mechanisms to maintain the high levels of Myosin II activity. First, Sma-

and Mad-related protein 2 (SMAD2)-CITED1 driven transcription are activated by transforming growth factor beta (TGFβ) secreted by amoeboid melanoma cells. The TGFβ-SMAD2-CITED1 axis regulates and sustains actomyosin force and then promotes melanoma progression [346]. Next, lower levels of Reactive Oxygen Species (ROS) in amoeboid melanoma cells can promote Myosin II activity by reducing ARHGAP5 which suppresses Rho-ROCK-MLC2 signaling [347]. Moreover, a recent report shows that WNT11/5B-FZD7-DAAM1 signaling axis directly activate RhoA-ROCK to support the amoeboid phenotype [249].

Adoption of an amoeboid phenotype likely contributes to metastatic dissemination in many ways. First, cells in the blood circulation are subjected to high levels of hemodynamic shear stress that can range over four orders of magnitude, causing the rapid death of most of the tumor circulating cells [348]. Although little is known about the direct role of the amoeboid phenotype in the protection from shear stress, there is evidence that inhibiting ROCK can reduce the survival of cells subjected to shear stress *in vitro* [349] and that spheroid morphology, characteristic of the amoeboid cells, can withstand this harsh environment better and survive high shear stress [350, 351].

It has been shown that amoeboid invasive cells are enriched near the invasive front area and the edge of human and mouse melanoma tumors, while the cells near the core of tumor are most in the elongated-mesenchymal state [249, 339, 346, 352, 353]. These amoeboid cells typically located at the edge of tumor are more active in communication with the surrounding tissues, which also support our findings. As we showed, the invasive amoeboid cells are associated with and interact with endothelial cell monolayers in adhesion, trans-endothelial migration, and modification of membrane integrity. Besides the endothelial cells in tumor microenvironment, a variety of normal cells such as stromal and immune cells contribute to tumorigenesis through communication with the cancer cells [354]. Typically, the monocytes can be attracted and polarized into CD163+CD206+ tumor-associated macrophages by secretion driven by crosstalk of ROCK-MLC2-NF-κB. These transformed macrophages facilitate melanoma cell growth [353].

Moreover, the abrogated endothelial junctions and increased permeability in endothelial cell monolayers are due to the ROCK-MLC2-driven IL-1α secretion and NF-κB activation in amoeboid melanoma cells [353]. Additionally, the drug resistant melanoma tumors with high levels of MLC2 can recruit immunosuppressive FoxP3+ T cells [339].

So far, morphological-based markers have not been utilized to select potential treatment strategies. We have shown here that the amoeboid phenotype in melanoma has a high preference for migration and invasion and is associated with drug resistance, providing evidence that potential risk for metastasis could be inferred through the study of cell morphology and signaling. These potential amoeboid markers, including high levels of ROCK-MLC2 pathway regulators [352] and high expression of CITED1 [346], are highly associated with worse prognosis. Alternately, our findings with HDAC8 suggest that the amoeboid state might be associated with a broader, more aggressive melanoma phenotype that contributes to both metastasis and drug resistance. Taken together, these markers could be used for prediction of worse outcomes in melanoma patients and improve the clinical outcomes.

Here, we demonstrated that noncanonical EphA2 signaling, especially EphA2 S897 phosphorylation, is the key driver that promotes the invasive MAT phenotype was also associated with acquired drug resistance in melanoma. In agreement with this, the high level of EphA2 S897 phosphorylation and Akt S473 phosphorylation were co-localized in human glioma specimens [298]. The EphA2 S897 phosphorylation catalyzed by Akt was also observed in our study, and we showed that PI3K inhibition could reverse the aggressive MAT phenotype in melanoma. Other evidence from the study of prostate and pancreatic cancer, has shown that EphA2 S897 can be phosphorylated by protein kinase A (PKA) [297].

We further observed that the morphological changes driven by noncanonical EphA2 signaling are also seen in melanoma cells cultured in 3D collagen. Consistent with our observations, it has been demonstrated that high levels of EphA2 S897 phosphorylation are found at the migrating front in lamellipodia [303]. In this instance, phosphorylated EphA2 was found to regulate the

assembly of the actin cytoskeleton and extension of lamellipodia, controlling cell motility and morphology [303]. A further role for EphA2 in metastatic behavior was also suggested by the co-localization of S897-EphA2 and MT1-MMP in ovarian carcinoma, but not in cells of the normal ovary [355, 356].

The co-localization of RSK S380 and S897-EphA2 have been widely detected in multiple cancer tissues including lung, stomach, colorectal, liver and thyroid specimens, where they are associated with poor survival. It therefore seems likely that across tumor types noncanonical EphA2 signaling is linked to tumor aggressiveness [303]. Further studies also suggest noncanonical EphA2 signaling is associated with drug resistance with our study implicating it acquired resistance to BRAF inhibitors [327], and others showing a link to EGFR inhibitor resistance in NSCLC [304].

Since the high expression of EphA2, especially the S897 phosphorylation, correlated with later stage tumors, the aggressive progression and shorter survival in patients [286, 295, 315, 327, 328], inhibition of EphA2 and its S897 phosphorylation could represent a novel therapeutic target in melanoma (and other tumors as well). Tyrosine kinase inhibitors directed against EphA2 would not be a good option due to diverse interactions of EphA2 with Akt, RSK and PKA [297, 299, 303]. Instead, agonists targeting the EphA2 receptor and antibody-based immunotherapy could be utilized to block S897-EphA2 signaling andl potentially abrogate metastatic dissemination [254]. First, artificial ligands such as soluble ephrin A1 induce EphA2 internalization and downregulation in a paracrine manner, which significantly alter the cell morphology, and also suppress the migration in GBM and human breast cancer cells [357, 358]. Besides ephrin A1, ephrin A1-Fc which dimerization by fusion of recombinant Ephrin A1 and human IgG Fc potentially induce the EphA2 degradation to inhibit gastric cancer cell growth and pancreatic cancer cell motility and invasion [359, 360]. Second, the EphA2 monoclonal antibodies mimic the ligands. The malignant features of EphA2 are strongly attenuated by its internalization and degradation induced by these agonist monoclonal antibodies. For example, one monoclonal antibody SHM16 interacting with

an EphA2 epitope other than ephrin A1 cause antibody internalization and inhibit migration and invasion in melanoma cells [361]. In addition, small molecules targeting the ligand-binding domain of EphA2 inhibit the Eph-ephrin interaction and further block the EphA2 phosphorylation [362, 363]. Furthermore, a tumor immunotherapeutic approach-chimeric antigen receptors (CARs) modified T (CAR-T) cell therapy has been developed to target EphA2 specifically. It has been demonstrated that EphA2-expressing glioblastoma cells can be identified and killed by these EphA2-specific T cells [364]. In combination with current immunotherapies, such as anti-PD1 or anti-CTLA4, inhibition of EphA2 could be an excellent strategy to improve the response and overcome resistance.

In response to multiple stresses, melanoma cells upregulate a transcriptional program that downregulates apoptosis, increases MAPK signaling, and leads to reorganization of the actin cytoskeleton and increased invasive capacity [163, 337]. In this study, we showed that HDAC8 is responsible for maintaining EphA2 noncanonical signaling, as we found that HDAC8 silencing inhibits both EphA2 S897 phosphorylation and Akt phosphorylation and abrogates the invasion associated with drug resistance. Increased expression of HDAC8 was associated with the enrichment of an EphA2 transcriptional program, the adoption of a MAT-like state, and increased adhesion to endothelial cells. Our observations are supported by other studies demonstrating that resistance to both BRAF inhibitor therapy and immunotherapy is associated with increased MLC2 and ROCK signaling and the adoption of an amoeboid phenotype [339]. Although systemic BRAF inhibitor therapy is only used in the metastatic setting, our findings do not suggest that all melanoma metastases are drug resistant. Rather, it is likely that there is cell-state plasticity and that metastases are seeded by minor subpopulations of cells that then revert to a more drug-sensitive, proliferative, and less invasive state once established in new organs [337, 365, 366]. A better understanding of this process is expected to lead to the development of novel treatment strategies such as the use of epigenetic inhibitors that may abrogate the transcriptional plasticity

that underlies adaptation to BRAF and BRAF/MAPK/extracellular signal–regulated kinase inhibitor therapy.

REFERENCES

1. Guy, G.P., Jr., et al., *Vital signs: melanoma incidence and mortality trends and projections - United States, 1982-2030.* MMWR Morb Mortal Wkly Rep, 2015. **64**(21): p. 591-6.
2. Guy, G.P., Jr., et al., *Prevalence and costs of skin cancer treatment in the U.S., 2002-2006 and 2007-2011.* Am J Prev Med, 2015. **48**(2): p. 183-187.
3. Rogers, H.W., et al., *Incidence Estimate of Nonmelanoma Skin Cancer (Keratinocyte Carcinomas) in the U.S. Population, 2012.* JAMA Dermatol, 2015. **151**(10): p. 1081-6.
4. *Cancer Facts & Figures 2020*. 2020; Available from: https://www.cancer.org/research/cancer-facts-statistics/all-cancer-facts-figures/cancer-facts-figures-2020.html.
5. Stern, R.S., *Prevalence of a history of skin cancer in 2007: results of an incidence-based model.* Arch Dermatol, 2010. **146**(3): p. 279-82.
6. *Skin Cancer Facts & Statistics*. 2021; Available from: https://www.skincancer.org/skin-cancer-information/skin-cancer-facts/.
7. *What Are Basal and Squamous Cell Skin Cancers?* 2019; Available from: https://www.cancer.org/cancer/basal-and-squamous-cell-skin-cancer/about/what-is-basal-and-squamous-cell.html.
8. Samarasinghe, V. and V. Madan, *Nonmelanoma skin cancer.* J Cutan Aesthet Surg, 2012. **5**(1): p. 3-10.
9. Paolino, G., et al., *Histology of Non-Melanoma Skin Cancers: An Update.* Biomedicines, 2017. **5**(4).
10. Becker, J.C., et al., *Merkel cell carcinoma.* Nat Rev Dis Primers, 2017. **3**: p. 17077.
11. Pulitzer, M., *Merkel Cell Carcinoma.* Surg Pathol Clin, 2017. **10**(2): p. 399-408.
12. *Cancer Facts & Figures 2019*. 2019; Available from: https://www.cancer.org/research/cancer-facts-statistics/all-cancer-facts-figures/cancer-facts-figures-2019.html.
13. Whiteman, D.C., A.C. Green, and C.M. Olsen, *The Growing Burden of Invasive Melanoma: Projections of Incidence Rates and Numbers of New Cases in Six Susceptible Populations through 2031.* J Invest Dermatol, 2016. **136**(6): p. 1161-1171.
14. *Cancer Facts & Figures 2021*. 2021, Atlanta: American Cancer Society.
15. Gupta, A.K., M. Bharadwaj, and R. Mehrotra, *Skin Cancer Concerns in People of Color: Risk Factors and Prevention.* Asian Pac J Cancer Prev, 2016. **17**(12): p. 5257-5264.
16. *Key Statistics for Melanoma Skin Cancer*. 2021; Available from: https://www.cancer.org/cancer/melanoma-skin-cancer/about/key-statistics.html.
17. Swetter, S.M., A.C. Geller, and J.M. Kirkwood, *Melanoma in the older person.* Oncology (Williston Park), 2004. **18**(9): p. 1187-96; discussion 1196-7.
18. Reed, K.B., et al., *Increasing incidence of melanoma among young adults: an epidemiological study in Olmsted County, Minnesota.* Mayo Clin Proc, 2012. **87**(4): p. 328-34.
19. Fidler, M.M., et al., *Cancer incidence and mortality among young adults aged 20-39 years worldwide in 2012: a population-based study.* Lancet Oncol, 2017. **18**(12): p. 1579-1589.

20. Weir, H.K., et al., *Melanoma in adolescents and young adults (ages 15-39 years): United States, 1999-2006.* J Am Acad Dermatol, 2011. **65**(5 Suppl 1): p. S38-49.
21. American Academy of Dermatology Ad Hoc Task Force for the, A.o.M., et al., *Early detection of melanoma: reviewing the ABCDEs.* J Am Acad Dermatol, 2015. **72**(4): p. 717-23.
22. Benvenuto-Andrade, C., et al., *Cutaneous melanoma: surveillance of patients for recurrence and new primary melanomas.* Dermatol Ther, 2005. **18**(6): p. 423-35.
23. Abbasi, N.R., et al., *Early diagnosis of cutaneous melanoma: revisiting the ABCD criteria.* JAMA, 2004. **292**(22): p. 2771-6.
24. Bronsnick, T., et al., *From mole to scar: the unintended consequence of treatment with an over-the-counter mole removal cream.* Skinmed, 2013. **11**(6): p. 364-6.
25. McAllister, J.C., C.R. Petzold, and P.A. Lio, *Adverse effects of a mole removal cream.* Pediatr Dermatol, 2009. **26**(5): p. 628-9.
26. Pollock, P.M., et al., *High frequency of BRAF mutations in nevi.* Nat Genet, 2003. **33**(1): p. 19-20.
27. Poynter, J.N., et al., *BRAF and NRAS mutations in melanoma and melanocytic nevi.* Melanoma Res, 2006. **16**(4): p. 267-73.
28. Thomas, N.E., *BRAF somatic mutations in malignant melanoma and melanocytic naevi.* Melanoma Res, 2006. **16**(2): p. 97-103.
29. Bauer, J., et al., *Congenital melanocytic nevi frequently harbor NRAS mutations but no BRAF mutations.* J Invest Dermatol, 2007. **127**(1): p. 179-82.
30. Tsao, H., et al., *The transformation rate of moles (melanocytic nevi) into cutaneous melanoma: a population-based estimate.* Arch Dermatol, 2003. **139**(3): p. 282-8.
31. Shain, A.H., et al., *Genomic and Transcriptomic Analysis Reveals Incremental Disruption of Key Signaling Pathways during Melanoma Evolution.* Cancer Cell, 2018. **34**(1): p. 45-55 e4.
32. Marks, R., A.P. Dorevitch, and G. Mason, *Do all melanomas come from "moles"? A study of the histological association between melanocytic naevi and melanoma.* Australas J Dermatol, 1990. **31**(2): p. 77-80.
33. Marks, R., *An overview of skin cancers. Incidence and causation.* Cancer, 1995. **75**(2 Suppl): p. 607-12.
34. Bevona, C., et al., *Cutaneous melanomas associated with nevi.* Arch Dermatol, 2003. **139**(12): p. 1620-4; discussion 1624.
35. Scolyer, R.A., G.V. Long, and J.F. Thompson, *Evolving concepts in melanoma classification and their relevance to multidisciplinary melanoma patient care.* Mol Oncol, 2011. **5**(2): p. 124-36.
36. Greenwald, H.S., E.B. Friedman, and I. Osman, *Superficial spreading and nodular melanoma are distinct biological entities: a challenge to the linear progression model.* Melanoma Res, 2012. **22**(1): p. 1-8.
37. Clark, W.H., Jr., et al., *The histogenesis and biologic behavior of primary human malignant melanomas of the skin.* Cancer Res, 1969. **29**(3): p. 705-27.
38. Rabbie, R., et al., *Melanoma subtypes: genomic profiles, prognostic molecular markers and therapeutic possibilities.* J Pathol, 2019. **247**(5): p. 539-551.
39. Whiteman, D.C., et al., *Anatomic site, sun exposure, and risk of cutaneous melanoma.* J Clin Oncol, 2006. **24**(19): p. 3172-7.
40. Porras, B.H. and C.J. Cockerell, *Cutaneous malignant melanoma: classification and clinical diagnosis.* Semin Cutan Med Surg, 1997. **16**(2): p. 88-96.
41. Linos, E., et al., *Increasing burden of melanoma in the United States.* J Invest Dermatol, 2009. **129**(7): p. 1666-74.
42. Kalkhoran, S., et al., *Historical, clinical, and dermoscopic characteristics of thin nodular melanoma.* Arch Dermatol, 2010. **146**(3): p. 311-8.

43. Langholz, B., et al., *Skin characteristics and risk of superficial spreading and nodular melanoma (United States).* Cancer Causes Control, 2000. **11**(8): p. 741-50.
44. Elwood, J.M. and R.P. Gallagher, *Site distribution of malignant melanoma.* Can Med Assoc J, 1983. **128**(12): p. 1400-4.
45. Gaudy-Marqueste, C., et al., *Risk factors in elderly people for lentigo maligna compared with other melanomas: a double case-control study.* Arch Dermatol, 2009. **145**(4): p. 418-23.
46. Bradford, P.T., et al., *Acral lentiginous melanoma: incidence and survival patterns in the United States, 1986-2005.* Arch Dermatol, 2009. **145**(4): p. 427-34.
47. Goydos, J.S. and S.L. Shoen, *Acral Lentiginous Melanoma.* Cancer Treat Res, 2016. **167**: p. 321-9.
48. Kim, S.Y. and S.J. Yun, *Cutaneous Melanoma in Asians.* Chonnam Med J, 2016. **52**(3): p. 185-93.
49. Egger, M.E., et al., *Unique prognostic factors in acral lentiginous melanoma.* Am J Surg, 2012. **204**(6): p. 874-9; discussion 879-80.
50. Chang, J.W., *Acral melanoma: a unique disease in Asia.* JAMA Dermatol, 2013. **149**(11): p. 1272-3.
51. Merkel, E.A. and P. Gerami, *Malignant melanoma of sun-protected sites: a review of clinical, histological, and molecular features.* Lab Invest, 2017. **97**(6): p. 630-635.
52. Koh, H.K., et al., *Prevention and early detection strategies for melanoma and skin cancer. Current status.* Arch Dermatol, 1996. **132**(4): p. 436-43.
53. El Ghissassi, F., et al., *A review of human carcinogens--part D: radiation.* Lancet Oncol, 2009. **10**(8): p. 751-2.
54. Le Clair, M.Z. and M.G. Cockburn, *Tanning bed use and melanoma: Establishing risk and improving prevention interventions.* Prev Med Rep, 2016. **3**: p. 139-44.
55. Dennis, L.K., et al., *Sunburns and risk of cutaneous melanoma: does age matter? A comprehensive meta-analysis.* Ann Epidemiol, 2008. **18**(8): p. 614-27.
56. Oliveria, S.A., et al., *Sun exposure and risk of melanoma.* Arch Dis Child, 2006. **91**(2): p. 131-8.
57. Greene, M.H., et al., *High risk of malignant melanoma in melanoma-prone families with dysplastic nevi.* Ann Intern Med, 1985. **102**(4): p. 458-65.
58. Titus-Ernstoff, L., et al., *Pigmentary characteristics and moles in relation to melanoma risk.* Int J Cancer, 2005. **116**(1): p. 144-9.
59. Frank, C., et al., *Risk of other Cancers in Families with Melanoma: Novel Familial Links.* Sci Rep, 2017. **7**: p. 42601.
60. Ford, D., et al., *Risk of cutaneous melanoma associated with a family history of the disease. The International Melanoma Analysis Group (IMAGE).* Int J Cancer, 1995. **62**(4): p. 377-81.
61. Rangwala, S. and K.Y. Tsai, *Roles of the immune system in skin cancer.* Br J Dermatol, 2011. **165**(5): p. 953-65.
62. Psaty, E.L., et al., *Defining the patient at high risk for melanoma.* Int J Dermatol, 2010. **49**(4): p. 362-76.
63. Siskind, V., et al., *Nevi, family history, and fair skin increase the risk of second primary melanoma.* J Invest Dermatol, 2011. **131**(2): p. 461-7.
64. Reiche, E.M., S.O. Nunes, and H.K. Morimoto, *Stress, depression, the immune system, and cancer.* Lancet Oncol, 2004. **5**(10): p. 617-25.
65. Dickson, P.V. and J.E. Gershenwald, *Staging and prognosis of cutaneous melanoma.* Surg Oncol Clin N Am, 2011. **20**(1): p. 1-17.
66. Sandru, A., et al., *Survival rates of patients with metastatic malignant melanoma.* J Med Life, 2014. **7**(4): p. 572-6.

67. Tas, F., *Metastatic behavior in melanoma: timing, pattern, survival, and influencing factors.* J Oncol, 2012. **2012**: p. 647684.
68. Owen, S.A., et al., *Identification of higher risk thin melanomas should be based on Breslow depth not Clark level IV.* Cancer, 2001. **91**(5): p. 983-91.
69. Cherobin, A., et al., *Prognostic factors for metastasis in cutaneous melanoma.* An Bras Dermatol, 2018. **93**(1): p. 19-26.
70. von Schuckmann, L.A., et al., *Risk of Melanoma Recurrence After Diagnosis of a High-Risk Primary Tumor.* JAMA Dermatol, 2019. **155**(6): p. 688-693.
71. Zbytek, B., et al., *Current concepts of metastasis in melanoma.* Expert Rev Dermatol, 2008. **3**(5): p. 569-585.
72. Damsky, W.E., L.E. Rosenbaum, and M. Bosenberg, *Decoding melanoma metastasis.* Cancers (Basel), 2010. **3**(1): p. 126-63.
73. Gershenwald, J.E., et al., *Melanoma staging: Evidence-based changes in the American Joint Committee on Cancer eighth edition cancer staging manual.* CA Cancer J Clin, 2017. **67**(6): p. 472-492.
74. Dinnes, J., et al., *Ultrasound, CT, MRI, or PET-CT for staging and re-staging of adults with cutaneous melanoma.* Cochrane Database Syst Rev, 2019. **7**: p. CD012806.
75. Volkovova, K., et al., *Associations between environmental factors and incidence of cutaneous melanoma. Review.* Environ Health, 2012. **11 Suppl 1**: p. S12.
76. Burden, A.D., et al., *Genetic and environmental influences in the development of multiple primary melanoma.* Arch Dermatol, 1999. **135**(3): p. 261-5.
77. Khan, A.Q., J.B. Travers, and M.G. Kemp, *Roles of UVA radiation and DNA damage responses in melanoma pathogenesis.* Environ Mol Mutagen, 2018. **59**(5): p. 438-460.
78. Schuch, A.P., et al., *Sunlight damage to cellular DNA: Focus on oxidatively generated lesions.* Free Radic Biol Med, 2017. **107**: p. 110-124.
79. Denat, L., et al., *Melanocytes as instigators and victims of oxidative stress.* J Invest Dermatol, 2014. **134**(6): p. 1512-1518.
80. Potrony, M., et al., *Update in genetic susceptibility in melanoma.* Ann Transl Med, 2015. **3**(15): p. 210.
81. Bertolotto, C., *Melanoma: from melanocyte to genetic alterations and clinical options.* Scientifica (Cairo), 2013. **2013**: p. 635203.
82. Leonardi, G.C., et al., *Cutaneous melanoma: From pathogenesis to therapy (Review).* Int J Oncol, 2018. **52**(4): p. 1071-1080.
83. Chin, L., L.A. Garraway, and D.E. Fisher, *Malignant melanoma: genetics and therapeutics in the genomic era.* Genes Dev, 2006. **20**(16): p. 2149-82.
84. Reddy, B.Y., D.M. Miller, and H. Tsao, *Somatic driver mutations in melanoma.* Cancer, 2017. **123**(S11): p. 2104-2117.
85. Alexandrov, L.B., et al., *Signatures of mutational processes in human cancer.* Nature, 2013. **500**(7463): p. 415-21.
86. Mehnert, J.M. and H.M. Kluger, *Driver mutations in melanoma: lessons learned from bench-to-bedside studies.* Curr Oncol Rep, 2012. **14**(5): p. 449-57.
87. Cheng, L., et al., *Molecular testing for BRAF mutations to inform melanoma treatment decisions: a move toward precision medicine.* Mod Pathol, 2018. **31**(1): p. 24-38.
88. Kudchadkar, R., K.H. Paraiso, and K.S. Smalley, *Targeting mutant BRAF in melanoma: current status and future development of combination therapy strategies.* Cancer J, 2012. **18**(2): p. 124-31.
89. Eriksson, H., et al., *BRAFV600E protein expression in primary cutaneous malignant melanomas and paired metastases.* JAMA Dermatol, 2015. **151**(4): p. 410-6.
90. Ascierto, P.A., et al., *The role of BRAF V600 mutation in melanoma.* J Transl Med, 2012. **10**: p. 85.

91. Klein, O., et al., *BRAF inhibitor activity in V600R metastatic melanoma--response.* Eur J Cancer, 2013. **49**(7): p. 1797-8.
92. Munoz-Couselo, E., et al., *NRAS-mutant melanoma: current challenges and future prospect.* Onco Targets Ther, 2017. **10**: p. 3941-3947.
93. Newell, F., et al., *Whole-genome landscape of mucosal melanoma reveals diverse drivers and therapeutic targets.* Nat Commun, 2019. **10**(1): p. 3163.
94. Tyrrell, H. and M. Payne, *Combatting mucosal melanoma: recent advances and future perspectives.* Melanoma Manag, 2018. **5**(3): p. MMT11.
95. Satzger, I., et al., *Analysis of c-KIT expression and KIT gene mutation in human mucosal melanomas.* Br J Cancer, 2008. **99**(12): p. 2065-9.
96. Beadling, C., et al., *KIT gene mutations and copy number in melanoma subtypes.* Clin Cancer Res, 2008. **14**(21): p. 6821-8.
97. Kong, Y., et al., *Large-scale analysis of KIT aberrations in Chinese patients with melanoma.* Clin Cancer Res, 2011. **17**(7): p. 1684-91.
98. Pho, L., D. Grossman, and S.A. Leachman, *Melanoma genetics: a review of genetic factors and clinical phenotypes in familial melanoma.* Curr Opin Oncol, 2006. **18**(2): p. 173-9.
99. Soura, E., et al., *Hereditary melanoma: Update on syndromes and management: Genetics of familial atypical multiple mole melanoma syndrome.* J Am Acad Dermatol, 2016. **74**(3): p. 395-407; quiz 408-10.
100. Helgadottir, H., et al., *CDKN2a mutation-negative melanoma families have increased risk exclusively for skin cancers but not for other malignancies.* Int J Cancer, 2015. **137**(9): p. 2220-6.
101. Hussussian, C.J., et al., *Germline p16 mutations in familial melanoma.* Nat Genet, 1994. **8**(1): p. 15-21.
102. Cancer Genome Atlas, N., *Genomic Classification of Cutaneous Melanoma.* Cell, 2015. **161**(7): p. 1681-96.
103. Stahl, J.M., et al., *Loss of PTEN promotes tumor development in malignant melanoma.* Cancer Res, 2003. **63**(11): p. 2881-90.
104. Wu, H., V. Goel, and F.G. Haluska, *PTEN signaling pathways in melanoma.* Oncogene, 2003. **22**(20): p. 3113-22.
105. Stahl, J.M., et al., *Deregulated Akt3 activity promotes development of malignant melanoma.* Cancer Res, 2004. **64**(19): p. 7002-10.
106. Rossi, M., et al., *Familial Melanoma: Diagnostic and Management Implications.* Dermatol Pract Concept, 2019. **9**(1): p. 10-16.
107. Sheppard, K.E. and G.A. McArthur, *The cell-cycle regulator CDK4: an emerging therapeutic target in melanoma.* Clin Cancer Res, 2013. **19**(19): p. 5320-8.
108. Merlino, G., et al., *The state of melanoma: challenges and opportunities.* Pigment Cell Melanoma Res, 2016. **29**(4): p. 404-16.
109. Ticha, I., et al., *A comprehensive evaluation of pathogenic mutations in primary cutaneous melanomas, including the identification of novel loss-of-function variants.* Sci Rep, 2019. **9**(1): p. 17050.
110. Toledo, F. and G.M. Wahl, *MDM2 and MDM4: p53 regulators as targets in anticancer therapy.* Int J Biochem Cell Biol, 2007. **39**(7-8): p. 1476-82.
111. Gembarska, A., et al., *MDM4 is a key therapeutic target in cutaneous melanoma.* Nat Med, 2012. **18**(8): p. 1239-47.
112. Li, Q. and G. Lozano, *Molecular pathways: targeting Mdm2 and Mdm4 in cancer therapy.* Clin Cancer Res, 2013. **19**(1): p. 34-41.
113. Tirosh, I., et al., *Dissecting the multicellular ecosystem of metastatic melanoma by single-cell RNA-seq.* Science, 2016. **352**(6282): p. 189-96.

114. Zhang, Z., et al., *Activation of the AXL kinase causes resistance to EGFR-targeted therapy in lung cancer.* Nat Genet, 2012. **44**(8): p. 852-60.
115. Wu, X., et al., *AXL kinase as a novel target for cancer therapy.* Oncotarget, 2014. **5**(20): p. 9546-63.
116. Hoek, K.S., et al., *In vivo switching of human melanoma cells between proliferative and invasive states.* Cancer Res, 2008. **68**(3): p. 650-6.
117. Konieczkowski, D.J., et al., *A melanoma cell state distinction influences sensitivity to MAPK pathway inhibitors.* Cancer Discov, 2014. **4**(7): p. 816-27.
118. Rambow, F., et al., *Toward Minimal Residual Disease-Directed Therapy in Melanoma.* Cell, 2018. **174**(4): p. 843-855 e19.
119. Garraway, L.A., et al., *Integrative genomic analyses identify MITF as a lineage survival oncogene amplified in malignant melanoma.* Nature, 2005. **436**(7047): p. 117-22.
120. Muller, J., et al., *Low MITF/AXL ratio predicts early resistance to multiple targeted drugs in melanoma.* Nat Commun, 2014. **5**: p. 5712.
121. Lister, J.A., et al., *A conditional zebrafish MITF mutation reveals MITF levels are critical for melanoma promotion vs. regression in vivo.* J Invest Dermatol, 2014. **134**(1): p. 133-140.
122. Carreira, S., et al., *Mitf regulation of Dia1 controls melanoma proliferation and invasiveness.* Genes Dev, 2006. **20**(24): p. 3426-39.
123. Hartman, M.L. and M. Czyz, *MITF in melanoma: mechanisms behind its expression and activity.* Cell Mol Life Sci, 2015. **72**(7): p. 1249-60.
124. Feige, E., et al., *Hypoxia-induced transcriptional repression of the melanoma-associated oncogene MITF.* Proc Natl Acad Sci U S A, 2011. **108**(43): p. E924-33.
125. Rambow, F., J.C. Marine, and C.R. Goding, *Melanoma plasticity and phenotypic diversity: therapeutic barriers and opportunities.* Genes Dev, 2019. **33**(19-20): p. 1295-1318.
126. Booy, E.P., E.S. Henson, and S.B. Gibson, *Epidermal growth factor regulates Mcl-1 expression through the MAPK-Elk-1 signalling pathway contributing to cell survival in breast cancer.* Oncogene, 2011. **30**(20): p. 2367-78.
127. Lavoie, J.N., et al., *Cyclin D1 expression is regulated positively by the p42/p44MAPK and negatively by the p38/HOGMAPK pathway.* J Biol Chem, 1996. **271**(34): p. 20608-16.
128. Schmelzle, T., et al., *Functional role and oncogene-regulated expression of the BH3-only factor Bmf in mammary epithelial anoikis and morphogenesis.* Proc Natl Acad Sci U S A, 2007. **104**(10): p. 3787-92.
129. Paraiso, K.H., et al., *PTEN loss confers BRAF inhibitor resistance to melanoma cells through the suppression of BIM expression.* Cancer Res, 2011. **71**(7): p. 2750-60.
130. Balmanno, K. and S.J. Cook, *Tumour cell survival signalling by the ERK1/2 pathway.* Cell Death Differ, 2009. **16**(3): p. 368-77.
131. Gallo, A., et al., *Menin uncouples Elk-1, JunD and c-Jun phosphorylation from MAP kinase activation.* Oncogene, 2002. **21**(42): p. 6434-45.
132. Reddy, K.B., et al., *Mitogen-activated protein kinase (MAPK) regulates the expression of progelatinase B (MMP-9) in breast epithelial cells.* Int J Cancer, 1999. **82**(2): p. 268-73.
133. Kumar, B., et al., *p38 mitogen-activated protein kinase-driven MAPKAPK2 regulates invasion of bladder cancer by modulation of MMP-2 and MMP-9 activity.* Cancer Res, 2010. **70**(2): p. 832-41.
134. Berra, E., G. Pages, and J. Pouyssegur, *MAP kinases and hypoxia in the control of VEGF expression.* Cancer Metastasis Rev, 2000. **19**(1-2): p. 139-45.
135. Wilhelm, S., et al., *Discovery and development of sorafenib: a multikinase inhibitor for treating cancer.* Nat Rev Drug Discov, 2006. **5**(10): p. 835-44.

136. Eisen, T., et al., *Sorafenib in advanced melanoma: a Phase II randomised discontinuation trial analysis.* Br J Cancer, 2006. **95**(5): p. 581-6.
137. Hauschild, A., et al., *Results of a phase III, randomized, placebo-controlled study of sorafenib in combination with carboplatin and paclitaxel as second-line treatment in patients with unresectable stage III or stage IV melanoma.* J Clin Oncol, 2009. **27**(17): p. 2823-30.
138. Flaherty, K.T., et al., *Phase III trial of carboplatin and paclitaxel with or without sorafenib in metastatic melanoma.* J Clin Oncol, 2013. **31**(3): p. 373-9.
139. Kane, R.C., et al., *Sorafenib for the treatment of advanced renal cell carcinoma.* Clin Cancer Res, 2006. **12**(24): p. 7271-8.
140. Joseph, E.W., et al., *The RAF inhibitor PLX4032 inhibits ERK signaling and tumor cell proliferation in a V600E BRAF-selective manner.* Proc Natl Acad Sci U S A, 2010. **107**(33): p. 14903-8.
141. Bollag, G., et al., *Clinical efficacy of a RAF inhibitor needs broad target blockade in BRAF-mutant melanoma.* Nature, 2010. **467**(7315): p. 596-9.
142. Chapman, P.B., et al., *Vemurafenib in patients with BRAFV600 mutation-positive metastatic melanoma: final overall survival results of the randomized BRIM-3 study.* Ann Oncol, 2017. **28**(10): p. 2581-2587.
143. Kim, G., et al., *FDA approval summary: vemurafenib for treatment of unresectable or metastatic melanoma with the BRAFV600E mutation.* Clin Cancer Res, 2014. **20**(19): p. 4994-5000.
144. Hauschild, A., et al., *Dabrafenib in BRAF-mutated metastatic melanoma: a multicentre, open-label, phase 3 randomised controlled trial.* Lancet, 2012. **380**(9839): p. 358-65.
145. Hauschild, A., et al., *Long-term outcomes in patients with BRAF V600-mutant metastatic melanoma receiving dabrafenib monotherapy: Analysis from phase 2 and 3 clinical trials.* Eur J Cancer, 2020. **125**: p. 114-120.
146. Long, G.V., et al., *Dabrafenib in patients with Val600Glu or Val600Lys BRAF-mutant melanoma metastatic to the brain (BREAK-MB): a multicentre, open-label, phase 2 trial.* Lancet Oncol, 2012. **13**(11): p. 1087-95.
147. Grob, J.J., et al., *Patient perception of the benefit of a BRAF inhibitor in metastatic melanoma: quality-of-life analyses of the BREAK-3 study comparing dabrafenib with dacarbazine.* Ann Oncol, 2014. **25**(7): p. 1428-1436.
148. Falchook, G.S., et al., *Dabrafenib in patients with melanoma, untreated brain metastases, and other solid tumours: a phase 1 dose-escalation trial.* Lancet, 2012. **379**(9829): p. 1893-901.
149. Sullivan, R.J. and K. Flaherty, *MAP kinase signaling and inhibition in melanoma.* Oncogene, 2013. **32**(19): p. 2373-9.
150. Flaherty, K.T., et al., *Improved survival with MEK inhibition in BRAF-mutated melanoma.* N Engl J Med, 2012. **367**(2): p. 107-14.
151. Wright, C.J. and P.L. McCormack, *Trametinib: first global approval.* Drugs, 2013. **73**(11): p. 1245-54.
152. Ascierto, P.A., et al., *Phase II trial (BREAK-2) of the BRAF inhibitor dabrafenib (GSK2118436) in patients with metastatic melanoma.* J Clin Oncol, 2013. **31**(26): p. 3205-11.
153. Sullivan, R.J. and K.T. Flaherty, *Resistance to BRAF-targeted therapy in melanoma.* Eur J Cancer, 2013. **49**(6): p. 1297-304.
154. Kugel, C.H., 3rd and A.E. Aplin, *Adaptive resistance to RAF inhibitors in melanoma.* Pigment Cell Melanoma Res, 2014. **27**(6): p. 1032-8.
155. Shi, H., et al., *Melanoma whole-exome sequencing identifies (V600E)B-RAF amplification-mediated acquired B-RAF inhibitor resistance.* Nat Commun, 2012. **3**: p. 724.

156. Fedorenko, I.V., et al., *BRAF Inhibition Generates a Host-Tumor Niche that Mediates Therapeutic Escape.* J Invest Dermatol, 2015. **135**(12): p. 3115-3124.
157. Smalley, K.S. and K.T. Flaherty, *Integrating BRAF/MEK inhibitors into combination therapy for melanoma.* Br J Cancer, 2009. **100**(3): p. 431-5.
158. Smalley, K.S., Z. Eroglu, and V.K. Sondak, *Combination Therapies for Melanoma: A New Standard of Care?* Am J Clin Dermatol, 2016. **17**(2): p. 99-105.
159. Solit, D.B. and N. Rosen, *Towards a unified model of RAF inhibitor resistance.* Cancer Discov, 2014. **4**(1): p. 27-30.
160. Lito, P., N. Rosen, and D.B. Solit, *Tumor adaptation and resistance to RAF inhibitors.* Nat Med, 2013. **19**(11): p. 1401-9.
161. Solit, D.B., et al., *BRAF mutation predicts sensitivity to MEK inhibition.* Nature, 2006. **439**(7074): p. 358-62.
162. Escuin-Ordinas, H., et al., *Cutaneous wound healing through paradoxical MAPK activation by BRAF inhibitors.* Nat Commun, 2016. **7**: p. 12348.
163. Hugo, W., et al., *Non-genomic and Immune Evolution of Melanoma Acquiring MAPKi Resistance.* Cell, 2015. **162**(6): p. 1271-85.
164. Moriceau, G., et al., *Tunable-combinatorial mechanisms of acquired resistance limit the efficacy of BRAF/MEK cotargeting but result in melanoma drug addiction.* Cancer Cell, 2015. **27**(2): p. 240-56.
165. Menzies, A.M. and G.V. Long, *Dabrafenib and trametinib, alone and in combination for BRAF-mutant metastatic melanoma.* Clin Cancer Res, 2014. **20**(8): p. 2035-43.
166. Long, G.V., et al., *Combined BRAF and MEK inhibition versus BRAF inhibition alone in melanoma.* N Engl J Med, 2014. **371**(20): p. 1877-88.
167. Ascierto, P.A., et al., *Cobimetinib combined with vemurafenib in advanced BRAF(V600)-mutant melanoma (coBRIM): updated efficacy results from a randomised, double-blind, phase 3 trial.* Lancet Oncol, 2016. **17**(9): p. 1248-60.
168. Eroglu, Z. and A. Ribas, *Combination therapy with BRAF and MEK inhibitors for melanoma: latest evidence and place in therapy.* Ther Adv Med Oncol, 2016. **8**(1): p. 48-56.
169. Robert, C., et al., *Five-Year Outcomes with Dabrafenib plus Trametinib in Metastatic Melanoma.* N Engl J Med, 2019. **381**(7): p. 626-636.
170. Larkin, J., et al., *Five-Year Survival with Combined Nivolumab and Ipilimumab in Advanced Melanoma.* N Engl J Med, 2019. **381**(16): p. 1535-1546.
171. Sarkisian, S., S. Nair, and R. Sharma, *Current Clinical Trials in the Treatment of Advanced Melanomas.* Surg Clin North Am, 2020. **100**(1): p. 201-208.
172. D'Aniello, C., et al., *Melanoma Adjuvant Treatment: Current Insight and Clinical Features.* Curr Cancer Drug Targets, 2018. **18**(5): p. 442-456.
173. Paraiso, K.H. and K.S. Smalley, *Making sense of MEK1 mutations in intrinsic and acquired BRAF inhibitor resistance.* Cancer Discov, 2012. **2**(5): p. 390-2.
174. Fedorenko, I.V., K.H. Paraiso, and K.S. Smalley, *Acquired and intrinsic BRAF inhibitor resistance in BRAF V600E mutant melanoma.* Biochem Pharmacol, 2011. **82**(3): p. 201-9.
175. Aplin, A.E., F.M. Kaplan, and Y. Shao, *Mechanisms of resistance to RAF inhibitors in melanoma.* J Invest Dermatol, 2011. **131**(9): p. 1817-20.
176. Verduzco, D., et al., *Ceritinib Enhances the Efficacy of Trametinib in BRAF/NRAS-Wild-Type Melanoma Cell Lines.* Mol Cancer Ther, 2018. **17**(1): p. 73-83.
177. Smalley, K.S., et al., *Multiple signaling pathways must be targeted to overcome drug resistance in cell lines derived from melanoma metastases.* Mol Cancer Ther, 2006. **5**(5): p. 1136-44.
178. Xue, Y., et al., *An approach to suppress the evolution of resistance in BRAF(V600E)-mutant cancer.* Nat Med, 2017. **23**(8): p. 929-937.

179. Solit, D.B. and N. Rosen, *Resistance to BRAF inhibition in melanomas.* N Engl J Med, 2011. **364**(8): p. 772-4.
180. Nazarian, R., et al., *Melanomas acquire resistance to B-RAF(V600E) inhibition by RTK or N-RAS upregulation.* Nature, 2010. **468**(7326): p. 973-7.
181. Manzano, J.L., et al., *Resistant mechanisms to BRAF inhibitors in melanoma.* Ann Transl Med, 2016. **4**(12): p. 237.
182. Dumaz, N., et al., *In melanoma, RAS mutations are accompanied by switching signaling from BRAF to CRAF and disrupted cyclic AMP signaling.* Cancer Res, 2006. **66**(19): p. 9483-91.
183. Montagut, C., et al., *Elevated CRAF as a potential mechanism of acquired resistance to BRAF inhibition in melanoma.* Cancer Res, 2008. **68**(12): p. 4853-61.
184. Dumaz, N., *Mechanism of RAF isoform switching induced by oncogenic RAS in melanoma.* Small GTPases, 2011. **2**(5): p. 289-292.
185. Poulikakos, P.I., et al., *RAF inhibitor resistance is mediated by dimerization of aberrantly spliced BRAF(V600E).* Nature, 2011. **480**(7377): p. 387-90.
186. Paraiso, K.H., et al., *Measurement of constitutive MAPK and PI3K/AKT signaling activity in human cancer cell lines.* Methods Enzymol, 2010. **484**: p. 549-67.
187. Davies, M.A., et al., *Integrated Molecular and Clinical Analysis of AKT Activation in Metastatic Melanoma.* Clin Cancer Res, 2009. **15**(24): p. 7538-7546.
188. Meier, F., et al., *The RAS/RAF/MEK/ERK and PI3K/AKT signaling pathways present molecular targets for the effective treatment of advanced melanoma.* Front Biosci, 2005. **10**: p. 2986-3001.
189. Valastyan, S. and R.A. Weinberg, *Tumor metastasis: molecular insights and evolving paradigms.* Cell, 2011. **147**(2): p. 275-92.
190. Lambert, A.W., D.R. Pattabiraman, and R.A. Weinberg, *Emerging Biological Principles of Metastasis.* Cell, 2017. **168**(4): p. 670-691.
191. van Zijl, F., G. Krupitza, and W. Mikulits, *Initial steps of metastasis: cell invasion and endothelial transmigration.* Mutat Res, 2011. **728**(1-2): p. 23-34.
192. Kessenbrock, K., V. Plaks, and Z. Werb, *Matrix metalloproteinases: regulators of the tumor microenvironment.* Cell, 2010. **141**(1): p. 52-67.
193. Plantureux, L., et al., *Impacts of Cancer on Platelet Production, Activation and Education and Mechanisms of Cancer-Associated Thrombosis.* Cancers (Basel), 2018. **10**(11).
194. Rejniak, K.A., *Circulating Tumor Cells: When a Solid Tumor Meets a Fluid Microenvironment.* Adv Exp Med Biol, 2016. **936**: p. 93-106.
195. Davies, M.A., et al., *Prognostic factors for survival in melanoma patients with brain metastases.* Cancer, 2011. **117**(8): p. 1687-96.
196. Davies, M.A., et al., *Dabrafenib plus trametinib in patients with BRAF(V600)-mutant melanoma brain metastases (COMBI-MB): a multicentre, multicohort, open-label, phase 2 trial.* Lancet Oncol, 2017. **18**(7): p. 863-873.
197. Cohen, J.V., et al., *Melanoma central nervous system metastases: current approaches, challenges, and opportunities.* Pigment Cell Melanoma Res, 2016. **29**(6): p. 627-642.
198. Ballabh, P., A. Braun, and M. Nedergaard, *The blood-brain barrier: an overview: structure, regulation, and clinical implications.* Neurobiol Dis, 2004. **16**(1): p. 1-13.
199. Lyle, L.T., et al., *Alterations in Pericyte Subpopulations Are Associated with Elevated Blood-Tumor Barrier Permeability in Experimental Brain Metastasis of Breast Cancer.* Clin Cancer Res, 2016. **22**(21): p. 5287-5299.
200. Abate-Daga, D., et al., *The biology and therapeutic management of melanoma brain metastases.* Biochem Pharmacol, 2018. **153**: p. 35-45.
201. Janzer, R.C. and M.C. Raff, *Astrocytes induce blood-brain barrier properties in endothelial cells.* Nature, 1987. **325**(6101): p. 253-7.

202. Abbott, N.J., *Astrocyte-endothelial interactions and blood-brain barrier permeability.* J Anat, 2002. **200**(6): p. 629-38.
203. Abbott, N.J., L. Ronnback, and E. Hansson, *Astrocyte-endothelial interactions at the blood-brain barrier.* Nat Rev Neurosci, 2006. **7**(1): p. 41-53.
204. Daneman, R. and A. Prat, *The blood-brain barrier.* Cold Spring Harb Perspect Biol, 2015. **7**(1): p. a020412.
205. Michinaga, S. and Y. Koyama, *Dual Roles of Astrocyte-Derived Factors in Regulation of Blood-Brain Barrier Function after Brain Damage.* Int J Mol Sci, 2019. **20**(3).
206. Alvarez, J.I., T. Katayama, and A. Prat, *Glial influence on the blood brain barrier.* Glia, 2013. **61**(12): p. 1939-58.
207. Wang, D.D. and A. Bordey, *The astrocyte odyssey.* Prog Neurobiol, 2008. **86**(4): p. 342-67.
208. Alvarez, J.I., et al., *The Hedgehog pathway promotes blood-brain barrier integrity and CNS immune quiescence.* Science, 2011. **334**(6063): p. 1727-31.
209. Argaw, A.T., et al., *VEGF-mediated disruption of endothelial CLN-5 promotes blood-brain barrier breakdown.* Proc Natl Acad Sci U S A, 2009. **106**(6): p. 1977-82.
210. Argaw, A.T., et al., *Astrocyte-derived VEGF-A drives blood-brain barrier disruption in CNS inflammatory disease.* J Clin Invest, 2012. **122**(7): p. 2454-68.
211. Shen, F., et al., *Coexpression of angiopoietin-1 with VEGF increases the structural integrity of the blood-brain barrier and reduces atrophy volume.* J Cereb Blood Flow Metab, 2011. **31**(12): p. 2343-51.
212. Wosik, K., et al., *Angiotensin II controls occludin function and is required for blood brain barrier maintenance: relevance to multiple sclerosis.* J Neurosci, 2007. **27**(34): p. 9032-42.
213. Daneman, R., et al., *Pericytes are required for blood-brain barrier integrity during embryogenesis.* Nature, 2010. **468**(7323): p. 562-6.
214. Winkler, E.A., R.D. Bell, and B.V. Zlokovic, *Central nervous system pericytes in health and disease.* Nat Neurosci, 2011. **14**(11): p. 1398-1405.
215. Gaengel, K., et al., *Endothelial-mural cell signaling in vascular development and angiogenesis.* Arterioscler Thromb Vasc Biol, 2009. **29**(5): p. 630-8.
216. Armulik, A., et al., *Pericytes regulate the blood-brain barrier.* Nature, 2010. **468**(7323): p. 557-61.
217. Dohgu, S., et al., *Brain pericytes contribute to the induction and up-regulation of blood-brain barrier functions through transforming growth factor-beta production.* Brain Res, 2005. **1038**(2): p. 208-15.
218. Winkler, E.A., R.D. Bell, and B.V. Zlokovic, *Lack of Smad or Notch leads to a fatal game of brain pericyte hopscotch.* Dev Cell, 2011. **20**(3): p. 279-80.
219. Regan, J.N. and M.W. Majesky, *Building a vessel wall with notch signaling.* Circ Res, 2009. **104**(4): p. 419-21.
220. Avraham, H.K., et al., *Angiopoietin-2 mediates blood-brain barrier impairment and colonization of triple-negative breast cancer cells in brain.* J Pathol, 2014. **232**(3): p. 369-81.
221. Sevenich, L., et al., *Analysis of tumour- and stroma-supplied proteolytic networks reveals a brain-metastasis-promoting role for cathepsin S.* Nat Cell Biol, 2014. **16**(9): p. 876-88.
222. Pereira, A.M., M. Strasberg-Rieber, and M. Rieber, *Invasion-associated MMP-2 and MMP-9 are up-regulated intracellularly in concert with apoptosis linked to melanoma cell detachment.* Clin Exp Metastasis, 2005. **22**(4): p. 285-95.
223. Sofroniew, M.V. and H.V. Vinters, *Astrocytes: biology and pathology.* Acta Neuropathol, 2010. **119**(1): p. 7-35.

224. Placone, A.L., A. Quinones-Hinojosa, and P.C. Searson, *The role of astrocytes in the progression of brain cancer: complicating the picture of the tumor microenvironment.* Tumour Biol, 2016. **37**(1): p. 61-9.
225. Skelly, D.T., et al., *A systematic analysis of the peripheral and CNS effects of systemic LPS, IL-1beta, [corrected] TNF-alpha and IL-6 challenges in C57BL/6 mice.* PLoS One, 2013. **8**(7): p. e69123.
226. Kim, S.J., et al., *Astrocytes upregulate survival genes in tumor cells and induce protection from chemotherapy.* Neoplasia, 2011. **13**(3): p. 286-98.
227. Lin, Q., et al., *Reactive astrocytes protect melanoma cells from chemotherapy by sequestering intracellular calcium through gap junction communication channels.* Neoplasia, 2010. **12**(9): p. 748-54.
228. Wang, L., et al., *Astrocytes directly influence tumor cell invasion and metastasis in vivo.* PLoS One, 2013. **8**(12): p. e80933.
229. Zhang, L., et al., *Microenvironment-induced PTEN loss by exosomal microRNA primes brain metastasis outgrowth.* Nature, 2015. **527**(7576): p. 100-104.
230. Bucheit, A.D., et al., *Complete loss of PTEN protein expression correlates with shorter time to brain metastasis and survival in stage IIIB/C melanoma patients with BRAFV600 mutations.* Clin Cancer Res, 2014. **20**(21): p. 5527-36.
231. Jilaveanu, L.B., et al., *PLEKHA5 as a Biomarker and Potential Mediator of Melanoma Brain Metastasis.* Clin Cancer Res, 2015. **21**(9): p. 2138-47.
232. Xie, T.X., et al., *Activation of stat3 in human melanoma promotes brain metastasis.* Cancer Res, 2006. **66**(6): p. 3188-96.
233. Brastianos, P.K., et al., *Genomic Characterization of Brain Metastases Reveals Branched Evolution and Potential Therapeutic Targets.* Cancer Discov, 2015. **5**(11): p. 1164-1177.
234. Kienast, Y., et al., *Real-time imaging reveals the single steps of brain metastasis formation.* Nat Med, 2010. **16**(1): p. 116-22.
235. Obenauf, A.C. and J. Massague, *Surviving at a Distance: Organ-Specific Metastasis.* Trends Cancer, 2015. **1**(1): p. 76-91.
236. Friedl, P., K.S. Zanker, and E.B. Brocker, *Cell migration strategies in 3-D extracellular matrix: differences in morphology, cell matrix interactions, and integrin function.* Microsc Res Tech, 1998. **43**(5): p. 369-78.
237. Sahai, E. and C.J. Marshall, *Differing modes of tumour cell invasion have distinct requirements for Rho/ROCK signalling and extracellular proteolysis.* Nat Cell Biol, 2003. **5**(8): p. 711-9.
238. Friedl, P., *Prespecification and plasticity: shifting mechanisms of cell migration.* Curr Opin Cell Biol, 2004. **16**(1): p. 14-23.
239. Wolf, K., et al., *Compensation mechanism in tumor cell migration: mesenchymal-amoeboid transition after blocking of pericellular proteolysis.* J Cell Biol, 2003. **160**(2): p. 267-77.
240. Wyckoff, J.B., et al., *ROCK- and myosin-dependent matrix deformation enables protease-independent tumor-cell invasion in vivo.* Curr Biol, 2006. **16**(15): p. 1515-23.
241. Pankova, K., et al., *The molecular mechanisms of transition between mesenchymal and amoeboid invasiveness in tumor cells.* Cell Mol Life Sci, 2010. **67**(1): p. 63-71.
242. Pinner, S. and E. Sahai, *Imaging amoeboid cancer cell motility in vivo.* J Microsc, 2008. **231**(3): p. 441-5.
243. Sanz-Moreno, V., et al., *Rac activation and inactivation control plasticity of tumor cell movement.* Cell, 2008. **135**(3): p. 510-23.
244. Nobes, C.D. and A. Hall, *Rho, rac, and cdc42 GTPases regulate the assembly of multimolecular focal complexes associated with actin stress fibers, lamellipodia, and filopodia.* Cell, 1995. **81**(1): p. 53-62.

245. Wilkinson, S., H.F. Paterson, and C.J. Marshall, *Cdc42-MRCK and Rho-ROCK signalling cooperate in myosin phosphorylation and cell invasion.* Nat Cell Biol, 2005. **7**(3): p. 255-61.
246. Yamazaki, D., S. Kurisu, and T. Takenawa, *Involvement of Rac and Rho signaling in cancer cell motility in 3D substrates.* Oncogene, 2009. **28**(13): p. 1570-83.
247. Gadea, G., et al., *DOCK10-mediated Cdc42 activation is necessary for amoeboid invasion of melanoma cells.* Curr Biol, 2008. **18**(19): p. 1456-65.
248. Parri, M., et al., *EphA2 reexpression prompts invasion of melanoma cells shifting from mesenchymal to amoeboid-like motility style.* Cancer Res, 2009. **69**(5): p. 2072-81.
249. Rodriguez-Hernandez, I., et al., *WNT11-FZD7-DAAM1 signalling supports tumour initiating abilities and melanoma amoeboid invasion.* Nat Commun, 2020. **11**(1): p. 5315.
250. Drescher, U., *The Eph family in the patterning of neural development.* Curr Biol, 1997. **7**(12): p. R799-807.
251. Holland, S.J., et al., *Cell-contact-dependent signalling in axon growth and guidance: Eph receptor tyrosine kinases and receptor protein tyrosine phosphatase beta.* Curr Opin Neurobiol, 1998. **8**(1): p. 117-27.
252. O'Leary, D.D. and D.G. Wilkinson, *Eph receptors and ephrins in neural development.* Curr Opin Neurobiol, 1999. **9**(1): p. 65-73.
253. Gale, N.W., et al., *Eph receptors and ligands comprise two major specificity subclasses and are reciprocally compartmentalized during embryogenesis.* Neuron, 1996. **17**(1): p. 9-19.
254. Darling, T.K. and T.J. Lamb, *Emerging Roles for Eph Receptors and Ephrin Ligands in Immunity.* Front Immunol, 2019. **10**: p. 1473.
255. Himanen, J.P., et al., *Architecture of Eph receptor clusters.* Proc Natl Acad Sci U S A, 2010. **107**(24): p. 10860-5.
256. Flanagan, J.G. and P. Vanderhaeghen, *The ephrins and Eph receptors in neural development.* Annu Rev Neurosci, 1998. **21**: p. 309-45.
257. Pasquale, E.B., *Eph receptor signalling casts a wide net on cell behaviour.* Nat Rev Mol Cell Biol, 2005. **6**(6): p. 462-75.
258. Dodelet, V.C. and E.B. Pasquale, *Eph receptors and ephrin ligands: embryogenesis to tumorigenesis.* Oncogene, 2000. **19**(49): p. 5614-9.
259. Park, J.E., A.I. Son, and R. Zhou, *Roles of EphA2 in Development and Disease.* Genes (Basel), 2013. **4**(3): p. 334-57.
260. Pasquale, E.B., *Eph-ephrin bidirectional signaling in physiology and disease.* Cell, 2008. **133**(1): p. 38-52.
261. Adams, R.H., et al., *Roles of ephrinB ligands and EphB receptors in cardiovascular development: demarcation of arterial/venous domains, vascular morphogenesis, and sprouting angiogenesis.* Genes Dev, 1999. **13**(3): p. 295-306.
262. Kullander, K. and R. Klein, *Mechanisms and functions of Eph and ephrin signalling.* Nat Rev Mol Cell Biol, 2002. **3**(7): p. 475-86.
263. Lindberg, R.A. and T. Hunter, *cDNA cloning and characterization of eck, an epithelial cell receptor protein-tyrosine kinase in the eph/elk family of protein kinases.* Mol Cell Biol, 1990. **10**(12): p. 6316-24.
264. Pasquale, E.B., *Eph receptors and ephrins in cancer: bidirectional signalling and beyond.* Nat Rev Cancer, 2010. **10**(3): p. 165-80.
265. Wykosky, J. and W. Debinski, *The EphA2 receptor and ephrinA1 ligand in solid tumors: function and therapeutic targeting.* Mol Cancer Res, 2008. **6**(12): p. 1795-806.
266. Singh, D.R., et al., *The EphA2 receptor is activated through induction of distinct, ligand-dependent oligomeric structures.* Commun Biol, 2018. **1**: p. 15.
267. Lisabeth, E.M., G. Falivelli, and E.B. Pasquale, *Eph receptor signaling and ephrins.* Cold Spring Harb Perspect Biol, 2013. **5**(9).

268. Pasquale, E.B., *The Eph family of receptors.* Curr Opin Cell Biol, 1997. **9**(5): p. 608-15.
269. Binns, K.L., et al., *Phosphorylation of tyrosine residues in the kinase domain and juxtamembrane region regulates the biological and catalytic activities of Eph receptors.* Mol Cell Biol, 2000. **20**(13): p. 4791-805.
270. Shi, X., et al., *A role of the SAM domain in EphA2 receptor activation.* Sci Rep, 2017. **7**: p. 45084.
271. Singh, D.R., et al., *The SAM domain inhibits EphA2 interactions in the plasma membrane.* Biochim Biophys Acta Mol Cell Res, 2017. **1864**(1): p. 31-38.
272. Qiao, F. and J.U. Bowie, *The many faces of SAM.* Sci STKE, 2005. **2005**(286): p. re7.
273. Hui, S., X. Xing, and G.D. Bader, *Predicting PDZ domain mediated protein interactions from structure.* BMC Bioinformatics, 2013. **14**: p. 27.
274. Son, A.I., et al., *Further analysis of the lens of ephrin-A5-/- mice: development of postnatal defects.* Mol Vis, 2013. **19**: p. 254-66.
275. Cooper, M.A., et al., *Loss of ephrin-A5 function disrupts lens fiber cell packing and leads to cataract.* Proc Natl Acad Sci U S A, 2008. **105**(43): p. 16620-5.
276. Jun, G., et al., *EPHA2 is associated with age-related cortical cataract in mice and humans.* PLoS Genet, 2009. **5**(7): p. e1000584.
277. Xu, H., et al., *EphA2: expression in the renal medulla and regulation by hypertonicity and urea stress in vitro and in vivo.* Am J Physiol Renal Physiol, 2005. **288**(4): p. F855-66.
278. Wakayama, Y., et al., *EphrinA1-EphA2 signal induces compaction and polarization of Madin-Darby canine kidney cells by inactivating Ezrin through negative regulation of RhoA.* J Biol Chem, 2011. **286**(51): p. 44243-44253.
279. Irie, N., et al., *Bidirectional signaling through ephrinA2-EphA2 enhances osteoclastogenesis and suppresses osteoblastogenesis.* J Biol Chem, 2009. **284**(21): p. 14637-44.
280. Zhao, C., et al., *Bidirectional ephrinB2-EphB4 signaling controls bone homeostasis.* Cell Metab, 2006. **4**(2): p. 111-21.
281. Kouros-Mehr, H. and Z. Werb, *Candidate regulators of mammary branching morphogenesis identified by genome-wide transcript analysis.* Dev Dyn, 2006. **235**(12): p. 3404-12.
282. Vaught, D., J. Chen, and D.M. Brantley-Sieders, *Regulation of mammary gland branching morphogenesis by EphA2 receptor tyrosine kinase.* Mol Biol Cell, 2009. **20**(10): p. 2572-81.
283. Saeger, B.M., M. Suhm, and A. Neubuser, *Ephrin/ephrin receptor expression during early stages of mouse inner ear development.* Dev Dyn, 2011. **240**(6): p. 1578-85.
284. Kurose, H., et al., *Elevated Expression of EPHA2 Is Associated With Poor Prognosis After Radical Prostatectomy in Prostate Cancer.* Anticancer Res, 2019. **39**(11): p. 6249-6257.
285. Amato, K.R., et al., *EPHA2 Blockade Overcomes Acquired Resistance to EGFR Kinase Inhibitors in Lung Cancer.* Cancer Res, 2016. **76**(2): p. 305-18.
286. Martini, G., et al., *EPHA2 Is a Predictive Biomarker of Resistance and a Potential Therapeutic Target for Improving Antiepidermal Growth Factor Receptor Therapy in Colorectal Cancer.* Mol Cancer Ther, 2019. **18**(4): p. 845-855.
287. Lin, Y.G., et al., *EphA2 overexpression is associated with angiogenesis in ovarian cancer.* Cancer, 2007. **109**(2): p. 332-40.
288. Chen, Z., et al., *Spatially modulated ephrinA1:EphA2 signaling increases local contractility and global focal adhesion dynamics to promote cell motility.* Proc Natl Acad Sci U S A, 2018. **115**(25): p. E5696-E5705.
289. Singh, A., E. Winterbottom, and I.O. Daar, *Eph/ephrin signaling in cell-cell and cell-substrate adhesion.* Front Biosci (Landmark Ed), 2012. **17**: p. 473-97.

290. Himanen, J.P., N. Saha, and D.B. Nikolov, *Cell-cell signaling via Eph receptors and ephrins.* Curr Opin Cell Biol, 2007. **19**(5): p. 534-42.
291. Davis, S., et al., *Ligands for EPH-related receptor tyrosine kinases that require membrane attachment or clustering for activity.* Science, 1994. **266**(5186): p. 816-9.
292. Fang, W.B., et al., *Identification and functional analysis of phosphorylated tyrosine residues within EphA2 receptor tyrosine kinase.* J Biol Chem, 2008. **283**(23): p. 16017-26.
293. Zhou, Y. and H. Sakurai, *Emerging and Diverse Functions of the EphA2 Noncanonical Pathway in Cancer Progression.* Biol Pharm Bull, 2017. **40**(10): p. 1616-1624.
294. De Robertis, M., et al., *Dysregulation of EGFR Pathway in EphA2 Cell Subpopulation Significantly Associates with Poor Prognosis in Colorectal Cancer.* Clin Cancer Res, 2017. **23**(1): p. 159-170.
295. Dunne, P.D., et al., *EphA2 Expression Is a Key Driver of Migration and Invasion and a Poor Prognostic Marker in Colorectal Cancer.* Clin Cancer Res, 2016. **22**(1): p. 230-242.
296. Li, X., et al., *Up-regulation of EphA2 and down-regulation of EphrinA1 are associated with the aggressive phenotype and poor prognosis of malignant glioma.* Tumour Biol, 2010. **31**(5): p. 477-88.
297. Barquilla, A., et al., *Protein kinase A can block EphA2 receptor-mediated cell repulsion by increasing EphA2 S897 phosphorylation.* Mol Biol Cell, 2016. **27**(17): p. 2757-70.
298. Miao, H., et al., *EphA2 mediates ligand-dependent inhibition and ligand-independent promotion of cell migration and invasion via a reciprocal regulatory loop with Akt.* Cancer Cell, 2009. **16**(1): p. 9-20.
299. Yang, N.Y., et al., *Crosstalk of the EphA2 receptor with a serine/threonine phosphatase suppresses the Akt-mTORC1 pathway in cancer cells.* Cell Signal, 2011. **23**(1): p. 201-12.
300. Miao, H., et al., *Activation of EphA2 kinase suppresses integrin function and causes focal-adhesion-kinase dephosphorylation.* Nat Cell Biol, 2000. **2**(2): p. 62-9.
301. Boyd, A.W., P.F. Bartlett, and M. Lackmann, *Therapeutic targeting of EPH receptors and their ligands.* Nat Rev Drug Discov, 2014. **13**(1): p. 39-62.
302. Biao-xue, R., et al., *EphA2-dependent molecular targeting therapy for malignant tumors.* Curr Cancer Drug Targets, 2011. **11**(9): p. 1082-97.
303. Zhou, Y., et al., *Crucial roles of RSK in cell motility by catalysing serine phosphorylation of EphA2.* Nat Commun, 2015. **6**: p. 7679.
304. Volz, C., et al., *Inhibition of Tumor VEGFR2 Induces Serine 897 EphA2-Dependent Tumor Cell Invasion and Metastasis in NSCLC.* Cell Rep, 2020. **31**(4): p. 107568.
305. Tandon, M., S.V. Vemula, and S.K. Mittal, *Emerging strategies for EphA2 receptor targeting for cancer therapeutics.* Expert Opin Ther Targets, 2011. **15**(1): p. 31-51.
306. Liu, Y., et al., *Clinical significance of EphA2 expression in squamous-cell carcinoma of the head and neck.* J Cancer Res Clin Oncol, 2011. **137**(5): p. 761-9.
307. Binda, E., et al., *The EphA2 receptor drives self-renewal and tumorigenicity in stem-like tumor-propagating cells from human glioblastomas.* Cancer Cell, 2012. **22**(6): p. 765-80.
308. Ponti, D., et al., *Isolation and in vitro propagation of tumorigenic breast cancer cells with stem/progenitor cell properties.* Cancer Res, 2005. **65**(13): p. 5506-11.
309. Ricci-Vitiani, L., et al., *Colon cancer stem cells.* J Mol Med (Berl), 2009. **87**(11): p. 1097-104.
310. Buzzeo, M.P., E.W. Scott, and C.R. Cogle, *The hunt for cancer-initiating cells: a history stemming from leukemia.* Leukemia, 2007. **21**(8): p. 1619-27.
311. Hadjipanayis, C.G. and E.G. Van Meir, *Tumor initiating cells in malignant gliomas: biology and implications for therapy.* J Mol Med (Berl), 2009. **87**(4): p. 363-74.
312. Galli, R., et al., *Isolation and characterization of tumorigenic, stem-like neural precursors from human glioblastoma.* Cancer Res, 2004. **64**(19): p. 7011-21.

313. Piccirillo, S.G., et al., *Bone morphogenetic proteins inhibit the tumorigenic potential of human brain tumour-initiating cells.* Nature, 2006. **444**(7120): p. 761-5.
314. Liu, D.P., et al., *Ephrin-A1 is a negative regulator in glioma through down-regulation of EphA2 and FAK.* Int J Oncol, 2007. **30**(4): p. 865-71.
315. Wykosky, J., et al., *EphA2 as a novel molecular marker and target in glioblastoma multiforme.* Mol Cancer Res, 2005. **3**(10): p. 541-51.
316. Miao, H., et al., *EphA2 promotes infiltrative invasion of glioma stem cells in vivo through cross-talk with Akt and regulates stem cell properties.* Oncogene, 2015. **34**(5): p. 558-67.
317. Venere, M., et al., *Cancer stem cells in gliomas: identifying and understanding the apex cell in cancer's hierarchy.* Glia, 2011. **59**(8): p. 1148-54.
318. Singh, S.K., et al., *Identification of a cancer stem cell in human brain tumors.* Cancer Res, 2003. **63**(18): p. 5821-8.
319. Hemmati, H.D., et al., *Cancerous stem cells can arise from pediatric brain tumors.* Proc Natl Acad Sci U S A, 2003. **100**(25): p. 15178-83.
320. Liu, G., et al., *Analysis of gene expression and chemoresistance of CD133+ cancer stem cells in glioblastoma.* Mol Cancer, 2006. **5**: p. 67.
321. Bao, S., et al., *Glioma stem cells promote radioresistance by preferential activation of the DNA damage response.* Nature, 2006. **444**(7120): p. 756-60.
322. Cheng, L., et al., *Elevated invasive potential of glioblastoma stem cells.* Biochem Biophys Res Commun, 2011. **406**(4): p. 643-8.
323. Garcia, J.L., et al., *Molecular analysis of ex-vivo CD133+ GBM cells revealed a common invasive and angiogenic profile but different proliferative signatures among high grade gliomas.* BMC Cancer, 2010. **10**: p. 454.
324. Gordon, K., et al., *Alteration of the EphA2/Ephrin-A signaling axis in psoriatic epidermis.* J Invest Dermatol, 2013. **133**(3): p. 712-722.
325. Garcia-Monclus, S., et al., *EphA2 receptor is a key player in the metastatic onset of Ewing sarcoma.* Int J Cancer, 2018. **143**(5): p. 1188-1201.
326. Williams, R.F., I. Fernandez-Pineda, and A. Gosain, *Pediatric Sarcomas.* Surg Clin North Am, 2016. **96**(5): p. 1107-25.
327. Paraiso, K.H., et al., *Ligand-independent EPHA2 signaling drives the adoption of a targeted therapy-mediated metastatic melanoma phenotype.* Cancer Discov, 2015. **5**(3): p. 264-73.
328. Tawadros, T., et al., *Ligand-independent activation of EphA2 by arachidonic acid induces metastasis-like behaviour in prostate cancer cells.* Br J Cancer, 2012. **107**(10): p. 1737-44.
329. Hill, V.K., et al., *The genetics of melanoma: recent advances.* Annu Rev Genomics Hum Genet, 2013. **14**: p. 257-79.
330. Avci, P., et al., *Animal models of skin disease for drug discovery.* Expert Opin Drug Discov, 2013. **8**(3): p. 331-55.
331. Kuzu, O.F., et al., *Current State of Animal (Mouse) Modeling in Melanoma Research.* Cancer Growth Metastasis, 2015. **8**(Suppl 1): p. 81-94.
332. Damsky, W.E., et al., *beta-catenin signaling controls metastasis in Braf-activated Pten-deficient melanomas.* Cancer Cell, 2011. **20**(6): p. 741-54.
333. Damsky, W., et al., *mTORC1 activation blocks BrafV600E-induced growth arrest but is insufficient for melanoma formation.* Cancer Cell, 2015. **27**(1): p. 41-56.
334. Viros, A., et al., *Ultraviolet radiation accelerates BRAF-driven melanomagenesis by targeting TP53.* Nature, 2014. **511**(7510): p. 478-482.
335. Marsh Durban, V., et al., *Differential AKT dependency displayed by mouse models of BRAFV600E-initiated melanoma.* J Clin Invest, 2013. **123**(12): p. 5104-18.
336. Bok, I., et al., *A Versatile ES Cell-Based Melanoma Mouse Modeling Platform.* Cancer Res, 2020. **80**(4): p. 912-921.

337. Emmons, M.F., et al., *HDAC8 Regulates a Stress Response Pathway in Melanoma to Mediate Escape from BRAF Inhibitor Therapy.* Cancer Res, 2019. **79**(11): p. 2947-2961.
338. Cardama, G.A., et al., *Relevance of small GTPase Rac1 pathway in drug and radio-resistance mechanisms: Opportunities in cancer therapeutics.* Crit Rev Oncol Hematol, 2018. **124**: p. 29-36.
339. Orgaz, J.L., et al., *Myosin II Reactivation and Cytoskeletal Remodeling as a Hallmark and a Vulnerability in Melanoma Therapy Resistance.* Cancer Cell, 2020. **37**(1): p. 85-103 e9.
340. Frenard, C., et al., *Development of brain metastases in patients with metastatic melanoma while receiving ipilimumab.* J Neurooncol, 2016. **126**(2): p. 355-60.
341. Hassel, J.C., et al., *Progression patterns under BRAF inhibitor treatment and treatment beyond progression in patients with metastatic melanoma.* Cancer Med, 2018. **7**(1): p. 95-104.
342. Kenchappa, R.S., et al., *Novel treatments for melanoma brain metastases.* Cancer Control, 2013. **20**(4): p. 298-306.
343. Ridley, A.J., et al., *The small GTP-binding protein rac regulates growth factor-induced membrane ruffling.* Cell, 1992. **70**(3): p. 401-10.
344. Amano, M., et al., *Formation of actin stress fibers and focal adhesions enhanced by Rho-kinase.* Science, 1997. **275**(5304): p. 1308-11.
345. Kimura, K., et al., *Regulation of myosin phosphatase by Rho and Rho-associated kinase (Rho-kinase).* Science, 1996. **273**(5272): p. 245-8.
346. Cantelli, G., et al., *TGF-beta-Induced Transcription Sustains Amoeboid Melanoma Migration and Dissemination.* Curr Biol, 2015. **25**(22): p. 2899-914.
347. Herraiz, C., et al., *Reactivation of p53 by a Cytoskeletal Sensor to Control the Balance Between DNA Damage and Tumor Dissemination.* J Natl Cancer Inst, 2016. **108**(1).
348. Fidler, I.J., *Metastasis: quantitative analysis of distribution and fate of tumor emboli labeled with 125 I-5-iodo-2'-deoxyuridine.* J Natl Cancer Inst, 1970. **45**(4): p. 773-82.
349. Barnes, J.M., J.T. Nauseef, and M.D. Henry, *Resistance to fluid shear stress is a conserved biophysical property of malignant cells.* PLoS One, 2012. **7**(12): p. e50973.
350. Hyler, A.R., et al., *Fluid shear stress impacts ovarian cancer cell viability, subcellular organization, and promotes genomic instability.* PLoS One, 2018. **13**(3): p. e0194170.
351. Sahai, E., *Illuminating the metastatic process.* Nat Rev Cancer, 2007. **7**(10): p. 737-49.
352. Sanz-Moreno, V., et al., *ROCK and JAK1 signaling cooperate to control actomyosin contractility in tumor cells and stroma.* Cancer Cell, 2011. **20**(2): p. 229-45.
353. Georgouli, M., et al., *Regional Activation of Myosin II in Cancer Cells Drives Tumor Progression via a Secretory Cross-Talk with the Immune Microenvironment.* Cell, 2019. **176**(4): p. 757-774 e23.
354. Quail, D.F. and J.A. Joyce, *Microenvironmental regulation of tumor progression and metastasis.* Nat Med, 2013. **19**(11): p. 1423-37.
355. Sugiyama, N., et al., *EphA2 cleavage by MT1-MMP triggers single cancer cell invasion via homotypic cell repulsion.* J Cell Biol, 2013. **201**(3): p. 467-84.
356. Koshikawa, N., et al., *Proteolysis of EphA2 Converts It from a Tumor Suppressor to an Oncoprotein.* Cancer Res, 2015. **75**(16): p. 3327-39.
357. Wykosky, J., et al., *Soluble monomeric EphrinA1 is released from tumor cells and is a functional ligand for the EphA2 receptor.* Oncogene, 2008. **27**(58): p. 7260-73.
358. Xu, Q., et al., *EphA2 receptor activation by monomeric Ephrin-A1 on supported membranes.* Biophys J, 2011. **101**(11): p. 2731-9.
359. Duxbury, M.S., et al., *Ligation of EphA2 by Ephrin A1-Fc inhibits pancreatic adenocarcinoma cellular invasiveness.* Biochem Biophys Res Commun, 2004. **320**(4): p. 1096-102.

360. Nakamura, R., et al., *EPHA2/EFNA1 expression in human gastric cancer.* Cancer Sci, 2005. **96**(1): p. 42-7.
361. Sakamoto, A., et al., *An Agonistic Antibody to EPHA2 Exhibits Antitumor Effects on Human Melanoma Cells.* Anticancer Res, 2018. **38**(6): p. 3273-3282.
362. Giorgio, C., et al., *Lithocholic acid is an Eph-ephrin ligand interfering with Eph-kinase activation.* PLoS One, 2011. **6**(3): p. e18128.
363. Mohamed, I.H., et al., *Polyphenol rich botanicals used as food supplements interfere with EphA2-ephrinA1 system.* Pharmacol Res, 2011. **64**(5): p. 464-70.
364. Chow, K.K., et al., *T cells redirected to EphA2 for the immunotherapy of glioblastoma.* Mol Ther, 2013. **21**(3): p. 629-37.
365. Bai, X., D.E. Fisher, and K.T. Flaherty, *Cell-state dynamics and therapeutic resistance in melanoma from the perspective of MITF and IFNgamma pathways.* Nat Rev Clin Oncol, 2019. **16**(9): p. 549-562.
366. Smalley, I., et al., *Leveraging transcriptional dynamics to improve BRAF inhibitor responses in melanoma.* EBioMedicine, 2019. **48**: p. 178-190.